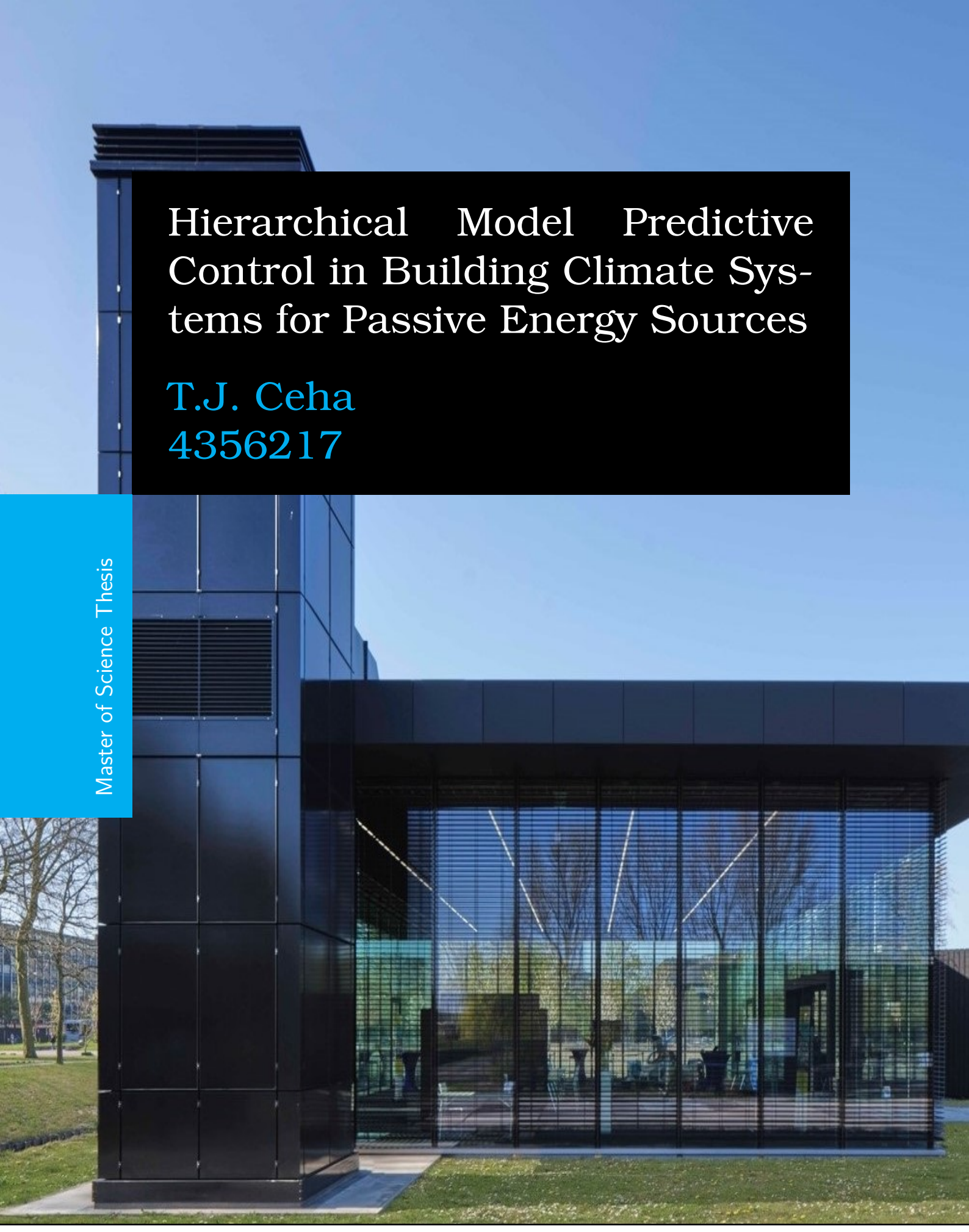

Hierarchical Model Predictive Control in Building Climate Systems for Passive Energy Sources

T.J. Ceha
4356217

Master of Science Thesis

TU Delft Delft University of Technology

Delft Center for Systems and Control

Hierarchical Model Predictive Control in Building Climate Systems for Passive Energy Sources

Master of Science Thesis

For the degree of Master of Science in Systems and Control at Delft University of Technology

T.J. Ceha
4356217

June 23, 2021

Faculty of Mechanical, Maritime and Materials Engineering (3mE) · Delft University of Technology

Abstract

There is an urgent need for technical innovations in the construction industry to meet the European Parliament's qualifications for reducing the energy footprint of buildings. This thesis is devoted to conducting research on control strategies that optimally manage passive energy sources, e.g., natural ventilation and solar irradiance, in combination with an active energy source. The main objective is to develop a control strategy that is both on-line applicable and maximizes the performance of the building energy management system in terms of passive fraction of energy while maintaining indoor thermal comfort.

Energy-saving model predictive control (MPC) structures have been extensively researched in the literature on building energy management systems. These studies usually focus on the energy distribution in multi-zoned buildings and rarely consider optimal control of a single or multiple passive energy sources. In addition, most studied building models are based on general buildings and are established by means of simulation software tools. A more experimental study has not yet been conducted on optimal energy management systems for a building that is maximized in harvesting passive energy.

This work investigates five MPC strategies as a way to optimize the operations of four solar blinds, a thermal chimney, and an active energy source. In these strategies, linear and nonlinear MPC are considered in the forms of centralized and hierarchical architectures. White-box modeling and linearization methods are adopted to develop the required linear and nonlinear building models. Thereafter, the proposed modeling methodology is validated by using experimental data. The hierarchical MPC architecture that considers a hybrid structure with a linear MPC agent for solar blind operations, a nonlinear MPC tracker for ventilation, a linear Kalman filter, and separated state-update loops appears to be the best-performing strategy. This control structure is also applied in a case study, in which it is tested on experimental data from the real-case office building, which is controlled by a rule-based control structure. The results show that the developed control structure is able to outperform the rule-based controller in terms of minimizing energy consumption and maintaining thermal comfort.

Table of Contents

Acknowledgements **xi**

1 Introduction **1**

1-1 Nearly zero energy buildings . . . 1

1-2 CONVERGE project . . . 2

1-3 Problem statement . . . 2

1-4 Report outline . . . 3

2 Literature Review: Sustainable Energy Management of Office Buildings **5**

2-1 Fundamentals of building energy dynamics . . . 5

2-1-1 Thermal transient behavior . . . 5

2-1-2 Solar irradiance . . . 9

2-1-3 Natural ventilation . . . 11

2-2 Building modeling approaches . . . 12

2-2-1 White-box: Software tool utilization . . . 13

2-2-2 Black-box: Statistical models and training data . . . 13

2-2-3 Grey-box: RC-network application . . . 14

2-2-4 Numerical validation methods . . . 15

2-3 MPC for indoor climate control . . . 15

2-3-1 Performance feasibility of MPC . . . 15

2-3-2 Control architectures . . . 17

2-3-3 Design and optimization of control objectives . . . 18

2-4 Conclusions . . . 19

3 Proposal of Control Systems **21**
3-1 Thermal system modeling . . . 21
3-1-1 System configuration . . . 22
3-1-2 Actuator modeling . . . 27
3-1-3 The nonlinear plant model . . . 28
3-1-4 The computational cost problem . . . 28
3-1-5 Linearization strategies . . . 30
3-2 MPC architecture study . . . 32
3-2-1 General MPC problem setup . . . 32
3-2-2 Convexity analysis . . . 34
3-2-3 Centralized structure . . . 35
3-2-4 Hierarchical structure . . . 39
3-2-5 The most promising structure . . . 42
3-2-6 State-update estimation . . . 42
3-3 Multi-objective control problem . . . 44
3-3-1 ϵ-constraint method . . . 45
3-3-2 Pareto front construction . . . 45
3-4 Conclusions . . . 46

4 Case Study **47**
4-1 Case study details . . . 47
4-1-1 Model validation setup . . . 47
4-1-2 Control case formulation . . . 49
4-1-3 MPC framework . . . 50
4-1-4 CPU specifications . . . 52
4-2 Case study results . . . 52
4-2-1 Validation results . . . 52
4-2-2 Control performance of grey-box model . . . 53
4-2-3 Control comparison with rule-based controller . . . 54
4-3 Conclusions . . . 58

5 Conclusions and Future Work **59**
5-1 Conclusions . . . 59
5-2 Recommendations for future work . . . 61

A Models for Solar-Based Parameters **63**

B Model Predictive Control **65**
B-1 Overview . . . 65
B-2 General Model Predictive Control Framework . . . 66
B-3 Objective Function Formulation . . . 67
B-4 Constraints Formulation . . . 68

C Supportive Tables with Optimization and Validation Results **71**

D Conference Paper **73**

E Draft of Journal Paper **81**

Bibliography **83**

Glossary **89**

List of Acronyms 89

List of Symbols 89

List of Figures

3-1 CCC-building with initial chimney design. 22
3-2 Occupancy distribution over a day. 33
3-3 Convexity of 2D solution space. 35
3-4 Convexity of 4D solution space. 35
3-5 Convexity of 8D solution space. 35
3-6 Convexity of 2D solution space. 35
3-7 Convexity of 4D solution space. 35
3-8 Convexity of 8D solution space. 35
3-9 NLMPC structure flowchart. 36
3-10 T_z progression for a 14-day period: $\Delta t = 3600 \wedge N_p = 8$. 37
3-11 LMPC structure flowchart. 38
3-12 T_z progression for a 14-day period: $\Delta t = 3600 \wedge N_p^* = 24$. 39
3-13 HMPC-1 structure flowchart. 41
3-14 HMPC-2 structure flowchart. 41
3-15 T_z progression for a 14-day period: $N_p^* = 24 \wedge N_p = 4$. 41
3-16 T_z progression for a 14-day period: $N_p^* = 24 \wedge N_p = 4$. 41
3-17 HMPC-2a structure flowchart. 44
3-18 HMPC-2b structure flowchart. 44
3-19 200 Pareto trade-off points. 46
3-20 Mean computational costs. 46

4-1 Final HMPC-2b structure flowchart. 50
4-2 Validation on 10-day period. 52
4-3 Validation on 3-day period. 52
4-4 Training on 10-day period. 53
4-5 Validation on 3-day period. 53

4-6 13-day progression of T_z: $N_p^* = 72 \wedge N_p = 9$. 55
4-7 Supplied air through natural ventilation. 55
4-8 States of the 4 blinds to control solar irradiance. 56
4-9 Auxiliary energy supply to ensure thermal comfort. 56
4-10 13-day progression of the measured T_z of the CCC-building. 56
4-11 Supplied air through fans. 56

B-1 Schematic representation of the discrete MPC scheme [54]. 65

List of Tables

2-1 Comparison of 7 models for oriented diffused radiation [23]. 11

3-1 General expressions. 22
3-2 Dimensions and material properties of each considered building component. . . . 22
3-3 Results of the NLMPC scheme for a 40-day simulation period. 37
3-4 Results of the LMPC scheme for a 40-day simulation period. 39
3-5 Results of the HMPC schemes for a 40-day simulation period. 40
3-6 ${}^{a}N_{\mathrm{p}}^{*}$ is 24 for the linear agent controller. 42
3-7 Results of the HMPC-2 extensions for a 40-day simulation period. 44

4-1 White-box model validation results: April 2 to 11. 52
4-2 White-box model validation results: May 22 to 24. 52
4-3 Grey-box model validation results on training data: April 2 to 11. 53
4-4 Grey-box model validation results on validation data: May 22 to 24. 53
4-5 Model comparison on 200-day period, using the HMPC-2b scheme. 54
4-6 Results of the HMPC-2b structure for a 13-day field experiment period. 55
4-7 Additional energy comparison to realize thermal comfort and IAQ. 57

B-1 Common types of objective functions [45]. 68
B-2 Common types of constraints [45]. 69

C-1 Results of the nonlinear convection coefficient fitted models. 71
C-2 Results of the linear convection coefficient fitted models. 72
C-3 Results of the optimized parameters for the grey-box model. 72

Acknowledgements

I am very grateful to complete the MSc study Systems & Control with this thesis project. Throughout the Master's program and my thesis, I experienced a strong and steep learning curve. This gave me the opportunity to develop myself in state-of-the-art techniques, but also in perseverance. I have enjoyed all aspects of my thesis research and am grateful for the additional opportunities this thesis has provided, like presenting my paper on the MED2021 conference and writing a second paper for an international journal. In addition, I gained experience in the practice of sensor installation, data management, and building actuators while working on the field experiment preparations at the Green Village.

First, I would like to thank my daily supervisor dr.ir. Luigi Antonio de Araujo Passos for his assistance during the thesis. Our numerous discussions took the outcome of this thesis to the next level. In addition, his cooperation and enthusiasm were indispensable for writing the papers.

I would also like to thank my main supervisor prof.dr.ir. Bart De Schutter for providing crucial insights and feedback on important aspects of the work. Although there were few meetings, the discussions were very helpful.

Furthermore, I owe gratitude to dr. Regina Bokel and dr. Alfredo Nunez Vicencio for their willingness to participate as members of the thesis committee.

Last of all, I want to thank the CONVERGE team and my fellow study colleagues. The project team provided relevant information and the opportunity to take field measurements, which supported the results of the thesis. In addition, my fellow students gave me different perspectives on the work, which resulted in new insights and enjoyment in the research.

Delft, University of Technology
4356217
June 23, 2021

T.J. Ceha

Chapter 1

Introduction

1-1 Nearly zero energy buildings

The urban environment in Europe is accounted for 40% of the total energy consumption in the EU [26], making it the highest-ranked sector in energy consumption. Two-thirds of this portion is consumed for indoor climate control. Therefore, 25% of the total energy consumption is used for creating a pleasant indoor climate. In 2015, the Dutch government proposed new construction laws, aiming to reduce the sector's energy consumption. From January 2021, all new constructions must comply with the Nearly Zero Energy Buildings-requirements (BENG-requirements) [52]. The new laws are a response to Directive 2010/31/EU of the European Parliament and the Council, which relates to the energy demand of buildings [1].

The main goal of BENG is to reduce the CO_2 emissions of new buildings in three steps.

1. Reducing the energy demand of buildings;
2. Limiting the use of fossil energy;
3. Utilizing renewable energy;

The final values of the three BENG-requirements were published in June 2019. For example, newly constructed average-sized offices may have a maximum energy demand of 90 kWh/m^2 per year. A maximum energy consumption of 40 kWh/m^2 may come from fossil energy and at least 30% of the total energy consumption has to come from renewable energy sources [43].

The building type determines the feasibility of the BENG-requirements. A terraced building generally has no problems satisfying the requirement. Since, the energy losses are limited to solely the front and back sides, due to adjacent buildings. Whereas a detached office building has more loss area. Therefore, the energy demand of such buildings is often between 100-150 kWh/m^2 per year [50]. This is why technical innovations for reducing the energy demand are more than welcome in the building construction industry. Therefore, the sector is in search for advanced techniques. Such innovations may emerge from the TU Delft CONVERGE project.

1-2 CONVERGE project

Passive climate control sources are suitable for reducing a building's energy demand. Much research is conducted in these sources. For instance, optimally controlled operable windows and solar blinds or integrated Phase Change Materials (PCM) and optimized building architectures can drastically reduce the energy demand. The current state-of-the-art is the "Earth, Wind & Fire" project, a TU Delft project in 2014. In this project, a thermal chimney for natural ventilation has been proposed and integrated into practice [17].

In 2018, the Green Village foundation on the TU Delft campus started a project for a nearly zero energy building, which was initially based on the "Earth, Wind & Fire" project. The CONVERGE project, standing for comfortable natural ventilation and energy reduction in the urban environment, has two main targets. Firstly, the integration of passive climate control systems into the building energy management system (BEMS), such that the auxiliary energy demand is reduced by at least 80% relative to conventional climate control practices. Secondly, it serves as a testbed to gain knowledge through research and education and to apply this knowledge quickly and easily in practice. Several partners play a role in this project. TU Delft contributes knowledge by assigning its researchers and students to the project. The companies Van Dorp, Hunter Douglas, and Priva, provide software and hardware as they are interested in the gained knowledge. Furthermore, the Green Village has a wide network of interested parties, included the Dutch government. This network helps to raise attention for this project [2]. The CONVERGE project is unique as it makes use of multiple passive climate sources and a blanket on-line control system. Dozens of actuators and more than a hundred sensors are integrated into the building to make the control of these sources possible. On-line smart energy management will be one of the main focuses of the CONVERGE project.

1-3 Problem statement

To reduce the building energy demand for indoor climate control, optimal control of active and passive energy sources by an advanced building energy management system (BEMS) is required. The literature study done prior to the MSc thesis project indicates that a vast amount of research has been conducted on MPC to reduce the energy demand by means of such sources and advanced control architectures. However, most studies are simulated-based and focused on one type of active or passive climate control source. They rather adapt their strategies to different building types instead of combining multiple climate control sources. To the best of the author's knowledge, a literature gap appears in the research field of BEMS for building climate control and the field of optimal control of climate control sources, especially passive sources, in real-case buildings. This thesis offers an opportunity to close this gap, as access is provided to measurements and control of active and passive climate control methods in a real-case building. Therefore, the aim of this MSc thesis is focused on advanced and on-line applicable model predictive control strategies to optimally control multiple climate control sources. Here, the building of the CONVERGE project will serve as support for the modeling and controller comparison. The following research question is proposed:

"What is the best model predictive control strategy for on-line building energy management systems that combines solar shading with passive ventilation in order to maximize performance in terms of passive fraction of energy while maintaining indoor thermal comfort?"

This main question is divided into a number of sub-questions to formulate an answer to the research question. The concluding answers of the sub-questions are provided in the last chapter.

1. *In what way can a building be modeled such that the model has a high degree of accuracy but is not too computationally complex, so that it is suitable for model-based control?*

2. *How does the developed building model perform compared to the thermal progressions in a real-case building?*

3. *In what way can an on-line applicable model predictive control strategy be developed such that it optimally combines the control of the two passive energy sources?*

4. *How does the developed model predictive control strategy optimally combines passive and active energy sources, while maintaining thermal comfort? Is it then possible to reduce the energy consumption of such a building compared to a real-case rule-based controller?*

1-4 Report outline

The structure of the remainder of this thesis report is as follows. First of all, Chapter 2 provides a literature review on the state-of-the-art techniques and research in the field of sustainable energy management of office buildings. Chapter 3 discusses the applied modeling techniques and, subsequently, proposes some promising control strategies for this MSc thesis project. Then, in Chapter 4 a model validation is performed and the best-performing control strategy will be compared in a case study with a more conventional controller. Lastly, Chapter 5 concludes the MSc thesis and provides recommendations for future work.

Chapter 2

Literature Review: Sustainable Energy Management of Office Buildings

This chapter provides an overview of state-of-the-art techniques and research in sustainable energy management of office buildings. First of all, Section 2-1 presents all relevant dynamical laws and models, found in the literature, to describe the energy-flow behavior in buildings. Subsequently, Section 2-2 introduces the three modeling paradigms and illustrates their application for building modeling. Hereafter, Section 2-3 describes the applications of MPC for indoor climate control. Lastly, Section 2-4 provides the conclusions about the literature.

2-1 Fundamentals of building energy dynamics

From a research point of view, it is crucial to follow the fundamentals of thermal energy-flow behavior in buildings. These fundamentals are expressed mathematically in proven dynamic equations and studied correlations. Such expressions often consider assumptions that may deteriorate the model accuracy. This section provides the main equations and assumptions, commonly considered in studies and books on thermodynamic system modeling [3, 41, 33].

2-1-1 Thermal transient behavior

In a building, thermal energy can be generated by heat sources, stored in building components, and transferred among those components or to the environment. Such components represent building exterior and interior masses or indoor air-filled zones and are able to store thermal energy in their mass by absorption according to the conservation law. When heat energy, Q, is considered and work, W, is omitted, the conservation law can be described as:

$$\Delta U = Q + \cancel{W} = \rho V c_{\mathrm{p}} \Delta T \tag{2-1}$$

where ΔU denotes the changes of internal mass energy and ΔT the thermal difference of the mass. The density ρ, volume V, and the constant-pressure specific heat c_{p} of the considered

mass determine how much energy can be absorbed before the temperature of the mass reaches the surrounding temperature. In practice, all masses in a system absorb or reject energy at non-uniformly rates, which leads to complex thermodynamics. This is simplified by only considering heavy masses, e.g., walls, ceiling, and floor, assuming the absorption and rejection to evolve uniformly per mass, and assuming that a component is made of one mass type. However, the change of energy in a component over time is described by the derivative of ΔU. This derivative describes the continuous energy gain rate of a component in three dimensions and is generally expressed as:

$$\rho V c_{\mathrm{p}} \frac{dT}{dt} = \dot{Q}_{\mathrm{gen}} + \dot{Q}_{\mathrm{vent}} + \dot{Q}_{\mathrm{in}} - \dot{Q}_{\mathrm{out}} \tag{2-2}$$

A component's stored energy gain rate depends on the internally generated $\dot{Q}_{\mathrm{gen}}$, ventilated $\dot{Q}_{\mathrm{vent}}$, absorbed $\dot{Q}_{\mathrm{in}}$, and transferred $\dot{Q}_{\mathrm{out}}$ energy gain rates. The component's characteristics determine in what amount the four gain rates affect the component's gain rate. For instance, exterior components absorb energy from solar irradiance and an air-filled zone is often affected by heat generation due to, e.g., HVAC systems. The energy gain rate types will be discussed in more detail by four different modes. The first three modes are members of the transferred energy gain rate, $\dot{Q}_{\mathrm{out}}$, as is presented in the equation below. The gain rates due to internal generation, ventilation, and absorption are addressed in the last mode.

$$\dot{Q}_{\mathrm{out}} = \dot{Q}_{\mathrm{cond}} + \dot{Q}_{\mathrm{conv}} + \dot{Q}_{\mathrm{rad}} \tag{2-3}$$

Conduction

The primary mode of heat transfer is derived from Fourier's law of thermal conduction. This three dimensional law is applied when temperature differences occur in or between static objects. For example, this mode occurs when insulation material is integrated between two building envelope components. The one-directional conductive heat gain rate is described as:

$$\dot{Q}_{\mathrm{cond}} = \kappa A_{\vec{x}} \frac{\partial T}{\partial \vec{x}} \tag{2-4}$$

where κ denotes the thermal conductivity of the solid in which energy transfers and $A_{\vec{x}}$ refers to the area perpendicular to the transfer direction $\vec{x}$ of energy. ∂T and $\partial \vec{x}$ are the partial derivatives of temperature and distance over the direction's length of the transferred energy.

Convection

When heat transfer occurs between a solid and a non-solid, the convection mode is required. Strictly speaking, this mode is derived from the conduction and radiation modes, because fluid or gas that is close to the surface is stationary. However, it is commonly accepted to consider convection more broadly when heat transfer occurs from a surface to a moving fluid or gas. Convective heat transfer follows out of Newton's law of cooling, formulated here as:

$$\dot{Q}_{\mathrm{conv}} = \overline{h} A_{\vec{x}} (T_{\mathrm{s}} - T_{\mathrm{M}}) \tag{2-5}$$

where $\overline{h}$ is the average heat transfer coefficient for an isothermal surface area $A_{\vec{x}}$. T_{s} and T_{M} denote the temperatures of the surface and adjacent medium, respectively. In thermodynamic

models for building components, equation 2-5 is considered for situations where heat transfer occurs between ambient air and external masses, in cavities between external and internal masses, and between internal masses and indoor zones. However, the heat transfer coefficient term $\overline{h}$ is challenging to acquire. According to Obyn et al. in [44], $\overline{h}$ is experimentally computable when the convective heat flux density and temperatures of the surface and adjacent medium are known. However, since this heat flux density is often the desired parameter, $\overline{h}$ is estimated as a function of the dimensionless Nusselt number as:

$$\overline{h} = \frac{\lambda \frac{dT}{d\vec{x}}|\vec{x}=0}{T_{\mathrm{s}} - T_{\mathrm{M}}} \approx \frac{Nu\lambda}{l} \tag{2-6}$$

where λ denotes the thermal conductivity of a fluid or gas and together with the distance derivative of the temperature difference, it forms the convective heat flux density. In addition, l represents the characteristic length in the moving direction of the air, and Nu is the Nusselt number which applies for the air moving direction along characteristic length l.

The Nusselt number has therefore a crucial role, but there is no general expression to calculate this number. Obyn et al. reviewed around 90 different convection coefficient correlations out of more than 25 sources. These correlations were specifically considered for models for vertical and horizon surfaces in buildings. Obyn et al. classified them in [44] into four categories:

- Constant value, Nu is kept constant over the whole working space or differ per separated working spaces, defined by if-statements and suitable for linearized models.
- Function of temperature difference, Nu depends on temperature differences described through Prandtl or Rayleigh numbers. These functions assume the airflow to be laminar.
- Function of airflow, Nu depends on airflow described through Reynolds numbers or Air Change per Hour values. These functions assume the airflow to be turbulent.
- Mixed functions, Nu depends on both the temperature difference and airflow. These functions assume the airflow to be partly laminar and partly turbulent.

Prandtl, Rayleigh, and Reynolds numbers are, like the Nusselt number, dimensionless values, which describe the behavior of the flow. Prandtl and Rayleigh numbers illustrate the buoyancy-driven flow, also known as natural convection, and Reynolds numbers help to predict the flow patterns within turbulent flow. How the numbers distinguish laminar and turbulent flows depend on the geometry of the surface. In the case of a vertical wall, laminar flow can be considered when Rayleigh is less than 10^9. When Rayleigh is between the 10^9 and 10^{12}, the flow regime will show laminar and turbulent characteristics. For even higher Rayleigh numbers, full turbulent flow is assumed. For horizontal surfaces, other Rayleigh numbers determine the boundary between laminar and turbulent flow. In this case, the facing direction of the heated horizontal plate also affects the convective behavior. Namely, because heated fluids or gas rise, resulting in different flow characteristics in the vertical direction. Therefore, a distinction of correlations is made between heated plates facing upwards or downwards.

Radiation

The third mode of heat transfer is thermal radiation: the energy transport of electromagnetic waves or photons from one object to another. The radiant exchange between two surfaces is provided by the Stefan-Boltzmann law and becomes significant when the temperature

difference between the surfaces is large [3]. Building components are able to radiate energy among them or reject it to the environment. The Stefan-Boltzmann law is formulated as:

$$\dot{Q}_{rad} = \mathcal{F}_{12}\sigma A_{\vec{x},1}(T_1^4 - T_2^4) \tag{2-7}$$

where $A_{\vec{x},1}$ refers to the area of a considered surface with temperature T_1, which interacts with another surface with temperature T_2. The radiation transfer factor $\mathcal{F}_{12}$ determines the extent to which the two areas interact. This factor depends on the geometric proportions between the surfaces and whether or not they are black- or grey-body objects. For grey-body objects, the surface emissivity percentage term ϵ is adopted by $\mathcal{F}_{12}$. ϵ is different for each material. Many radiant transfer factors are described by Ref. [41], both for black- and grey-body objects. The σ term is the Stefan-Boltzmann constant, which makes the 4th-order of the black-body surface temperature linear proportional to the radiant heat transfer rate.

In case of no clear second surface, e.g., the interaction between the environment and the building exterior masses, $\mathcal{F}_{12}$ is equated with the surface emissivity ϵ of the component. In addition, the sky temperature should be considered as the temperature of the environment. According to Albatayneh et al. in [7], the ISO 13790 standard allows the sky temperature to be simply determined by means of subtracting the ambient temperature with a constant value. This value depends on the considered climate. For instance, 9, 11, and 13 are used for the sub-polar, temperate, and tropical climates, respectively.

Internal heat generation, absorption, and ventilation

Internal generation, absorption, and ventilation of energy in building components is caused by two types of sources, active and passive. Active energy sources affect the component's heat energy by using auxiliary energy. Examples of these sources are heaters, ventilation, and air-conditioning, i.e., HVAC systems. The amount of auxiliary energy used to equally affect the temperature of a specific component over an equal period of time differs per system based on its dynamics and efficiency. However, the shared advantage of HVAC systems is that they are fully controllable.

Passive energy sources do not use auxiliary energy to affect a component's temperature and some of these sources are uncontrollable, e.g., electronic devices and occupancy. Heat generation by modern electronic devices has decreased drastically in contrast to their older versions. Due to the reduced heat generation and the complexity of including them in a building model, these heat sources are often disregarded in research. However, occupants can affect the component's temperature significantly and are often considered in models. According to Ahmed et al. in [6], ISO standards indicate that the metabolic heat gain per person varies from 100 to 500 W, depending on the degree of activity. For light to standard office work, this is between 100 and 130 W. Occupancy can be scheduled or predicted by means of algorithms, such as Markov chain and Artificial Neural Networks (ANN) [20].

Some initially uncontrollable passive sources become controllable by using certain actuators. Major examples are solar irradiance, natural ventilation, and additional thermal mass:

Solar irradiance is the energy per unit area in the form of electromagnetic radiation. It is received from the Sun and absorbed by the building components. Exterior solar blinds are applied to control the incoming solar irradiance through the windows. The modeling method of this energy source is discussed further in detail in Section 2-1-2.

Natural ventilation of air is caused by pressure differences between interior and exterior air. The indoor zone temperature is altered due to airflow between the indoor zone and the environment, which is partly wind-driven and partly buoyancy-driven. Automated operational windows can be used to control this phenomenon, but wind-driven pressure differences are hard to predict and buoyancy forces tend to go upwards. Therefore, operational windows are not the optimal actuators to control natural ventilation. The state-of-the-art technique for controlling natural ventilation is developed by Bronsema et al. He proposed a concept of a thermal chimney, designed to optimize the buoyancy-driven airflow in a building [17]. The modeling method of this energy source is discussed further in detail in Section 2-1-3.

Additional thermal mass is used to store or release heat energy when there is a surplus or shortage of energy. Phase change materials are salines that have a relatively high thermal mass and can therefore store large amounts of energy [53]. By integrating a smart ventilation system that can choose to use or surpass this additional thermal mass, ventilated air can be heated or cooled passively. Due to the limited time period for the study, this research does not consider phase change materials, regardless of their high performance potential. Therefore, PCM will only be discussed in the thesis' recommendations.

2-1-2 Solar irradiance

The modeling of solar irradiance is challenging. This kind of radiation constantly changes due to multiple types of variables, e.g., the Sun's position and intensity and the building's location and geometries. The amount of energy absorbed by the components depends on the component's dimensions and mass properties. Ref. [30] suggests the correlation between the solar irradiance and the absorptive heat energy by a component is as:

$$\dot{Q}_{\text{in}} = I_{\text{o}} A \xi^n \alpha \tag{2-8}$$

The absorbed energy gain rate $\dot{Q}_{\text{in}}$ depends on the oriented incidence of solar irradiation per unit area I_{o}, the effective optical transparency ξ, and the mass' absorptance α. The ξ and α terms variate for each component, depending on the mass type, the transmittance rate of each glazing, and the number of glazings in series before the considered component, n. In addition, the oriented incidence I_{o} basically consists of three terms: direct beam, reflected, and diffused radiation, as is presented below. The basics of the three terms are discussed further in this section. In addition, Appendix A can be consulted for the full mathematical models of the oriented irradiance values and the two optical properties.

$$I_{\text{o}} = I_{\text{o,b}} + I_{\text{o,r}} + I_{\text{o,d}} \tag{2-9}$$

Direct beam radiation

The oriented direct beam radiation $I_{\text{o,b}}$ is the received portion of the direct beam radiation on an object's surface. Irradiance sensors are able to measure two types of direct beam radiation, one which is perpendicular to the Earth's horizon I_{bh} and one which is perpendicular to a tracking surface I_{bn}. I_{bh} is measured by fixed upwards-facing sensors, but modern sensors obtain I_{bn} values by rotating along with the Sun's position in the sky. According to Ref. [32, 48], the angle between the object's surface normal and the solar beam direction θ_{n}, and

the zenith angle θ_z can both be applied in following expressions to obtain the oriented beam radiation:

$$I_{o,b} = I_{bh}\frac{\cos(\theta_n)}{\cos(\theta_z)} = I_{bn}\cos(\theta_n) \tag{2-10}$$

Reflected radiation

The oriented reflected radiation $I_{o,r}$ is the received portion of horizontal solar radiation that is reflected by the surrounding Earth surface. This includes circumjacent objects such as buildings and trees. The horizontal solar radiation is determinable via the direct beam radiation that is perpendicular to the horizon I_{bh} and the diffused radiation I_d which is measurable by irradiation sensors. Assuming a total isotropic reflection and a surrounding diffuse reflectance of ρ_r for all irradiance, a commonly used expression for $I_{o,r}$ is according to Ref. [32, 48]:

$$I_{o,r} = (I_d + I_{bh})\rho_r\frac{1-\cos(\beta)}{2} \tag{2-11}$$

where β denotes the angle between the tilted surface and the horizon. The albedo value ρ_r depends on the type of surrounding ground. Common albedo values are 0.2 for humid climates, 0.5 for dry climates and 0.9 for snow covered ground [48].

Diffused radiation

The oriented diffused radiation $I_{o,d}$ is the received portion of the solar radiation that has changed direction due to atmospheric scattering. The amount of scattering depends on less predictable conditions, such as cloudiness and atmospheric clearness, and is therefore hard to model. The $I_{o,d}$ value consists of three radiation-type terms and can be described as:

$$I_{o,d} = I_{d,iso}\frac{1+\cos(\beta)}{2} + I_{d,cir}\frac{\cos(\theta_n)}{\cos(\theta_z)} + I_{d,hor}F_{c\text{-}hor} \tag{2-12}$$

Isotropic diffuse radiation $I_{d,iso}$ is received uniformly from the sky, circumsolar radiation $I_{d,cir}$ refers to the onward dispersion of irradiance and comes from the sky section surrounding the Sun, and horizon brightening radiation $I_{d,hor}$ is concentrated around the horizon and depends on the sky's clearness. Models that only consider $I_{d,iso}$ are called isotropic models. In addition, more complex models that consider all terms are called anisotropic models.

The $I_{d,iso}$, $I_{d,cir}$, and $I_{d,hor}$ are not separately determinable by sensors, but they are elements of the measurable I_d value, which makes it difficult to calculate $I_{o,d}$. Hence, a great number of models for the modeling of I_o have been developed by numerous research studies. Most models generally agree on the mathematical expressions for $I_{o,b}$ and $I_{o,r}$, but differ on the $I_{o,d}$ term. Simón-Martín et al. performed an extensive review and experimental comparison among 30 models in [23], considering different surface directions and sky conditions. The study conducted a statistical analysis on them using the root mean squared error (RMSE) and the coefficient of determination (R^2). A brief comparison between the good performing and more acknowledged models from that study is given in Table 2-1. The superior model in this study is the ANN-type Multi-Layer Perceptron model, trained on local data. In addition, the anisotropic models outperformed the isotropic models due to their increased complexity.

Model Name	Model Type	Complexity	Local Data Needed	Performance rate: 1 to 7	
				RMSE	R^2
Liu & Jordan [38]	Isotropic	Simple	-	7	6
Koronakis [37]	Isotropic	Simple	-	6	7
Hay & Davies [31]	Anisotropic	Simple	-	5	5
Muneer [42]	Anisotropic	Moderate	-	3	4
Perez [46]	Anisotropic	Moderate	-	4	3
Perez opt. [46, 23]	Anisotropic	Complex	✓	2	2
MLP [23]	ANN	Complex	✓	1	1

Table 2-1: Comparison of 7 models for oriented diffused radiation [23].

Especially the Perez models and the Muneer model are promising. However, locally obtained training data is required by the Perez optimized model, so this model and the ANN-type models are not applicable for this thesis, as such training data is not available. Research studies by Toledo et al. [49] and Loutzenhiser et al. [40] also compared the Muneer and Perez models, both concluding that the Perez model is slightly better under most sky conditions. Therefore, the Perez model was chosen for the remainder of the thesis.

2-1-3 Natural ventilation

The control of the indoor zone temperature by ventilation is based on thermal advection. Advection is known as the transport of a substance by motion to an area and affecting that area with its properties. In the case of thermal advection, the considered property is thermal energy. Therefore, the energy gain rate by ventilation in an air-filled zone, assuming constant air pressure and uniformly mixed airflows, can be expressed as:

$$\dot{Q}_{\text{vent}} = \dot{m} c_{\text{p,air}} \Delta T \tag{2-13}$$

where $\dot{m}$ refers to the air mass flow rate, $c_{\text{p,air}}$ the heat capacity of air under constant pressure, and ΔT the air temperature difference between the ventilation output and the zone. The ventilated air in active systems is actively heated or cooled and the mass flow rate is driven by fans. Passive systems use unmodified ambient air to alter the indoor climate and the mass flow rate is driven by natural ventilation forces, such as wind and buoyancy. As mentioned before, the ventilation system of interest is the thermal chimney, which is based on the concept of buoyancy forces. Therefore, wind-driven natural ventilation will not be discussed further. However, two models for mass flow behavior due to buoyancy forces are elaborated below.

Computational fluid dynamics

CFD models are numerical methods that can compute the mass flow behavior based on laws of fluid dynamics and the Navier-Stokes equations, the conservation of mass and momentum:

$$\nabla \cdot \mathbf{v} = 0 \tag{2-14}$$

$$\rho \frac{D\mathbf{v}}{Dt} = -\nabla P + \mu \nabla^2 \mathbf{v} + \rho \mathbf{g} \tag{2-15}$$

Equation 2-14 describes that the air mass difference between the in- and outlet of a system is equal to zero. In equation 2-15, the mass flow behavior is calculated. The left-hand side represents the rate of accumulation of momentum within the control volume of the fluid or gas in a directional vector. The right-hand side combines the terms: all directional differential pressures, all directional viscosity stresses, and external volume forces, to describe the flow direction and speed. Furthermore, CFD model methods, such as finite volume, element, and difference methods, solve the Navier-Stokes equations on fine element grids, resulting in highly accurate results and heavy computational loads. Therefore, CFD models are suitable for model validation and fault detection, but not for model-based control.

Andersen's fully mixed model

The actual mass flow is calculated by determining the velocity vector of the flow through the momentum conservation equation and selecting the flow's perpendicular facing area $A_{\vec{x}}$:

$$\dot{m} = \rho \mathbf{v} A_{\vec{x}} \tag{2-16}$$

When uniform indoor temperature is assumed in a single-zone with two openings, the fully mixed model of Andersen et al. [8] can be applied to model the mass flow behavior due to buoyancy forces in that zone. This model is derived from equation 2-16 and made suitable for a thermal chimney. Andersen's model is expressed as:

$$\dot{m} = C_{\mathrm{d}} \rho A^* \sqrt{2gH \frac{|T_{\mathrm{in}} - T_{\mathrm{out}}|}{T_{\mathrm{out}}}} \tag{2-17}$$

where C_{d} is the coefficient for discharge and friction, g the gravitation force, H the height difference between the two openings, and T_{in} and T_{out} refer to the in- and outdoor temperatures, respectively. In addition, the effective opening area A^* depends on the areas of the two openings. In practice, C_{d} is within the range of 0.5 and 0.7, but is still hard to determine accurately by hand. CFD models can help to estimate this value more precisely.

2-2 Building modeling approaches

For most studies, an accurate model of a building's energy-flow behavior is essential for their research topics. These models can be used for, e.g., energy demand analyses, construction optimization, fault detection, and model-based control [5]. The energy-flow behavior is mainly affected by five factors according to Boodi et al. in [15]:

1. Building dimensional, physical, and thermal properties;
2. Occupancy behavior and interaction with the building;
3. Indoor population size;
4. Building location and surroundings;
5. Climate conditions, such as ambient temperature, wind speed, solar irradiance, etc.;

The model's accuracy depends on the number of factors modeled and how detailed they are expressed in the model. Many modeling approaches are available to model these factors.

These approaches can be divided into three modeling paradigms: white-box, black-box, and grey-box. Each paradigm has its advantages and disadvantages with regard to modeling the factors. Hence, they are extensively researched in the literature on building modeling. In these studies, the models obtained are often validated on experimental or simulated building data by means of various validation methods. The three paradigms and validation methods relevant to this thesis are discussed below.

2-2-1 White-box: Software tool utilization

White-box models represent the building's thermal dynamic structure by using fundamental laws of physics, thermodynamics, and heat transfer in a set of mathematical expressions which can be derived and solved. These models can be of the distributed parameter type, meaning that the model is infinitely dimensional due to the lack of specific assumptions. However, assumptions, such as uniform heating in system components, are frequently assumed to make the model finite-dimensional, i.e., a lumped parameter type model [5]. In addition, accurate white-box models of buildings are initially nonlinear and continuous, but discretizing and linearizing techniques help to simplify the model. Nevertheless, the construction of accurate white-box models requires expert knowledge of the fundamental laws, building properties and location, and occupancy behavior. The model's accuracy also increases with full knowledge of system disturbances, such as ambient climate conditions and amount of occupants. This requires information which is not always accurate or available, making white-box modeling a complex and time-consuming approach. Hence, numerous software tools have been developed for building dynamics evaluation and energy demand analysis. These building energy simulation (BES) tools, often approved by the US Department of Energy, aim to make white-box modeling more affordable and reliable.

BES tools, such as EnergyPlus [21], TRNSYS [11], and ESP-r [57], are specialized in applying correct fundamental laws of thermodynamics for user-chosen building components and actuators. In addition, they employ optimized integrated solvers, resulting in a relatively fast simulation execution when the building's energy demand is calculated. The disadvantage is that these programs have difficulty supporting other use cases, such as exporting model information, modeling controllers, or reformulating equations into optimal control problems. To overcome these obstacles, co-simulation software, such as BCVTB [55] and MLE+ [13], is developed. This software couples white-box models in, e.g., EnergyPlus with control techniques written in dynamic computational software, such as MATLAB or Modelica [56], into a co-simulating scheme. However, Drgoňa et al. suggest in [25] that such schemes have shown to become computationally expensive due to communication lags between the software programs. Therefore, white-box modeling by BES tools is particularly suitable for building energy demand analysis, construction optimization, and fault detection. However, when research is focused on the assessment of controllers employed on white-box models, it may be preferable to create these models directly in MATLAB or Modelica, especially when the considered building is relatively less complex.

2-2-2 Black-box: Statistical models and training data

Black-box models are developed based on statistical models by quantifying historical data parameters to find optimal correlation patterns between controllable and disturbance input

data and building performance output data [15]. Therefore, no knowledge of the building's thermodynamic structure is required. This modeling approach is considered to be relatively less complex, highly accurate, and computationally inexpensive. The disadvantage is that the inner model process is mostly unknown. This leads to a reduction in control flexibility, system understanding, and model scalability. Black-box modeling requires large amounts of pre-collected, quality training data. If the training data is of low quality or not of a wide range, huge prediction errors can occur. Data can be collected by three sources:

- Real data collection from living buildings through sensors;
- Simulated data collection from BES tools; e.g., EnergyPlus and TRNSYS.
- Standard data sets available in public benchmark libraries, e.g., ASHRAE;

Lots of statistical models have been considered in the literature of building modeling. These black-box models have shown to be more suitable for building energy demand prediction and model-based control than for fault detection due to the lack of knowledge of the inner model process [15]. The models can be categorized into parametric linear models (Auto-Regressive with Moving-Average and eXogenous inputs, Subspace-based State-Space System Identification), parametric nonlinear models (Nonlinear Auto-Regressive Moving-Average with eXogenous inputs, ANN), and nonparametric nonlinear models (k-Nearest Neighbors, Support Vector Machines (SVM), Random Forest) [25]. The choice of a statistical model is based on the studied research question and preference for high accuracy or low computation load, which are often conflicting objectives.

2-2-3 Grey-box: RC-network application

Grey-box modeling is a hybrid approach, combining the physics-based structure from white-box models and the data-driven parameter estimation of the black-box modeling approach. Usually, in grey-box models, the physical structure is simplified through state-space dimensionality reduction or linearization. For building modeling, simplified models are able to maintain a similar accuracy level due to parameter estimation [47]. The RC network analogy is a typically used concept structure for a grey-box model. The resistor parameter represents the thermal resistance of energy flow between building components which is, in practice, caused by conduction and convection. The capacitance parameter symbolizes the capacity to store thermal energy in building components. The RC network is a linear network that is easily scalable by considering more building components. For example, an Interior-Ambient model that considers the building as one component can be described by a 1R1C network, but a model that distinguishes between indoor air, interior and external components, and ambient air requires, e.g., a 4R2C or 8R3C network [5].

The data to optimize model parameters can be obtained by the same sources as for the black-box modeling approach. However, the advantage over black-box is that less data is needed to optimize the grey-box parameters, as too much training data easily causes overfitted parameters. In addition, RC-networks are linearized models of the, in practice, nonlinear building system, and these estimable linearized parameters have the potential to capture the working range around the nonlinearities more accurately than white-box linearization techniques. As Picard et al. show in [47], the accuracy can remain high while the model's order is reduced, resulting in lower computational costs as opposed to white-box modeling.

Therefore, grey-box is suitable for building energy demand prediction, model-based control, and fault detection research due to the included detailed building structures in the models.

2-2-4 Numerical validation methods

Many numerical validation methods are available to validate a developed model. In this thesis, two of them will be considered. The first technique is the Variance Accounted For (VAF), useful to assess the predictive behavior capabilities of a model. The VAF takes the variance of the difference between the model output, $\hat{y}$, and the validation data, y, and divides this by the variance of the validation data to obtain the model's goodness of fit percentage. The VAF method is expressed as:

$$\text{VAF} = (1 - \frac{var(y - \hat{y})}{var(y)}) * 100\% \tag{2-18}$$

However, VAF only assesses the model's behavior and not the actual error between the two data sets [51]. For instance, two data sets that exhibit the same behavior, but differ by a constant error, still hold a VAF of 100%. That is why it is interesting to also evaluate the models on the basis of the root-mean-square error (RMSE). This method calculates the error between the two data sets and forces the larger errors to have a disproportionately greater effect on the RMSE value. This method indicates the accuracy of the model better than calculating the absolute mean error alone. However, RMSE is less useful for comparing multiple models under different conditions. Therefore, a normalized extension is added to obtain the NRMSE by dividing the RMSE by the value range of the data set, as is shown below. Finally, the higher the VAF and the lower the NRMSE, the better the validation fit of the model.

$$\text{RMSE} = \sqrt{\frac{1}{N}\sum_{i=1}^{N}(y(i) - \hat{y}(i))^2} \tag{2-19}$$

$$\text{NRMSE} = \frac{\text{RMSE}}{y_{max} - y_{min}} \tag{2-20}$$

2-3 MPC for indoor climate control

Nowadays, several types of building energy management systems (BEMS) are used to control the indoor climate in commercial buildings around the world. Those BEMS mainly contain simple rule-based and PID controllers. However, the extensive literature overview of Drgoňa et al. implies that the more advanced MPC strategy has become dominant in the literature on intelligent BEMS [25]. This section provides an overview of the relevant research on MPC for BEMS. For a more general description of MPC, the reader is referred to Appendix B.

2-3-1 Performance feasibility of MPC

An MPC controller is able to make control decisions that benefit the long-term performance of a system by considering future situations. This is an advantage over the less advanced

controllers which only consider current situations. MPC is well suited for indoor climate control, due to the building's ability to store thermal energy in its mass and the constantly changing future in- and outdoor conditions that are often predictable. MPC controllers use prediction models to anticipate on the building characteristics and future conditions by optimizing feasible control signals such that the building's thermal energy response for the receding horizon is enhanced. In theory, a prediction model consists of a horizon length of accumulation of successive models. Each model contains the dynamics, weather conditions, and disturbances for each single horizon step. The previously discussed modeling approaches can be adopted for such a prediction model. For instance, white- and grey-box based MPC are commonly used in the literature, but ANN and SVM-based MPC have also been considered.

An MPC controller calculates the control signals for a system through optimization. Such MPC optimizations are subjected to an objective function in which the priorities for one or more objectives are mathematically expressed. However, the feasibility of the optimization is often limited by model and actuator constraints. Such objective functions, constraints, and prediction models determine the complexity of the optimization problem, often creating a trade-off between the control performance and computation time. Hence, the problem complexity is highly dependent on the MPC type. In this thesis, the linear and nonlinear MPC types are studied and therefore elaborated further below.

Linear MPC

Theory speaks of linear MPC when the constraints and prediction model are both linear and a linear or quadratic objective function is applied [25]. The main advantage of linear MPC is that the accumulation of successive models, for linear time-invariant and linear parameter-varying models, can be done simply by recursive substitution of sequential state variables into large prediction matrices. The prediction matrices can then be substituted in an objective function to form the Hessian matrix. The Hessian matrix must be positive semi-definite or definite for the optimization problem to be convex. In this case, solvers, such as MATLAB functions *linprog* and *quadprog*, are able to determine the best solution by finding the minimum of the optimization problem that is guaranteed to be global and satisfies all constraints included. Linear MPC for buildings is suitable for on-line application due to the low computational costs, even for large-scale building models. However, the required models are linearized expressions of reality, making these models less accurate in contrast to nonlinear models.

Nonlinear MPC

Nonlinear MPC emerges when either the objective function, prediction model, or constraints is nonlinear [25]. As mentioned previously, some thermodynamics are nonlinear, e.g., convection and radiation, and therefore research studies often use nonlinear thermodynamics for accurate building modeling. The optimization problem is then formed by a nonlinear function that contains all successive dynamics for the full horizon length and an objective function. In this case, the optimization problem is not convex, which means that multiple local minima arise. The solver can therefore no longer guarantee that the solution found is the global minimum of the problem. However, there are solvers and solver algorithms designed to handle this problem. For example, MATLAB function *fmincon* is able to search through multiple local

minima around predetermined initial guess values to find the best solution that satisfies the set of constraints and algorithm tolerance thresholds. When a discovered local minimum satisfies the constraints, but does not meet these tolerance thresholds, new local minima will be analyzed until the thresholds are met or the maximum of solver iterations has been passed. The solver algorithms take care of how the search is executed. Some major algorithms are:

- Interior-point, able to solve both linear and nonlinear problems;
- Sequential quadratic programming (SQP), able to solve constraint nonlinear problems;
- Active-set, similar to SQP but takes larger steps and therefore is faster but less accurate;

Note that the choice of initial guess affects the optimization, as the search is done in the guess' neighborhood. To broaden the search and enhance the global solution approximation, solver methods can be used such as multi-start local optimization in which multiple initial guesses are examined sequentially during optimization, and genetic algorithms in which multiple search spaces are searched simultaneously. However, these methods are computationally heavy.

2-3-2 Control architectures

In the literature on BEMS, multiple control architectures have been considered. It has been shown that the right choice of architecture benefits both performance and computational costs of the overall problem. The architectures are divided into four structures which are discussed below.

Centralized MPC structures are the most considered architectures in theoretical and simulation-based research and often serve as benchmark for assessing other control architectures [25]. Note that centralized MPC has the potential to be the best performing structure as the agent controls the whole system. However, this comes with the expense of large computational costs, especially for nonlinear multi-zone building prediction models with large horizons. Therefore, few truly centralized MPC architectures are used for practical applications. Jorissen et al. presented in [34] an implementation strategy of a centralized linear MPC structure for a 27-zoned office building. The MPC structure replaced a rule-based controller for controlling the HVAC system, but a performance comparison was not carried out.

Decentralized MPC structures ease the computational costs by splitting the system into smaller subsystems and controlling them separately. The reliability of the overall system is high, since other subsystems are not affected when one agent fails. This is advantageous over all other architectures. However, the system's performance decreases, because no communication among agents is mathematically expressed in the structure. According to Afram et al. in [4], inefficient temperature differences might arise among zones by regulating different reference temperature setpoints for HVAC systems in adjacent zones. This results in poor control decisions.

Distributed MPC structures are based on the same principle as decentralized control, but differ in that the distributed agents do communicate with each other. Therefore, the agents can decide together the further course of action by sharing minimum amounts of information. This results in higher control performance at the expense of little increased computational loads. According to Drgoňa et al. in [25], the distributed structure is the most promising single-level control structure for HVAC systems in living multi-zone buildings.

Hierarchical MPC structures are multi-level control structures where the upper-layer agent controller manages one or more lower-layer slave controllers. This is suitable for subsystems that can be optimized for different timescales. This eases the computational load without much performance degradation compared to centralized cases [25]. The slave controllers can control the temperature for each zone individually and the agent coordinates potential conflicts for local decisions. Furthermore, Kim et al. in [35] and Long et al. in [39] optimized their office building models for different timescales to determine the reference trajectory by the agent controller and to track this reference by the slave controllers for controlling the HVAC systems. Their prediction models were linear and they both used one actuator type per considered zone.

2-3-3 Design and optimization of control objectives

The objective function is a mathematical expression of the main target of an optimization problem. The convergence towards this target is achieved by minimizing such objective functions. For BEMS, such targets can be reference temperature tracking to enhance occupant comfort levels, energy demand minimization, or economical cost minimization. The literature speaks of multi-objective optimization when multiple targets are set in an objective function. In such cases, the targets often conflict and a trade-off must be found among them. In BEMS, this trade-off is often caused by the conflicting occupant discomfort and auxiliary energy terms. Namely because minimizing discomfort often comes at the expense of minimizing auxiliary energy. Common approaches for multi-objective optimization are the Pareto front construction, the weighted sum method, and the ϵ-constraint method [16]. However, before discussing these approaches, indoor comfort conditions for occupants should be defined.

The indoor comfort conditions are determined by three factors: thermal comfort, visual comfort, and Indoor Air Quality (IAQ) [24]. The thermal comfort in a zone depends on the occupant's sensation experience of temperature, humidity, and air currents. Due to the varying thermal sensation experiences among occupants, there are no feasible climate conditions that satisfy all occupants. However, the mean thermal comfort per zone can be determined by Fanger's PMV/PDD model [29]. This method is based on local surveys among occupants and is adopted by both the ASHRAE and ISO standards. Moreover, visual comfort refers to the level of illumination, measured in lux, and the level of direct glare of the Sun. In addition, the indoor air quality depends on the CO_2 concentration in the zone and other pollutants. The use of solar blinds and ventilation can be optimized when the control problem is focused on visual comfort and IAQ. However, for the sake of simplicity, only thermal comfort is taken into account in this thesis. By considering visual comfort and IAQ complex multi-objective optimization problems will emerge, which are not relevant for this thesis topic.

Pareto front

The Pareto front is formed by a set of trade-off solutions in which the improvement of one objective is at the expense of the other conflicting objective(s). The advantage of this constructed front is that it allows the user to easily observe all trade-off outcomes and choose the outcome according to his preference. In theory, this is well suited for non-convex optimization problems, where non-convex solutions in the Pareto front can be located and avoided. In

practice, however, the construction of the optimal front is very time-consuming and the shape of this front differs per time step due to changing building model conditions and disturbances. Therefore, employing such a method for each time step is not practical.

Weighed sum method

The weighted sum method is the scaling of a set of objectives to a single objective function by adding each objective which is pre-multiplied by a user-supplied weight. The weights are chosen in proportion to the relative importance of the objectives. This proportion of weights represents one point of the Pareto front and the computational cost is therefore relatively low. However, it is hard to set the weights to obtain a Pareto-optimal solution in a desired region of the Pareto front, without knowing the shape of the front. Especially for non-convex problems, the solution found is not guaranteed to be Pareto-optimal.

ϵ-constraint method

The ϵ-constraint method is to constrain one or more objectives, such that the resulting objective function consists of only one objective to be minimized. This is done by adding inequality constraints on the model's output to the optimization problem and omitting the objective term of the output. This is suitable for both convex and non-convex problems, but the constraint should be carefully selected, such that a feasible solution for the optimization problem still exists.

2-4 Conclusions

Smart building energy management systems are used to maintain high indoor comfort levels for occupants while minimizing the building's energy demand or economical costs. To achieve such goals, smart BEMS make optimal use of passive and active energy sources, such as natural ventilation, solar energy, and HVAC systems. To control these sources, different actuators are needed to prevent under- or overheating of the indoor temperature. A lot of research is currently being done on BEMS that optimize such control signals by means of model predictive control. MPC has the ability to predict future system conditions and to optimize the system control signals that benefit those future conditions while handling system constraints and uncertainties. For the predictions, this control scheme applies discretized models that, when validated, mathematically represent the real system. Therefore, the control performance increases as the model accuracy of such prediction models increases. For buildings, multiple modeling paradigms can be used to obtain an accurate model. Hence, grey- and black-box approaches are well-studied in this literature topic. Multiple fashions in those paradigms have been shown to be suitable for model-based control, as their models can be accurate while being relatively computational inexpensive. However, unlike white-box modeling, the grey- and black-box paradigms require training data from real systems, which is not always readily available.

White-box models of buildings and actuators are developed by means of thermodynamic laws and full intelligence of the system parameters. This method requires expert knowledge on

modeling thermal energy transfer modes, heat generation sources, and solar irradiance dynamics. Building energy simulation tools, such as EnergyPlus and TRNSYS, are available to make white-box modeling more accessible. However, those tools are less suitable to directly assess different controllers on their control performance. Therefore, building models for model-based control are preferred to be developed in MATLAB, regardless of the complex thermodynamics involved. In particular, convection coefficients and oriented solar irradiance values prove to be challenging to determine. Lots of research is conducted in developing accurate convection correlations. These correlations determine the Nusselt number by means of the Prandtl, Rayleigh, and Reynolds numbers. In addition, several complex algorithms have been developed that process solar irradiance for tilted surfaces. From these algorithms, research has shown that the Perez model is a justifiable choice. Furthermore, an actuator model is adopted to represent the thermal chimney, which is called Andersen's model. This model is a simplified derivation of the Navier-Stokes equations and denotes natural ventilation due to buoyancy forces.

In the literature on BEMS, extensive research is done into different facets of MPC. Such studies often focused on minimizing computational costs while maintaining control performance, as an MPC controller can easily become too computationally expensive and therefore impractical for on-line application. Optimization conditions, such as the number of variables to be optimized, the amount of conflicting objectives, and system complexity, determine the computational cost of the optimization problem. For instance, it is less complex for a linear MPC controller to find the globally optimal solution than for a nonlinear MPC controller. However, nonlinear MPC in BEMS tends to produce better control performance, as some building thermodynamics are initially nonlinear. In order to apply nonlinear MPC and still solve complex optimization problems within a reasonable time, research is conducted in different control architectures for BEMS. It has been found that such structures can divide the blanket problem into smaller sub-problems, which are solvable in less time. Especially for multi-zone buildings, authors proposed innovative MPC architectures, such as decentralized, distributed, and hierarchical MPC, to regulate the room temperatures of the different zones. In these studies, one controllable HVAC system type was usually considered. However, research into optimal control of multiple active and passive energy sources by one BEMS has not yet been extensively conducted. Future research could therefore result in an innovative MPC architecture, which benefits the available energy resources rather than the multiple zones in a building. Hence, the aim of this thesis will be to find such an architecture.

Chapter 3

Proposal of Control Systems

This chapter describes the determination methodology of the best-performing control system which has potential for on-line application. For this, different control architectures that contain MPC-type controllers are analyzed. To apply MPC and determine the best structure through simulation-based analysis, prediction and plant models of the building's thermal transient behavior are required. Therefore, Section 3-1 presents modeling techniques to develop three model types. Section 3-2 provides the establishment and assessment of five distinct control architectures to determine the best-performing structure. In Section 3-3, multi-objective optimization in relation to this structure is discussed and the final control system for the case study is proposed. Lastly, the chapter's conclusions are given in Section 3-4.

3-1 Thermal system modeling

There are many possibilities in the construction and orientation of buildings, resulting in many different thermal response cases. For each case, a new building model is required to capture the building's thermal response as accurately as possible. The Co-Creation Centre, located at the Green Village and hereinafter referred to as CCC-building, serves as support for this thesis as the developed model is based on this building. The initial plan was to measure data of the CCC-building and apply grey-box modeling strategies. However, due to COVID-19, there was a delay in the sensor installation procedure by several months. This made both grey- and black-box modeling no longer optional, considering the thesis' time limit. Instead, three white-box models of the CCC-building are proposed:

- Nonlinear plant model, to accurately approximate the building's thermal response;
- Simplified nonlinear model, to lower computational costs compared to the plant model;
- Linear model, to approximate the thermal response loosely using linearized expressions;

In the models, the main components of the CCC-building are resembled by dynamical discreet expressions. The geometry and material types of the components are derived from the architectural drawings. The mass, thermal, and optical properties of all materials are obtained from the material database GRANTA EduPack [9] and presented in Table 3-2.

3-1-1 System configuration

Figure 3-1 illustrates the single-zoned CCC-building. No additional thermal coupling with other zones is considered. Hence, the model is relative simple as it only contains a roof, ceiling, raised and basement floor, four triple-glazed walls, and an inner zone. These components are affected by 7 disturbances, i.e., ambient and ground temperature (T_{a}, T_{g}), air pressure (p_{air}), ambient wind speed (v_{a}), oriented solar irradiance (I_{o}, $I_{\mathrm{o,b}}$, $I_{\mathrm{o,r}}$, $I_{\mathrm{o,d}}$), oriented optical properties (α_{o}, ξ_{o}), unshaded floor area (A_{u}), and occupancy (N_{occ}), and their temperatures are denoted by model states. Moreover, expressions that are generally applied in this work are shown in Table 3-1. Note that for convection the adjacent medium is denoted by M.

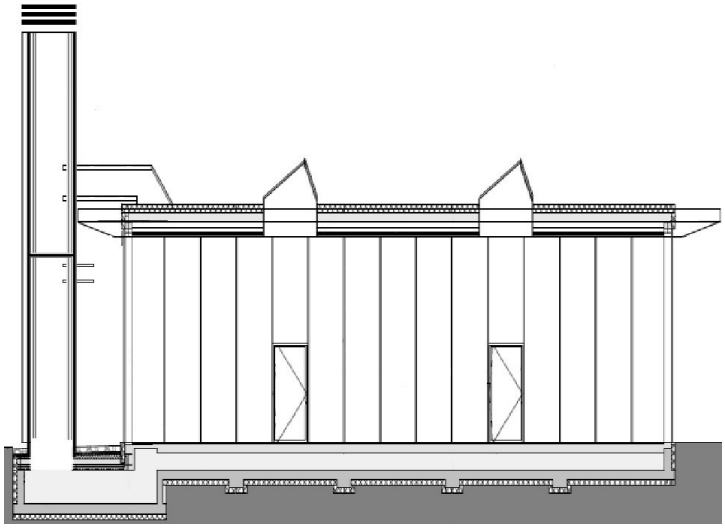

Figure 3-1: CCC-building with initial chimney design.

Symbol	Expression
g	9.81
p_{Ar}	101325
σ	5.67×10^{-8}
D	0.014
A	$X \times Y$
V	$X \times Y \times Z$
T_{sky}	$T_{\mathrm{a}} - 10$
Ra	$f(T_{\mathrm{i}}, T_{\mathrm{j}}, p_{\mathrm{M}}, Y, g, M)$
Re	$f(T_{\mathrm{j}}, p_{\mathrm{M}}, Y, v_{\mathrm{a}}, M)$
Pr	$f(T_{\mathrm{i}}, T_{\mathrm{j}}, p_{\mathrm{M}}, M)$
λ_{M}	$f(T_{\mathrm{i}}, T_{\mathrm{j}}, p_{\mathrm{M}}, M)$

Table 3-1: General expressions.

The energy transfer between the components is modeled to be one-directional and directed to the inner zone. Therefore, only components in series, such as the roof and ceiling, are mathematically coupled. Hence, no direct energy exchange is assumed between, e.g., the walls and floor. For simplicity, it is assumed that the components absorb and reject energy uniformly and that radiant energy transfer can be neglected between components surrounding the inner zone. Namely, since the temperature differences between those components are assumed to be small and the relatively large spaces and orientations between the interior components cause low viewing factors. Furthermore, the component dimensions width, length, and depth are denoted as X, Y, and Z, respectively. Hereafter, the models for each model state are presented.

State	X	Y	Z	ρ	$\mathrm{c_p}$	κ	α	ξ	ϵ	ϵ_{low}
T_{z}	13.5	22.5	5.2	1.225	1000	-	-	-	-	-
T_{r}	13.5	22.5	0.004	1050	1800	0.167	0.87	-	0.93	-
T_{c}	13.5	22.5	0.003	7850	500	0.167	-	-	-	-
$T_{\mathrm{n,j}}$, $T_{\mathrm{s,j}}$	13.5	5.2	0.01	2470	900	-	0.085	0.83	0.82	0.16
$T_{\mathrm{e,j}}$, $T_{\mathrm{w,j}}$	22.5	5.2	0.01	2470	900	-	0.085	0.83	0.82	0.16
T_{rf}	13.5	22.5	0.038	1550	800	-	0.2	-	-	-
T_{bf}	13.5	22.5	0.225	2000	840	0.3125	-	-	-	-

Table 3-2: Dimensions and material properties of each considered building component.

Roof & ceiling

The roof consists of thin bitumen layers and the ceiling contains corrugated galvanized steel sheets. Heat transfer between the roof and the environment is modeled with forced convection expressions using Zhukauskas' correlation, radiation, and absorption of solar irradiance. Between the roof and ceiling, conduction occurs through the insulation. The insulation material has an R-value of 6 $(m^2K)/W$. R-values denote the insulation quality and equal the inverse of the conduction coefficient κ. The heat transfer between the ceiling and the inner room is modeled by McAdams' convection correlations for downward-facing horizontal surfaces. A difference exists between downward-facing surfaces that heat or cool the adjacent medium since the flow behavior varies for the two cases. The heat balance of the roof is discretely modeled by using a time period Δt as:

$$\Delta T_{\mathrm{r}} = (\dot{Q}_{\mathrm{in}} - \dot{Q}_{\mathrm{cond}} - \dot{Q}_{\mathrm{rad}} - \dot{Q}_{\mathrm{conv}})\frac{\Delta t}{\rho V c_{\mathrm{p}}} \tag{3-1}$$

$$\dot{Q}_{\mathrm{in}} = I_{\mathrm{o}} A \alpha \tag{3-2}$$

$$\dot{Q}_{\mathrm{cond}} = \kappa A (T_{\mathrm{r}} - T_{\mathrm{c}}) \tag{3-3}$$

$$\dot{Q}_{\mathrm{rad}} = \epsilon \sigma A (T_{\mathrm{r}}^4 - T_{\mathrm{sky}}^4) \tag{3-4}$$

$$\dot{Q}_{\mathrm{conv}} = \overline{h}_{\mathrm{r,a}} A (T_{\mathrm{r}} - T_{\mathrm{a}}) \tag{3-5}$$

$$\overline{h}_{\mathrm{r,a}} = Nu \lambda_{\mathrm{air}} l^{-1} \tag{3-6}$$

$$l = \frac{A}{2X + 2Y} \tag{3-7}$$

$$Nu = 0.037 Re^{0.8} Pr^{0.3334} \tag{3-8}$$

In addition, the heat balance of the ceiling is modeled as:

$$\Delta T_{\mathrm{c}} = (-\dot{Q}_{\mathrm{cond}} - \dot{Q}_{\mathrm{conv}})\frac{\Delta t}{\rho V c_{\mathrm{p}}} \tag{3-9}$$

$$\dot{Q}_{\mathrm{cond}} = \kappa A (T_{\mathrm{c}} - T_{\mathrm{r}}) \tag{3-10}$$

$$\dot{Q}_{\mathrm{conv}} = \overline{h}_{\mathrm{c,z}} A (T_{\mathrm{c}} - T_{\mathrm{z}}) \tag{3-11}$$

$$\overline{h}_{\mathrm{c,z}} = Nu_{\downarrow} \lambda_{\mathrm{air}} l^{-1} \tag{3-12}$$

$$l = \frac{A}{2X + 2Y} \tag{3-13}$$

$$Nu_{\downarrow} = \begin{cases} 0.54 Ra^{0.25}, & T_{\mathrm{c}} < T_{\mathrm{z}} \ \wedge \ Ra \leq 10^7 \\ 0.15 Ra^{0.3334}, & T_{\mathrm{c}} < T_{\mathrm{z}} \ \wedge \ Ra > 10^7 \\ 0.27 Ra^{0.25}, & T_{\mathrm{c}} > T_{\mathrm{z}} \end{cases} \tag{3-14}$$

Four triple-glazed walls

The four walls consist of transparent glass. Each wall is triple-glazed with argon (Ar) filled cavities. Such a totally glazed wall construction is unique and therefore not well-studied in the literature on BEMS. However, this is not a popular construction strategy, because, without proper use of solar blinds, heat surpluses will occur during warm and sunny days.

The heat transfer among all glazings is modeled using expressions for convection, radiation, and absorption, as shown below. Zhukauskas' correlation is used to model forced convection between the environment and exterior glazing. MacGregor's correlation is applied for natural convection in the cavities, as it is developed for vertical cavities with large ratios between the cavity's height and thickness (D). The Churchill & Chu correlation for vertical surfaces is used to model convection between the interior glazing and the inner zone. Furthermore, the radiant heat transfer is normally substantial in these cavities due to the relatively small cavity thickness and high emissivity of glass. However, innovative low-ϵ glass is applied in the CCC-building. Low-ϵ glass is manufactured with metal-oxide coatings that lower the surface emissivity without significantly reducing transparency. These coatings are only located on the cavity side of the exterior and interior glazings, not on the middle glazing. Note that the subscript numbers 1, 2, and 3 denote the exterior, middle, and interior glazings, respectively.

$$\Delta T_{\mathrm{i,j}} = (\dot{Q}_{\mathrm{in}} - \dot{Q}_{\mathrm{rad}} - \dot{Q}_{\mathrm{conv}})\frac{\Delta t}{\rho V c_{\mathrm{p}}}, \qquad \mathrm{i} \ni \{\mathrm{n,e,s,w}\} \tag{3-15}$$

$$\dot{Q}_{\mathrm{in}} = \begin{cases} A(I_{\mathrm{o,b}}\alpha_{\mathrm{o}} + (I_{\mathrm{o,r}} + I_{\mathrm{o,d}})\alpha), & \mathrm{j} = 1 \\ A(I_{\mathrm{o,b}}\xi_{\mathrm{o}}\alpha_{\mathrm{o}} + (I_{\mathrm{o,r}} + I_{\mathrm{o,d}})\xi\alpha), & \mathrm{j} = 2 \\ A(I_{\mathrm{o,b}}\xi_{\mathrm{o}}^2\alpha_{\mathrm{o}} + (I_{\mathrm{o,r}} + I_{\mathrm{o,d}})\xi^2\alpha), & \mathrm{j} = 3 \end{cases} \tag{3-16}$$

$$\dot{Q}_{\mathrm{rad}} = \begin{cases} \sigma A(\epsilon(T_{\mathrm{i,1}}^4 - T_{\mathrm{sky}}^4) + \mathcal{F}(T_{\mathrm{i,1}}^4 - T_{\mathrm{i,2}}^4)), & \mathrm{j} = 1 \\ \sigma A\mathcal{F}(2T_{\mathrm{i,2}}^4 - T_{\mathrm{i,1}}^4 - T_{\mathrm{i,3}}^4), & \mathrm{j} = 2 \\ \sigma A\mathcal{F}(T_{\mathrm{i,3}}^4 - T_{\mathrm{i,2}}^4), & \mathrm{j} = 3 \end{cases} \tag{3-17}$$

$$\mathcal{F} = (\epsilon^{-1} + \epsilon_{\mathrm{low}}^{-1} - 1)^{-1} \tag{3-18}$$

$$\dot{Q}_{\mathrm{conv}} = \begin{cases} A(\overline{h}_{1,\mathrm{a}}(T_{\mathrm{i,1}} - T_{\mathrm{a}}) + \overline{h}_{1,2}(T_{\mathrm{i,1}} - T_{\mathrm{i,2}})), & \mathrm{j} = 1 \\ A(\overline{h}_{2,1}(T_{\mathrm{i,2}} - T_{\mathrm{i,1}}) + \overline{h}_{2,3}(T_{\mathrm{i,2}} - T_{\mathrm{i,3}})), & \mathrm{j} = 2 \\ A(\overline{h}_{3,2}(T_{\mathrm{i,3}} - T_{\mathrm{i,2}}) + \overline{h}_{3,\mathrm{z}}(T_{\mathrm{i,3}} - T_{\mathrm{z}})), & \mathrm{j} = 3 \end{cases} \tag{3-19}$$

$$\overline{h}_{\mathrm{j,j^*}} = \begin{cases} Nu_{\mathrm{j^*}}\lambda_{\mathrm{air}}Y^{-1}, & \mathrm{j^* = a,z} \wedge \mathrm{j} \neq \mathrm{j^*} \\ Nu_{\mathrm{j^*}}\lambda_{\mathrm{Ar}}Y^{-1}, & \mathrm{j^* = 1,2,3} \wedge \mathrm{j} \neq \mathrm{j^*} \end{cases} \tag{3-20}$$

The Nusselt number expressions for the three different situations are as follows:

Zhukauskas for $\mathrm{j^* = a}$: $$Nu_{\mathrm{j^*}} = 0.037Re^{0.8}Pr^{0.3334} \tag{3-21}$$

MacGregor for $\mathrm{j^* = 1,2,3}$: $$Nu_{\mathrm{j^*}} = 0.42Pr^{0.012}Ra^{0.25}(\frac{Y}{D})^{-0.3} \tag{3-22}$$

Churchill & Chu for $\mathrm{j^* = z}$: $$Nu_{\mathrm{j^*}} = \begin{cases} 0.68 + (\frac{0.670Ra^{0.25}}{1+(\frac{0.492}{Pr})^{0.5625}})^{0.4444}, & Ra < 10^9 \\ (0.825 + (\frac{0.387Ra^{0.1667}}{1+(\frac{0.492}{Pr})^{0.5625}})^{0.2963})^2, & Ra \geq 10^9 \end{cases} \tag{3-23}$$

Raised floor & basement floor

The raised floor consists of calcium sulfate tiles, resting on steel pedestals. Some tiles are perforated so that air can freely move between the inner zone and basement. Hence, the raised floor is modeled as a 'floating' plate of thermal mass in the inner zone, which absorbs incoming

solar irradiance and interacts with the inner zone through convection on both sides of the plate. Therefore, McAdams' correlation for both upwards- and downwards-facing horizontal surfaces is applied. The heat balance of the raised floor is modeled as:

$$\Delta T_{\mathrm{rf}} = (\dot{Q}_{\mathrm{in}} - \dot{Q}_{\mathrm{conv}})\frac{\Delta t}{\rho V c_{\mathrm{p}}} \tag{3-24}$$

$$\dot{Q}_{\mathrm{in}} = I_{\mathrm{o}} A_{\mathrm{u}} \xi_{\mathrm{o}}^{3} \alpha \tag{3-25}$$

$$\dot{Q}_{\mathrm{conv}} = \overline{h}_{\mathrm{rf,z}} A (T_{\mathrm{rf}} - T_{\mathrm{z}}) \tag{3-26}$$

$$\overline{h}_{\mathrm{rf,z}} = (Nu_{\uparrow} + Nu_{\downarrow})\lambda_{\mathrm{air}} l^{-1} \tag{3-27}$$

$$l = \frac{A}{2X + 2Y} \tag{3-28}$$

$$Nu_{\uparrow} = \begin{cases} 0.54 Ra^{0.25}, & T_{\mathrm{rf}} > T_{\mathrm{z}} \ \wedge \ Ra \leq 10^{7} \\ 0.15 Ra^{0.3334}, & T_{\mathrm{rf}} > T_{\mathrm{z}} \ \wedge \ Ra > 10^{7} \\ 0.27 Ra^{0.25}, & T_{\mathrm{rf}} < T_{\mathrm{z}} \end{cases} \tag{3-29}$$

$$Nu_{\downarrow} = \begin{cases} 0.54 Ra^{0.25}, & T_{\mathrm{rf}} < T_{\mathrm{z}} \ \wedge \ Ra \leq 10^{7} \\ 0.15 Ra^{0.3334}, & T_{\mathrm{rf}} < T_{\mathrm{z}} \ \wedge \ Ra > 10^{7} \\ 0.27 Ra^{0.25}, & T_{\mathrm{rf}} > T_{\mathrm{z}} \end{cases} \tag{3-30}$$

The concrete basement floor is adjacent to the underlying ground and the inner zone. Insulation material is integrated between the concrete and the ground and has an R-value quality of 3.2 $(\mathrm{m}^2\mathrm{K})/\mathrm{W}$. Therefore, the energy balance should be modeled with expressions for conduction and convection. For convective heat transfer, McAdams' correlation for upwards-facing horizontal surfaces is applied. The balance of the basement floor is modeled as:

$$\Delta T_{\mathrm{bf}} = (-\dot{Q}_{\mathrm{cond}} - \dot{Q}_{\mathrm{conv}})\frac{\Delta t}{\rho V c_{\mathrm{p}}} \tag{3-31}$$

$$\dot{Q}_{\mathrm{cond}} = \kappa A (T_{\mathrm{bf}} - T_{\mathrm{g}}) \tag{3-32}$$

$$\dot{Q}_{\mathrm{conv}} = \overline{h}_{\mathrm{bf,z}} A (T_{\mathrm{bf}} - T_{\mathrm{z}}) \tag{3-33}$$

$$\overline{h}_{\mathrm{bf,z}} = Nu_{\uparrow} \lambda_{\mathrm{air}} l^{-1} \tag{3-34}$$

$$l = \frac{A}{2X + 2Y} \tag{3-35}$$

$$Nu_{\uparrow} = \begin{cases} 0.54 Ra^{0.25}, & T_{\mathrm{bf}} > T_{\mathrm{z}} \ \wedge \ Ra \leq 10^{7} \\ 0.15 Ra^{0.3334}, & T_{\mathrm{bf}} > T_{\mathrm{z}} \ \wedge \ Ra > 10^{7} \\ 0.27 Ra^{0.25}, & T_{\mathrm{bf}} < T_{\mathrm{z}} \end{cases} \tag{3-36}$$

However, T_{g} is not measurable, as no ground sensors are placed under the CCC-building. Instead, a cosine model is developed by Algorithm 1, which approximates the daily ground temperature of one-meter depth, measured by the Royal Netherlands Meteorological Institute [36]. This data resembles the mean of two ground temperature data sets from weather stations located in Wilhelminadorp, $T_{\mathrm{g,w}}$, and De Bilt, $T_{\mathrm{g,b}}$, so that both coastal and continental climates are considered. Of three years of data, 70% is randomly selected to use as training data, on which the algorithm optimizes the amplitude a, horizontally shift c, and equilibrium point d. Note that the cosine model uses the day number of the year as an input. The

optimized variables a, c, and d have the values 5.3 K, 43.9 days, and 288.15 K, respectively. To verify the model's correctness, the VAF and RMSE are determined on the remaining 30% validation data. The VAF and RMSE turned out to be 97.6% and 0.591 K, respectively.

Algorithm 1 Ground temperature model **MATLAB**

Input: $\{T_{\mathrm{g,b}}, T_{\mathrm{g,w}}\} \in Data$
Output: Optimized values $\{a, c, d\} \in u$
Procedure:
$T_{\mathrm{g,m}} \leftarrow \mathbf{mean}(T_{\mathrm{g,b}}, T_{\mathrm{g,w}})$
$l \leftarrow \mathbf{length}(T_{\mathrm{g,m}})$
$p \leftarrow \mathbf{randperm}(l, 0.7l)$ % training set
$v \leftarrow \mathbf{setdiff}(1 \rightarrow l, p)$ % validation set
$fun \leftarrow @(u)\mathbf{function}(u, T_{\mathrm{g,m}}(p), p)$
$u_0 = [6, 45, 285]$
$u \leftarrow \mathbf{fminsearch}(fun, u_0)$
return u
$C = \mathbf{function}(u, T_{\mathrm{g,m}}, Day)$
$T_{\mathrm{g}} \leftarrow -a\ \cos\left(\frac{2\pi}{365}(Day - c)\right) + d$
$C \leftarrow \mathbf{VAF}(T_{\mathrm{g}}, T_{\mathrm{g,m}})^{-1} + \mathbf{RMSE}(T_{\mathrm{g}}, T_{\mathrm{g,m}})$
return C

Inner zone

The inner zone is affected by the surrounding components but is also directly influenced by energy sources. Hence, this state is subjected to convection and heat generation by HVAC actuators and occupants. Convection is modeled by using the natural convection correlations of Churchill & Chu and McAdams. In addition, the heat generation per occupant is set to 100 W and the HVAC system contains a heat pump and ventilation system. Therefore, the heat pump gain ($\dot{Q}_{\mathrm{hp}}$) and air mass flow ($\dot{m}$) are usable to regulate this state.

$$\Delta T_{\mathrm{z}} = (\dot{Q}_{\mathrm{gen}} + \dot{Q}_{\mathrm{vent}} - \dot{Q}_{\mathrm{conv}})\frac{\Delta t}{\rho V c_{\mathrm{p}}} \tag{3-37}$$

$$\dot{Q}_{\mathrm{gen}} = \dot{Q}_{\mathrm{hp}} + 100 N_{\mathrm{occ}} \tag{3-38}$$

$$\dot{Q}_{\mathrm{vent}} = \dot{m} c_{\mathrm{p}} (T_{\mathrm{a}} - T_{\mathrm{z}}) \tag{3-39}$$

$$\dot{Q}_{\mathrm{conv}} = \sum_i \overline{h}_{\mathrm{z,i}} A_{\mathrm{i}} (T_{\mathrm{z}} - T_{\mathrm{i}}), \qquad \mathrm{i} \ni \{\mathrm{bf, rf, c, n, e, s, w}\} \tag{3-40}$$

$$\overline{h}_{\mathrm{z,i}} = \begin{cases} Nu_{\mathrm{i}} \lambda_{\mathrm{air}} l^{-1}, & \mathrm{i} = \mathrm{bf, rf, c} \\ Nu_{\mathrm{i}} \lambda_{\mathrm{air}} Y^{-1}, & \mathrm{i} = \mathrm{n, e, s, w} \end{cases} \tag{3-41}$$

$$l = \frac{A_{\mathrm{i}}}{2X + 2Y}, \qquad \mathrm{i} = \mathrm{bf, rf, c} \tag{3-42}$$

$$Nu_{\mathrm{i}} = \begin{cases} \text{Churchill \& Chu eq. 3-23}, & \mathrm{i} = \mathrm{n, e, s, w} \\ \text{McAdams eq. 3-14}, & \mathrm{i} = \mathrm{c} \\ \text{McAdams eq. 3-29 \& 3-30}, & \mathrm{i} = \mathrm{rf} \\ \text{McAdams eq. 3-36}, & \mathrm{i} = \mathrm{bf} \end{cases} \tag{3-43}$$

3-1-2 Actuator modeling

Three actuator types are considered to control the inner zone's state. Automated solar blinds on each exterior glazing control incoming solar irradiance, the thermal chimney provides natural ventilation which is controlled by the adjustable flow aperture area, and the heat pump actively transfers heat energy between ambient air and the inner zone by means of the coolant's controllable and heat exchangers. The latter requires a complex model and is not the main focus of this work. Therefore, $\dot{Q}_{\mathrm{hp}}$ is a controllable input in equation 3-38. Then, the amount of active energy required to ensure thermal comfort will serve as assessment criteria in the case study. The models for the passive energy control actuators are discussed below.

Automated solar blind model

A model for the automated solar blinds is developed, assuming that the reduction of the incoming irradiation is linearly proportional to the downward position of the blind and that the movement is instantaneous relative to the control time step. Therefore, the control input on the solar irradiance (u_{b}) is denoted as a percentage. 100% indicates fully open blinds and 0% shows that they are closed. Note that only the floor and glazing states are directly affected by this control. In this case, equation 3-16 is extended as:

$$\dot{Q}_{\mathrm{in}} = \begin{cases} A(I_{\mathrm{o,b}}\alpha_{\mathrm{o}} + (I_{\mathrm{o,r}} + I_{\mathrm{o,d}})\alpha)u_{\mathrm{b}}, & \mathrm{j} = 1 \\ A(I_{\mathrm{o,b}}\xi_{\mathrm{o}}\alpha_{\mathrm{o}} + (I_{\mathrm{o,r}} + I_{\mathrm{o,d}})\xi\alpha)u_{\mathrm{b}}, & \mathrm{j} = 2 \\ A(I_{\mathrm{o,b}}\xi_{\mathrm{o}}^2\alpha_{\mathrm{o}} + (I_{\mathrm{o,r}} + I_{\mathrm{o,d}})\xi^2\alpha)u_{\mathrm{b}}, & \mathrm{j} = 3 \end{cases} \tag{3-44}$$

The four solar blinds for the four directions are independently controllable. Therefore, the extended expression for the solar irradiance absorption by the raised floor is more complex. The Sun's location needs to be considered in this model as closing one blind affects the floor's state differently than closing another. This is solved by calculating the eight fractions of solar irradiances, entering through the four glazings. Hence, equation 3-25 is extended as:

$$\dot{Q}_{\mathrm{in}} = A_{\mathrm{u}}\alpha(I_{\mathrm{o,b}}\sum_{\mathrm{i}} f_{\mathrm{b,i}}\xi_{\mathrm{o,i}}^3 u_{\mathrm{b,i}} + (I_{\mathrm{o,r}} + I_{\mathrm{o,d}})\sum_{\mathrm{i}} f_{\mathrm{rd,i}}\xi^3 u_{\mathrm{b,i}}), \qquad \mathrm{i} \ni \{\mathrm{n,e,s,w}\} \tag{3-45}$$

$$f_{\mathrm{b,i}} = \frac{I_{\mathrm{o,b,i}}}{\sum_{\mathrm{i}} I_{\mathrm{o,b,i}}}, \qquad \mathrm{i} \ni \{\mathrm{n,e,s,w}\} \tag{3-46}$$

$$f_{\mathrm{rd,i}} = \frac{I_{\mathrm{o,r,i}} + I_{\mathrm{o,d,i}}}{\sum_{\mathrm{i}}(I_{\mathrm{o,r,i}} + I_{\mathrm{o,d,i}})}, \qquad \mathrm{i} \ni \{\mathrm{n,e,s,w}\} \tag{3-47}$$

Thermal chimney model

The control model for natural ventilation through the thermal chimney consists of Andersen's fully-mixed model [8] with an additional controllable input u_{v}. This input regulates the air mass flow by opening and closing the ventilation shaft. The state of the shaft is denoted by a percentage. Therefore, the control input is linearly determinable between 0% and 100%, denoting a closed and open shaft, respectively. The C_{d} coefficient determines how effective natural ventilation is in the practical application. This coefficient decreases as more objects are integrated into the chimney and is therefore hard to determine by hand. A CFD model

of this specific thermal chimney is used to determine this value and to validate the control model. De Araujo Passos et al. estimated in [22] the C_d of the same thermal chimney design by using PHOENICS [19]. This commercial CFD software tool is widely considered for thermal systems and therefore reliable for code-to-code verification. The upper-layer chimney height H, inlet area A_t, and outlet area A_b are set on 4 m, 2.4 m^2, and 3.5 m^2, respectively. Note that the upper-layer chimney is above the inner zone exhaust valve. C_d was found to be 0.57.

$$\dot{Q}_\mathrm{vent} = \dot{m} c_\mathrm{p} (T_\mathrm{a} - T_\mathrm{z}) u_\mathrm{v} \tag{3-48}$$

$$\dot{m} = C_\mathrm{d} \rho A^* \sqrt{2gH \frac{|T_\mathrm{z} - T_\mathrm{a}|}{T_\mathrm{a}}} \tag{3-49}$$

$$A^* = \frac{A_\mathrm{t} A_\mathrm{b}}{\sqrt{A_\mathrm{t}^2 + A_\mathrm{b}^2}} \tag{3-50}$$

3-1-3 The nonlinear plant model

All previously discussed models together form the nonlinear plant model. This plant model serves as a simulation testbed to support the development of a suitable controller and should therefore be the best representation of the CCC-building. To perform simulations, the model is compressed into one function that contains 17 discreet balances, each for one state. During one simulation step, this system of equations calculates 'updated' state values for the current time step by considering all applicable parameters of that time step and the old states of the previous time step. The function is solved by the MATLAB nonlinear system solver *fsolve* with the Levenberg-Marquardt algorithm. Subsequently, the temperature change of each state is assessed. If this change is too great, the function will be resolved, using the same time step-dependent states and parameters, but replacing the old states, which serve as input for the convection correlations, with the updated states. The assessment of the temperature change continues until the benchmark, which indicates that all states have reached their steady-state for that time step, is reached. Hereafter, the next simulation step is executed.

This simulation strategy increases the model's accuracy as many convection correlation revisions are taken during a simulation step. This results in a more accurate model evolution. However, this also increases the computation time, mainly due to the Nusselt number correlations. Per model revision, 21 Nusselt numbers are determined. Therefore, the Rayleigh, Reynolds, and Prandtl numbers have to be calculated for each case by means of state and air properties. These properties are obtained by consulting the C++ CoolProp library [12] via a MATLAB wrapper. This library contains a collection of mass, liquid, and gas property data over a wide material, temperature, and pressure range. The wrapper consults this library for the required values per situation. However, the wrapper's computation time is relatively high in contrast to the execution cost of the rest of the plant model. Namely, the library contains an enormous amount of data and its search method is optimized for C++ software and not for MATLAB. Therefore, MATLAB users are limited to the search speed of the wrapper.

3-1-4 The computational cost problem

The nonlinear plant model appeared to be less suitable to serve as an MPC prediction model. Such a prediction model requires an acceptable level of accuracy, but cannot be too computa-

tionally expensive. However, due to the general robustness of MPC, the plant model can be simplified without dramatically deteriorating control performance. Two adjustments, which are both discussed below, are applied to create a simplified nonlinear model suitable for MPC. These adjustments caused a computation time reduction of 93.5%, as the computation time of a simulation step of the nonlinear plant model and simplified nonlinear model appeared to be 0.072 and 0.0047 seconds, respectively. When comparing the two model outputs, the VAF equals 99.7%, indicating high accuracy levels of the simplified nonlinear model.

Matrix formation

One adjustment to decrease the computation cost is the conversion of the model from function form to matrix form, so that the system is expressed in a nonlinear state-space model. The state-space is developed in continuous-time and has the dimensions of 17 states, 6 inputs, 1 output, and 1 disturbance variable. The latter denotes the amount of occupants. This continuous-time model is discretized using MATLAB function *c2d*, from the Control System Toolbox, with the zero-order hold discretization method and a sample time of Δt. The resulting nonlinear discreet state-space model has the form:

$$x_{k+1} = \mathcal{A}(x_k, p_k)x_k + \mathcal{B}(x_k, p_k)u_k + \mathcal{E}d_k \tag{3-51}$$

$$y_k = \mathcal{C}x_k \tag{3-52}$$

where x_k, u_k, y_k, p_k, and d_k denote the model state temperatures, inputs, outputs, time step-dependent parameters, and disturbances, respectively. In this form, the model matrices $\mathcal{A}_k$ and $\mathcal{B}_k$ depend on time-varying states and parameters. However, $\mathcal{E}$ and $\mathcal{C}$ are linear time-invariant matrices, denoting the disturbance source and measured building states, respectively. The state-space form holds lower computational costs than the function form, as MATLAB is heavily optimized in matrix operations and the optimizer *fsolve* is disregarded. Applying this conversion reduces the computation time of the building model by 10%.

Fit functions for convection coefficients

Another modification to reduce computational costs is to omit to assess the change in state values, such that no revisions of the state-space model are performed during a simulation step. This results in lower computational costs. Instead, black-box functions are applied to approximate the 21 convection correlations. Then, the model no longer relies on the C++ CoolProp library and MATLAB wrapper. MATLAB function *fit* of the Curve Fitting Toolbox allows to fit data on 2- and 3-dimensional models by using input and output training data. However, 3-dimensional models include more information and are therefore preferable. 21 data sets are created by simulating the plant model for a simulation period of a year. Each data set contains the temperature data of two states and corresponding convection coefficients. Hereafter, each set is randomly divided into 80% training data and 20% validation data. Multiple 3-dimensional model types can be selected in the function *fit*. Through trial and error, the nearest neighbor interpolation model turned out to perform best. The computation time of such a *fit* model appeared to be 50% lower than that of the MATLAB wrapper. By applying this modification, the simulation time of the building model is reduced by 92%.

In the fitted models for the 16 coupled components in which natural convection occurs, the values of any two coupled states serve as input data. In addition, the ambient temperature and wind speed serve as input data in the fitted models for the 5 exterior components that are exposed to forced convection. The convection coefficients of all 21 correlations, which are generated by the plant model, serve as output data for each model. Moreover, the VAF and NRMSE values of each fitted model are obtained by using the validation data to verify the correctness of each model. The validation results are presented in Table C-1 in Appendix C.

3-1-5 Linearization strategies

The speed and reliability of the MPC optimization is increased when linear MPC is considered. This claim is elaborated further in the next section. In this subsection, three linearization methods for the radiation, convection, and ventilation expressions are proposed. After employing the linearizations, the state and parameter-dependent system matrices $\mathcal{A}_\mathrm{k}$ and $\mathcal{B}_\mathrm{k}$ from equation 3-50 are converted to parameter-dependent matrices. These matrices form the linear time-variant state-space model that will serve as prediction model. Important to note here is that the inner zone state T_z plays a major role in the three nonlinear expressions, however, no state-dependent matrices can exist in the linear model. Therefore, the inner zone's state, obtained in the previous simulated time step, $T_\mathrm{z}(k-1)$, is made constant for all linear models for the MPC horizon. This constant is denoted as $T_{\mathrm{z},0}$ and presumably approximates T_z in the early horizon period. However, $T_{\mathrm{z},0}$ loses accuracy over the course of the horizon.

Radiation equations

The 4th-order temperatures, used in the radiant equations 3-4 and 3-17, are linearized as shown below. This linearization method is valid when the temperature difference is much lower than the temperature values considered [10]. In that case, T_i and T_j can both be approximated by a nominal temperature T_nom, while the temperature difference is multiplied linearly.

$$(T_\mathrm{i}^4 - T_\mathrm{j}^4) = (T_\mathrm{i} + T_\mathrm{j})(T_\mathrm{i}^2 + T_\mathrm{j}^2)(T_\mathrm{i} - T_\mathrm{j}) \tag{3-53}$$

$$\approx 4T_\mathrm{nom}^3(T_\mathrm{i} - T_\mathrm{j}) \tag{3-54}$$

Normally, T_nom is an average of two values of any coupled states. However, the application of state values must be omitted in order to employ any linear model. Applying constant averages for all cases would be acceptable, but due to presumably large temperature differences between night and day periods, this is not the most accurate method. Better is to determine T_nom for the exterior components by taking the average of the ambient and the sky temperatures, which are both known in present and future. For the interior components, T_sky is replaced by the inner zone temperature constant $T_{\mathrm{z},0}$. The linearized radiation term is expressed as:

$$\dot{Q}_\mathrm{rad} \approx 4\mathcal{F}\sigma A T_\mathrm{nom}^3(T_\mathrm{i} - T_\mathrm{j}) \tag{3-55}$$

$$T_\mathrm{nom} = \begin{cases} 0.5(T_\mathrm{a} + T_\mathrm{sky}), & \text{for exterior components} \\ 0.5(T_\mathrm{a} + T_{\mathrm{z},0}), & \text{for interior components} \end{cases} \tag{3-56}$$

Convection coefficients

The linearization of the convection coefficient correlations is challenging due to the dominant role of the states on the Nusselt number calculations. A common linearization method is to apply constant convection coefficients for each expression. In this case, the mean convection coefficient values in Table C-1 in Appendix C can be used. However, the fitting method of black-box models can outperform these constants in terms of accuracy. Still, the fitted model inputs cannot contain state variables. So the black-box models for natural convection should be refitted. The generated $\overline{h}_{\mathrm{i,j}}$ data is again applied as output data and possible input variables are $T_{\mathrm{z},0}$, T_{a}, and t_{h}. Note that t_{h} indicates the daily hours from 0 to 23.

After trial and error, the linear interpolation model appeared to be the best-performing fitting model and the highest correlation between the input and output training data was found when all three input variables were considered. However, the linear interpolation model is a 3-dimensional model which only supports two input variables. Therefore, $T_{\mathrm{z},0}$ and T_{a} are combined to input variable T_{diff}. The exact expression of T_{diff} is found by finding the correct ratio between $T_{\mathrm{z},0}$ and T_{a}. The optimization of this ratio and the development of the black-box models are provided in Algorithm 2. A similar method to validate the black-box models as before is performed and the results are also presented in Table C-2 in Appendix C.

Algorithm 2 Linearized convection models **MATLAB**

Input: $\{T_{\mathrm{z},0}(i), T_{\mathrm{a}}(i), t_{\mathrm{h}}(i), \overline{h}(i)\} \in Data$
Output: $x_{\mathrm{op}}, \mathrm{Model}(i)$
Procedure:
for $i = 1 \rightarrow 16$ **do** % all 16 models
$x0 \ni \pm\{10, 1, 0.1, 0.01, 10^{-3}, 10^{-4}\}$
$Fval \leftarrow \infty$
$[C, \mathrm{Model}(i)] \leftarrow @(x)$**function**$(x, Data(i))$
for $j = 1 \rightarrow 12$ **do** % multi-start
$[x, fval] \leftarrow$ **fminsearch**$(fun, x0(j))$
if $fval < Fval$ **then**
$Fval \leftarrow fval$
$x_{\mathrm{op}}(i) \leftarrow x$
end if
end for
end for
return $x_{\mathrm{op}}, Model(i)$
$[C, \mathrm{Model}] =$ **function**$(x, Data)$
$T_{\mathrm{diff}} \leftarrow |xT_{\mathrm{z},0} - T_{\mathrm{a}}|$
$l \leftarrow$ **length**(T_{diff})
$p \leftarrow$ **randperm**$(l, 0.8l)$ % training set
$v \leftarrow$ **setdiff**$(1 \rightarrow l, p)$ % validation set
$opts \leftarrow$ **'linearinterp'**
$\mathrm{Model} \leftarrow$ **fit**$([t_{\mathrm{h}}(p), T_{\mathrm{diff}}(p)], \overline{h}(p), opts)$
$y \leftarrow Model(t_{\mathrm{h}}(v), T_{\mathrm{diff}}(v))$
$C \leftarrow$ **VAF**$(y, \overline{h}(v))^{-1} +$ **NRMSE**$(y, \overline{h}(v))$
return C, Model

Thermal chimney model

The model for energy gain by natural ventilation through the thermal chimney, equation 3-48, depends on both the control input and the inner zone's state. Hence, classic linearization techniques are hard to apply for this model. Instead, the state T_z is replaced with the temperature constant $T_{z,0}$. Note that this model is located in the input matrix $\mathcal{B}$ and directly affects the inner zone's state. As mentioned before, $T_{z,0}$ is most accurate for the early horizon period. Thereafter, it loses its accuracy. This linearization scheme is therefore the main bottleneck of the linearized model in terms of model correctness compared to the nonlinear plant model. The expression for the linearized natural ventilation model is shown below.

$$\dot{Q}_{\text{vent}} \approx \dot{m} c_p (T_a - T_{z,0}) u_v \tag{3-57}$$

$$\dot{m} \approx C_d \rho A^* \sqrt{2gH \frac{|T_{z,0} - T_a|}{T_a}} \tag{3-58}$$

3-2 MPC architecture study

The main objective of the control design is to reduce the building's energy consumption while ensuring thermal comfort by means of controlling the present passive and active energy sources. The challenge is to find optimal control signals for all present actuators, while the computational cost of optimizing these signals is sufficiently suppressed. This section describes the study of assessing five different MPC architectures to address these objectives.

3-2-1 General MPC problem setup

To compare the MPC structures on their control performance and computation time, a setup of the MPC problem is defined and generalized for all structures. A general setup helps to single out the most promising structure and is defined by the following points of content.

Objective function basis

As mentioned in Chapter 2, MPC optimization problems are described by an objective function for a receding horizon that is subject to a prediction model and constraints. Such a function can be of the single- or multi-objective type. For the latter, the objectives are often conflicting and therefore finding the preferred Pareto optimum of the conflicting objectives is extra time-consuming. These conflicts will occur in a BEMS when thermal comfort cannot be achieved by the control of passive energy sources alone. Then, auxiliary energy is required to fill the thermal gaps. However, optimizing an additional control variable and dealing with conflicting objectives, increase the computation cost. Therefore, solely single-objective functions are considered when assessing the five architectures by assuming that only the passive energy sources are available and controllable. This makes thermal comfort the sole objective of the controller as no objective for auxiliary energy is considered, meaning that thermal comfort is unlikely to be constantly achieved. This is, however, not problematic for the comparison, as it is assumed that the best-performing MPC architecture will also outperform the others in the event that auxiliary energy is considered.

Assessment criteria

One reason why MPC is suitable for an office is that thermal comfort should only be achieved when the building is occupied. This means that when the building is unoccupied, e.g., during the night, an MPC controller can make preparatory decisions for the next morning's occupied period. Therefore, the objective function is only relevant to be minimized for the occupied hours, denoted as t_{occ}. Assumed is that thermal comfort is achieved when the inner zone reference temperature, T_{ref}, is reached. In the setup, the nonlinear plant model serves as a simulation testbed for each architecture and the squared and absolute errors, e, between T_{ref} and the model's output, T_{z}, denote the control performance. The error equation is presented below. In addition, the computation time of one optimization step, t_{op}, is evaluated per architecture. If these steps take too long, on-line control becomes impractical.

$$e = |T_{\text{ref}}(t_{\text{occ}}) - T_{\text{z}}(t_{\text{occ}})| \tag{3-59}$$

Disturbance data and control time step

As previously discussed, the nonlinear plant and prediction models depend on uncontrollable parameters, i.e., disturbances. However, these parameters are not all derived from one source. The oriented solar irradiance, unshaded floor area, and optical property parameters are obtained through Algorithms 4, 5, and 6, provided in Appendix A, and the occupancy is predetermined. Note that occupants denote when thermal comfort should be achieved and that they function as uncontrollable heat sources. Hence, full occupancy knowledge for the whole horizon benefits the control performance. Unfortunately, occupancy is hard to predict without assigning them in predetermined schedules. Therefore, an occupancy schedule, shown in Figure 3-2, of eight occupied hours is selected and applied in each MPC structure. In all result figures, the periods with occupancy are indicated by the small areas between two black dashed lines.

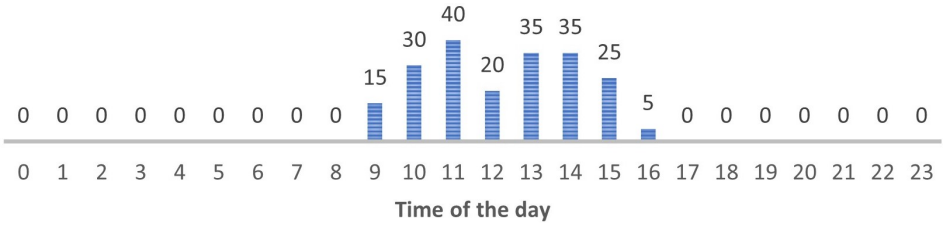

Figure 3-2: Occupancy distribution over a day.

The environmental climate data is accessible for both in present and future. Local weather stations are able to measure the data and local weather forecasts of various institutions have shown to be quite accurate for the near future of a few days. However, for the comparison, full knowledge of the environmental climate data is considered by using a Typical Meteorological Year (TMY) weather data set from EnergyPlus [27]. This set contains the annual period of typical weather data per hour, measured in Amsterdam. Climate data from forty consecutive days in the spring are selected for the assessment. This period is chosen because varying environmental climates occur during spring. In contrast to spring, summer or winter climates are predominantly warm or cold. These seasons are likely to result in consistently similar control actions. This would not demonstrate the full potential of the control structure.

The disturbance data set has an hourly sampling time. So, the MPC controller has to base its solutions on hourly data. Reasonable is to set the control time step, Δt, to an hour for each controller. Another option is to lower Δt to 30 minutes so that the MPC calculations become more robust, considering the mismatch between the plant and prediction models. Hence, both cases are analyzed. Note that shortening the control time step results in less time to optimize the inputs. So any reduction in the control time steps must be carefully considered.

3-2-2 Convexity analysis

A model convexity analysis has been conducted before the architecture comparison is performed. Through this analysis, the reliability of both the linear and nonlinear optimization problems becomes clear. The theory explains that for linear optimization problems, the Hessian matrix must be positive definite or semi-definite for the optimization problem to be convex. This is tested by obtaining the Hessian's eigenvalues for each time step and checking if these are nonnegative. All eigenvalues of the proposed linear model were found to be positive, meaning that the Hessian is positive definite and thus convex. Hence, there is complete reliability in finding the global solution to the linear optimization problems of all time steps.

Analyzing the nonlinear optimization problem convexity is more challenging as these problems are by definition non-convex. A common method for approaching the global solution of this optimization problem is to use *fmincon* in combination with multi-start. Applying multi-start performs multiple consecutive optimizations that address the same optimization problem, but use different sets of initial guesses. By executing the optimization from different and mostly randomly chosen starting points, multiple local minima will be found. The lowest local minimum resembles the best approximation of the global solution. The more starting points are considered, the greater the reliability that the solution found is the global solution.

Visualization of convexity

However, applying multi-start is time-consuming and the results did not appear to improve significantly. This can be caused by a non-convex optimization problem that is almost convex in practice. In this case, the local minima are very close to each other and therefore resemble about the same solution. To test this hypothesis, six simulation time steps are randomly selected to analyze the convexity of the corresponding nonlinear optimization problems. Multi-start with 400 starting points is applied during these time steps for the prediction horizons of 2, 4, and 8. In this test setup, only the ventilation inputs are analyzed, as the ventilation expressions contain most of the model nonlinearities. The 400 starting points are indicated by filled circles and the 400 optimal solutions are symbolized by crosses. The third dimension, resembling the objective function value, is denoted in color. Note that when prediction horizons of 4 and 8 are considered, large solution spaces will occur. In order to visualize those results, the solution space is reduced by summing the ventilation inputs into two solution values. Figures 3-2 and 3-5 provide the shape of the optimization problem, recognizable by the color distribution. Figures 3-3, 3-4, 3-6, and 3-7 indicate that even for larger horizons, there is only one small region in which all found local minima are located. These figures indicate that applying multi-start is redundant for these optimization problems and support the decision not to use multi-start for all optimizations.

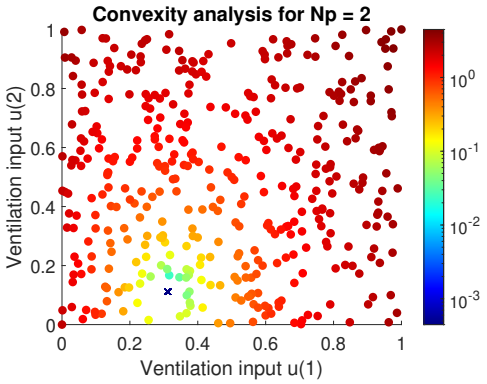

Figure 3-3: Convexity of 2D solution space.

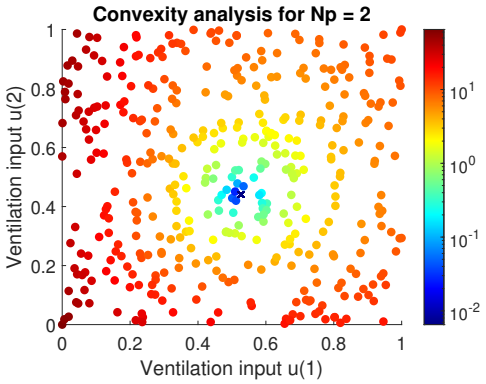

Figure 3-6: Convexity of 2D solution space.

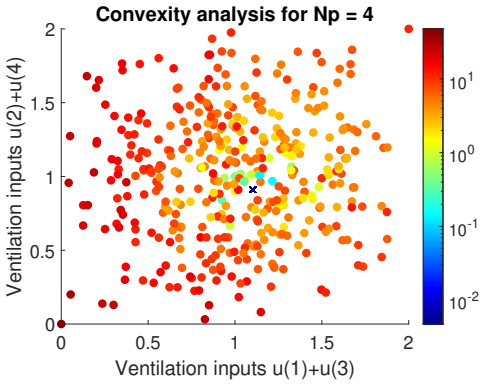

Figure 3-4: Convexity of 4D solution space.

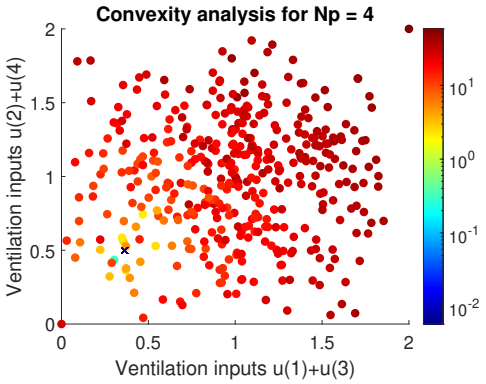

Figure 3-7: Convexity of 4D solution space.

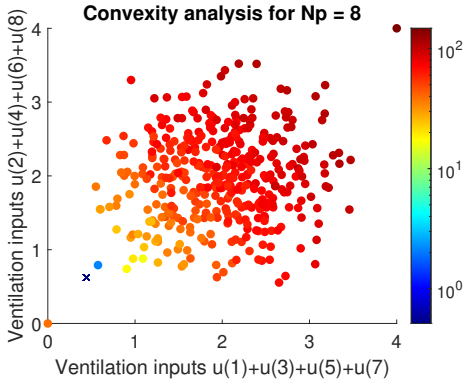

Figure 3-5: Convexity of 8D solution space.

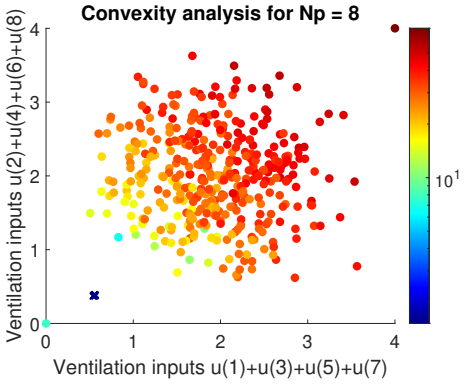

Figure 3-8: Convexity of 8D solution space.

3-2-3 Centralized structure

A centralized structure is characterized by the use of one controller to optimize all the system's control signals. Two centralized structures are assessed in this thesis: the linear and nonlinear MPC controller. The two controllers vary in their prediction model, objective function, and optimization strategy. These differences are clarified by the two following points of content.

Nonlinear MPC

The flowchart, presented in Figure 3-9, displays the centralized nonlinear MPC (NLMPC) scheme. The nonlinear parameter-varying prediction model consists of a set of consecutive nonlinear state-space models. Each state-space model denotes the building's thermal dynamics per prediction step, i, of the receding horizon, N_p. The model parameters are adjusted per prediction step by considering a new set of time, occupancy, weather data, and model states. The latter are set equal to the updated states of the previous prediction step or simulation step, x_0. The optimization algorithm, employed by the MATLAB solver *fmincon*, is active-set, as it shows similar control performance with faster convergence than interior-point and SQP. Another method to suppress calculation costs is to set the control horizon, N_c, lower than N_p. However, the control performance seemed to decrease when this strategy was considered. This is presumably caused by the dominant role of the time step-dependent parameters in the state-space matrices. Hence, for all structures, N_c is set equal to N_p. Furthermore, note that at each simulation time step k, the initial guess $\tilde{u}$ is set equal to the optimized input $\hat{u}$ of the previous time step. The full optimization problem per k is provided below.

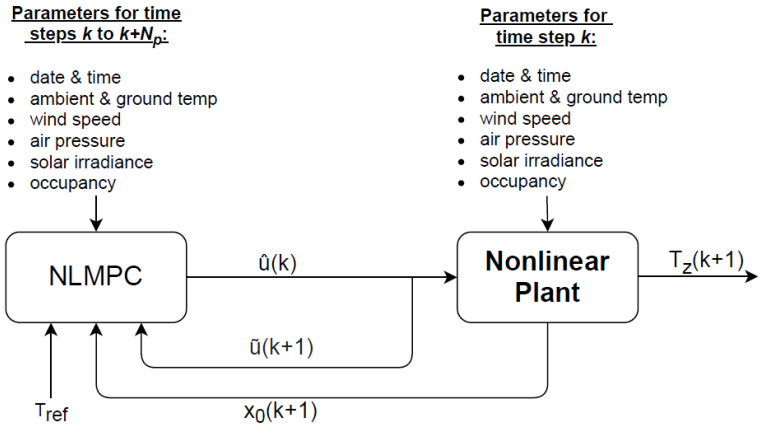

Figure 3-9: NLMPC structure flowchart.

$$\min_{U \hat{=} u(k),\ldots,u(k+N_\mathrm{p}-1)} \sum_{i=1}^{N_\mathrm{p}} (T_\mathrm{z}(k+i) - T_\mathrm{ref})^2 \tag{3-60}$$

$$\begin{aligned}
\text{s.t.} \quad & u(k+i) \geq 0, && i \ni \{0,\ldots,N_\mathrm{p}-1\} \\
& u(k+i) \leq 1, && i \ni \{0,\ldots,N_\mathrm{p}-1\} \\
& T_\mathrm{ref} = 293.15 && \\
& x(k+i+1) = f(x(k+i), u(k+i), p(k+i)) + \mathcal{E}d(k+i), && i \ni \{0,\ldots,N_\mathrm{p}-1\} \\
& T_\mathrm{z}(k+i) = \mathcal{C}x(k+i), && i \ni \{1,\ldots,N_\mathrm{p}\} \\
& x(k+i) = x_0, && i = 0 \\
& x(k+i) \in \mathbb{X}^{17}, && i \ni \{0,\ldots,N_\mathrm{p}\} \\
& u(k+i) \in \mathbb{U}^{5}, && i \ni \{0,\ldots,N_\mathrm{p}-1\} \\
& d(k+i) \in \mathbb{D}^{1}, && i \ni \{0,\ldots,N_\mathrm{p}-1\} \\
& T_\mathrm{z}(k+i) \in \mathbb{Y}^{1}, && i \ni \{1,\ldots,N_\mathrm{p}\}
\end{aligned}$$

In theory, the NLMPC scheme outperforms the other structures in terms of control performance. The simplified nonlinear model has a higher accuracy level than the linearized model and, as explained in Chapter 2, centralized structures are able to outperform other structures. However, a computational cost problem arises when the control time step is set at 30 minutes and the prediction horizon is set to bridge 15 hours. Then, the optimization time takes 18 minutes, which approaches the control time step. To make preparatory decisions during unoccupied hours, the prediction horizon should be set to a value that bridges at least the unoccupied period. Therefore, the minimum horizon length is 17 for hourly control actions, which takes about 4 minutes per optimization. However, if the control time step is 30 minutes, the minimum horizon should be 33, taking about 20 minutes. Therefore, this scheme's computation time exceeds the control time step when the control time step is further decreased, additional control variables are added, or multi-objective functions are considered.

Hence, the prediction horizon is reduced so that a maximum of 8 hours is bridged. In this case, the system converges to T_{ref} for all prediction steps, even for unoccupied hours. The results are provided in Table 3-3 and Figure 3-10. The absolute error is relatively low, indicating high control accuracy when the system can achieve T_{ref}. However, since there are no preparatory decisions, the squared error is relatively high, as T_{ref} is harder to reach in this structure.

Δt	3600 s			1800 s		
N_{p}	2	4	8	2	4	8
$\sum e^2$[K^2]	385	325	237	447	393	316
$\sum e$ [K]	191	176	157	203	189	170
t_{op} [s]	0.84	5.16	30.6	0.78	4.27	26.1

Table 3-3: Results of the NLMPC scheme for a 40-day simulation period.

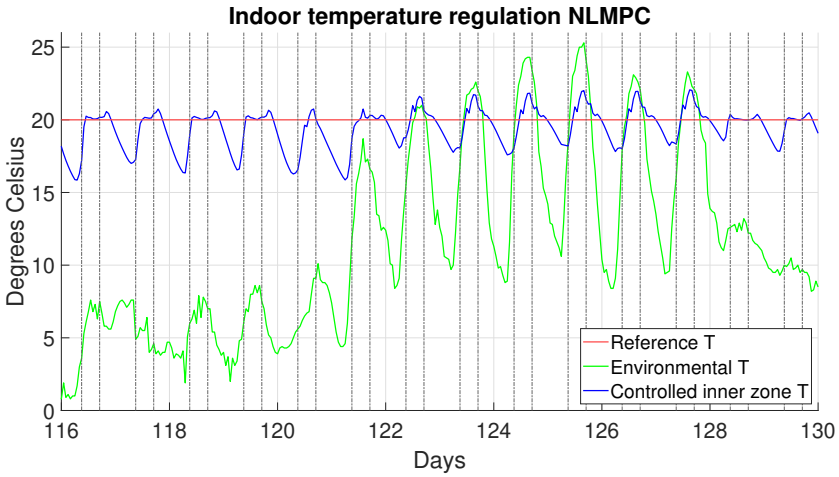

Figure 3-10: T_{z} progression for a 14-day period: $\Delta t = 3600 \wedge N_{\text{p}} = 8$.

Linear MPC

For linear MPC (LMPC), a quadratic programming optimization problem is adopted. The linear parameter-varying prediction model contains all linear state-space models for the LMPC prediction horizon N_{p}^*. Each state-space model denotes the building's thermal dynamics for

each new set of time, occupancy, and climate data. Afterward, the prediction model is substituted into a quadratic objective function with penalizing matrices on the stage and terminal costs. Note that the terminal matrix is calculated by the Riccati equation, using MATLAB function *idare* from the Control System Toolbox. The resulting optimization problem is in the form of an augmented Hessian matrix that is symmetric positive definite for each k. The LMPC structure optimizes 5 inputs that are bounded between 1 and 0. Figure 3-11 displays the LMPC scheme and the optimization problem for each k is provided below.

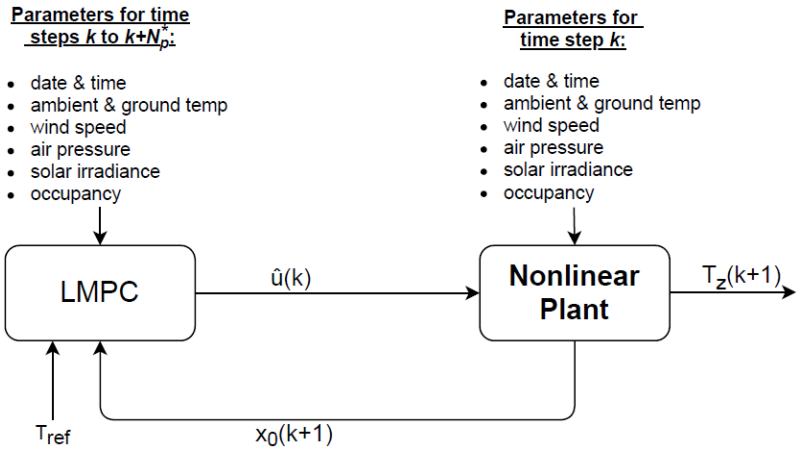

Figure 3-11: LMPC structure flowchart.

$$\min_{U \hat{=} u(k),\ldots,u(k+N_{\mathrm{p}}^*-1)} \sum_{i=0}^{N_{\mathrm{p}}^*-1} (\mathcal{Q}_{\mathrm{k+i}}(T_{\mathrm{z}}(k+i) - T_{\mathrm{ref}})^2 + (u(k+i) - u_{\mathrm{ref}})^T \ldots \mathcal{R}(u(k+i) - u_{\mathrm{ref}})) + \mathcal{P}(T_{\mathrm{z}}(k+N_{\mathrm{p}}^*) - T_{\mathrm{ref}})^2 \tag{3-61}$$

$$\begin{aligned}
\text{s.t.} \quad u(k+i) &\geq 0, && i \ni \{0,\ldots,N_{\mathrm{p}}^*-1\}\\
u(k+i) &\leq 1, && i \ni \{0,\ldots,N_{\mathrm{p}}^*-1\}\\
T_{\mathrm{ref}} &= 293.15\\
u_{\mathrm{ref}} &= [0,1,1,1,1]^T\\
x(k+i+1) &= \mathcal{A}(p(k+i))x(k+i) + \mathcal{B}(p(k+i))u(k+i) + \mathcal{E}d(k+i), && i \ni \{0,\ldots,N_{\mathrm{p}}^*-1\}\\
T_{\mathrm{z}}(k+i) &= \mathcal{C}x(k+i), && i \ni \{0,\ldots,N_{\mathrm{p}}^*\}\\
x(k+i) &= x_0, && i = 0\\
\mathcal{Q}_{\mathrm{k+i}} &= \begin{cases} 4000, & k+i \in t_{\mathrm{occ}} \\ 0, & k+i \notin t_{\mathrm{occ}} \end{cases} && i \ni \{0,\ldots,N_{\mathrm{p}}^*-1\}\\
\mathcal{R} &= \mathbf{diag}(3, 0.1, 0.1, 0.1, 0.1)\\
\mathcal{P} &= \mathbf{idare}(\mathcal{A}(p(k+i)), \mathcal{B}(p(k+i)), \mathcal{Q}_{\mathrm{k+i}}, \mathcal{R}), && i = N_{\mathrm{p}}^*\\
x(k+i) &\in \mathbb{X}^{17}, && i \ni \{0,\ldots,N_{\mathrm{p}}^*\}\\
u(k+i) &\in \mathbb{U}^5, && i \ni \{0,\ldots,N_{\mathrm{p}}^*-1\}\\
d(k+i) &\in \mathbb{D}^1, && i \ni \{0,\ldots,N_{\mathrm{p}}^*-1\}\\
T_{\mathrm{z}}(k+i) &\in \mathbb{Y}^1, && i \ni \{0,\ldots,N_{\mathrm{p}}^*\}
\end{aligned}$$

u_{ref} defines the preferred actuator modes, i.e., the initial blind mode is 100% and for ventilation 0%. Note that the objective function penalizes the inputs, which causes conflicting objectives. With this penalization, thermal control via shading is slightly preferred above ventilation. In this way, thermal regulation via thermal mass over a longer period is encouraged. To omit the conflict between the inputs and output, the penalty on the output is set exceedingly high.

In contrast to NLMPC, this optimization problem tends to be regularly solvable within the control time step. By converting the problem into a Hessian matrix, MATLAB solver *quadprog* can directly obtain the most optimal solutions, instead of considering multiple local minima when using *fmincon* for the NLMPC problems. Therefore, N_{p}^{*} can easily bridge the 16 unoccupied hours. However, the results in Table 3-4 indicate that the controller is more robust when considering horizons of 24 by an hourly sampling time and 48 by a 30 minute sampling time. These two horizons lead to more but lower convergence errors since their summed absolute error is not the best, but their summed squared error is the lowest. Furthermore, to omit the convergence to T_{ref} for unoccupied hours, the $\mathcal{Q}_{\text{k+i}}$ matrices are disregarded for the unoccupied prediction steps. During those hours, preparatory decisions are made to benefit future thermal control. This is visible in Figure 3-12. However, the small convergence errors are also visible around T_{ref} for t_{occ}. This main shortcoming of LMPC is caused by the model mismatch between the linearized prediction model and the nonlinear plant model.

Δt	3600 s				1800 s			
N_{p}^{*}	18	24	36	48	36	48	72	96
$\sum e^2$[K^2]	238	211	211	220	226	208	208	216
$\sum e$ [K]	150	177	178	186	145	177	178	186
t_{op} [s]	0.12	0.16	0.20	0.38	0.25	0.37	0.72	1.29

Table 3-4: Results of the LMPC scheme for a 40-day simulation period.

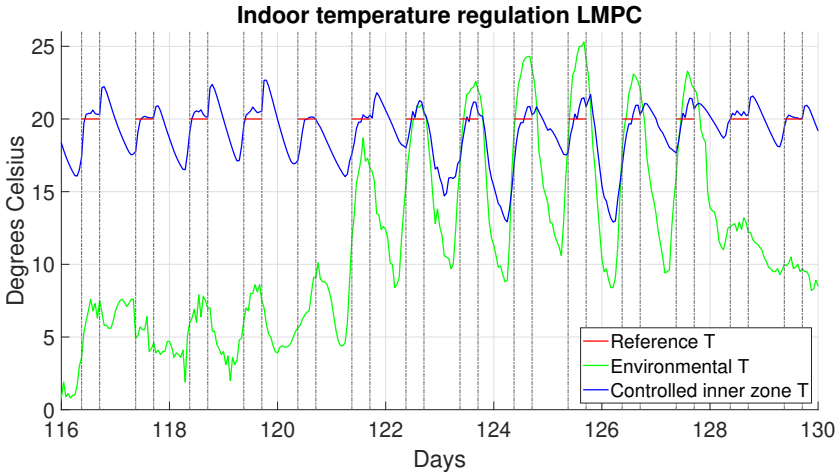

Figure 3-12: T_{z} progression for a 14-day period: $\Delta t = 3600 \wedge N_{\text{p}}^{*} = 24$.

3-2-4 Hierarchical structure

In this subsection, two hierarchical architectures are proposed. These structures contain two controllers that cooperate in an agent-slave relation: the upper-layer controller affects the op-

timization problem of the lower-layer controller. Then, control performance and computation time improvements can emerge. In this work, such improvements are uncovered and applied.

The proposed hierarchical MPC (HMPC) structures combine the advantages of the two centralized structures, i.e., using LMPC with large horizons and low computation times to optimize a reference temperature trajectory T_{traj} and using NLMPC with short horizons to accurately track this trajectory. T_{traj} is determined by solving the same LMPC optimization problem as is applied in the centralized LMPC structure. Hereafter, the optimized inputs are inserted in the linearized model to create a smooth inner zone state trajectory for the NLMPC horizon N_{p}. However, only the reference trajectory during unoccupied hours, T^*_{traj}, is relevant for the NLMPC slave controller, as this controller is unable to determine this optimal trajectory for itself. For occupied hours, T_{traj} is set equal to the conventional reference temperature of 293.15 K. In addition, the inputs, that are optimized by LMPC, are passed to the NLMPC controller for re-optimization, as good initial guesses help *fmincon* to converge faster to the optimized control signals. However, the re-optimization strategy is where the two proposed hierarchical structures differ.

Full input re-optimization

In HMPC-1, provided in Figure 3-13, all five pre-optimized control variable types are passed as initial guess set $\tilde{u}$ to the NLMPC slave. $\tilde{u}$ contains the input guesses, valid for the NLMPC prediction horizon N_{p}. These control variables are then re-optimized by solving a similar optimization problem as is discussed for the centralized NLMPC structure. However in this optimization problem, T_{ref} is replaced by T_{traj}. The re-optimized control signals $\hat{u}$ are applied in the nonlinear plant model and the results are presented in Table 3-5 and Figure 3-15.

Partly input re-optimization

In HMPC-2, presented in Figure 3-14, not all pre-optimized control variable types are applied as initial guess set $\tilde{u}$. In this case, the slave controller only considers the optimized inputs for ventilation as initial guesses for the ventilation input variable. The control signals for the blinds, optimized by the LMPC agent controller, are employed as stationary parameters for the NLMPC problem. A similar NLMPC optimization problem as discussed before is performed, but this time only one control variable is re-optimized. Subsequently, the optimized signals for the blinds and the re-optimized signal for the ventilation are applied in the nonlinear plant model. The results are presented in Table 3-5 and Figure 3-16.

	HMPC-1						HMPC-2					
Δt	$3600\,\text{s} \rightarrow N^*_{\text{p}} = 24$			$1800\,\text{s} \rightarrow N^*_{\text{p}} = 48$			$3600\,\text{s} \rightarrow N^*_{\text{p}} = 24$			$1800\,\text{s} \rightarrow N^*_{\text{p}} = 48$		
N_{p}	2	4	8	2	4	8	2	4	8	2	4	8
$\sum e^2$ [K^2]	275	215	187	306	267	222	207	201	199	204	201	196
$\sum e$ [K]	159	143	137	163	152	141	139	137	141	134	133	133
t_{op} [s]	1.23	5.92	35.0	1.38	5.71	32.7	0.63	2.56	12.8	0.81	2.41	11.5

Table 3-5: Results of the HMPC schemes for a 40-day simulation period.

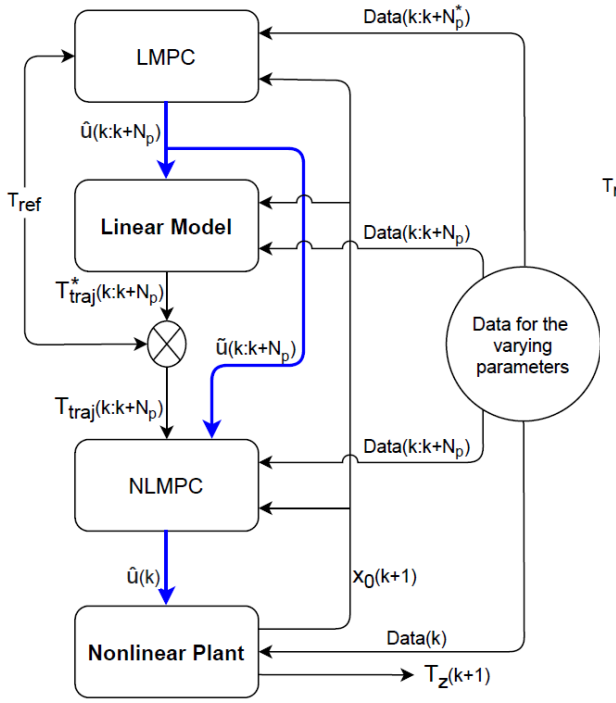

Figure 3-13: HMPC-1 structure flowchart.

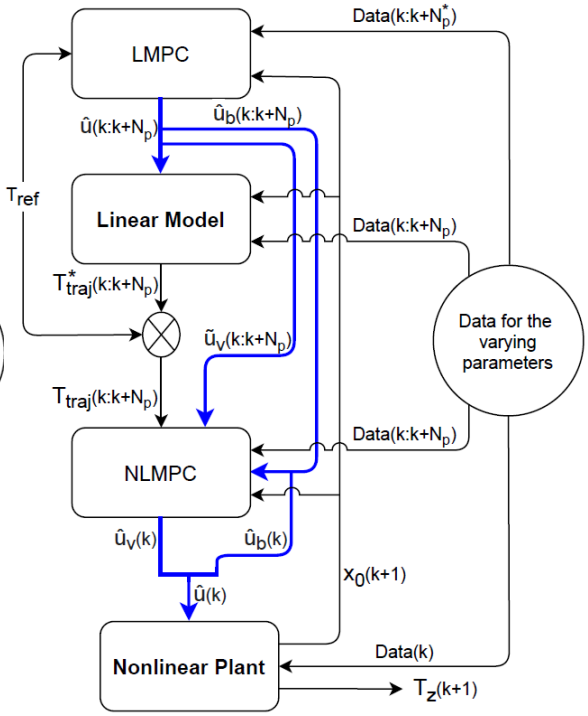

Figure 3-14: HMPC-2 structure flowchart.

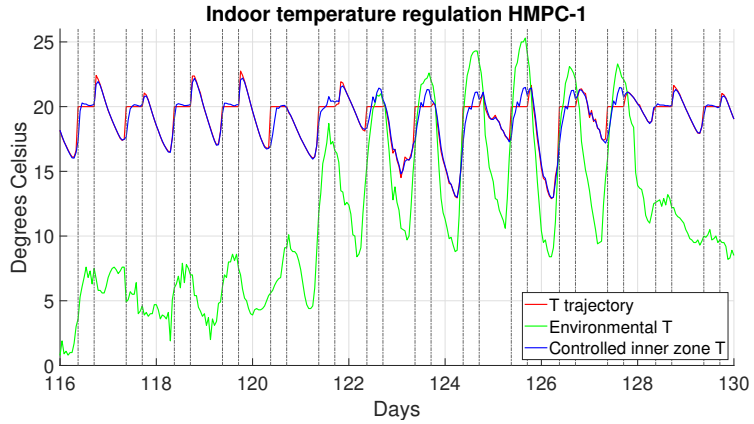

Figure 3-15: T_z progression for a 14-day period: $N_p^* = 24 \wedge N_p = 4$.

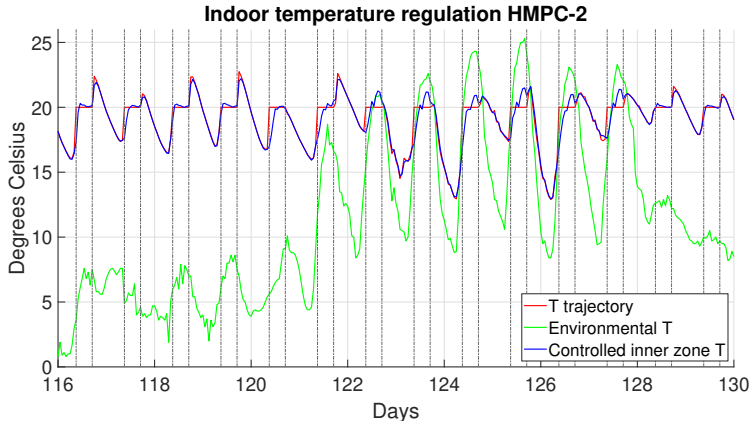

Figure 3-16: T_z progression for a 14-day period: $N_p^* = 24 \wedge N_p = 4$.

3-2-5 The most promising structure

Comparing the NLMPC and LMPC structures implies that applying LMPC with large prediction horizons is beneficial. The squared error is significantly reduced, indicating that making preparatory decisions benefit future occupied hours. However, the absolute error did not improve since the LMPC structure produces more small errors due to its model mismatch. HMPC-1 solves this problem as both the squared and absolute errors are reduced. However, the computational cost does not improve compared to NLMPC as a similar nonlinear optimization problem occurs in both structures. These costs increase even further with a higher N_p or extra climate control actuators. Therefore, HMPC-2 is the most promising structure as it generally outperforms HMPC-1 in both control performance and computation time. Moreover, HMPC-2 appears to be better applicable for shorter control time steps than HMPC-1, as the results do not appear to improve significantly when larger horizons are considered.

This is explainable by looking at the main problem of HMPC-1 that occurs when all input signals are re-optimized on a short N_p. Then, the NLMPC slave prefers ventilation over shading to control T_z, since the inner zone transient response via ventilation is faster. However, the blinds have a significant effect over the long period, due to their influence on thermal mass, benefiting future situations. For example, HMPC-1 may prioritize ventilation to cool T_z during a semi-warm day. However, when a warm day follows, a better solution might have been to close the blinds and decrease the ventilation. This is a typical scenario that may occur when the blind control inputs are re-optimized on little future disturbance knowledge. HMPC-2 solves this problem by assuming that the building's thermal response due to solar irradiance is relatively slow and therefore less sensitive to linearizations. Hence, the blind control inputs can be optimized by the LMPC agent on a large N_p^* with much disturbance knowledge. Then, the re-optimized ventilation control input can prevent small thermal errors on the short-term. This ensures the preservation of high control performance for the short period, while the re-optimization is solved faster by *fmincon* as only one input type is optimized.

Table 3-6 shows a percentage comparison between the four structures, each with a well-performing prediction horizon, simulated over a 200-day period in spring, summer, and autumn. These results are consistent with the result analysis of the 40-day simulation period.

Architecture	N_p	$\sum e^2$ [K^2]	$\sum e$ [K]	t_op [s]
NLMPC	8	1736	882	30.6
LMPC	24	-20.9%	+3.7%	-99.4%
HMPC-1	4^a	-20.7%	-10.0%	-78.6%
HMPC-2	4^a	-22.7%	-12.4%	-92.5%

Table 3-6: $^a N_\mathrm{p}^*$ is 24 for the linear agent controller.

3-2-6 State-update estimation

HMPC-2 outperforms the other structures in terms of maximum control performance with a minimum computational load. However, the conducted simulations are based on full state knowledge. This is not realistic as not all states are measurable in the CCC-building. Moreover, in general buildings, usually, only the indoor temperature is known. Therefore, a Kalman filter is added to the HMPC-2 structure. Kalman filters use data of measurable states to estimate the values of the immeasurable states. By adding the filter, two extensions of the

HMPC-2 structure are developed. They are referred to as HMPC-2a and HMPC-2b. The development of the Kalman filter and the two HMPC-2 extensions are discussed further below.

Kalman filter

Various Kalman filters can be considered for state estimation of the nonlinear dynamical plant [51]. Nonlinear Kalman filters, e.g., extended, unscented, or ensemble, are able to estimate the states of nonlinear systems. However, analyzing these filters is an entire thesis study and therefore beyond the scope of this thesis. Hence, a linear Kalman filter is included in the structure and the results appeared to be more than sufficient. The algorithm for producing the state estimation update $\hat{x}_{\text{est}}(k|k)$ in the Kalman filter is presented below.

Algorithm 3 State-update in Kalman filter **MATLAB**

Input: $\hat{x}_{\text{mod}}(k|k-1)$, $y_{\text{p}}(k)$, $w(k-1)$, $v(k)$, $\mathcal{A}_{\text{k-1}}$, $\mathcal{B}_{\text{k-1}}$, $\mathcal{C}$
Output: $\hat{x}_{\text{est}}(k|k)$
Procedure:
$r \leftarrow \textbf{obsv}(\mathcal{A}_{\text{k-1}}, \mathcal{C})$
$Rank \leftarrow \textbf{rank}(r)$
$States \leftarrow \textbf{length}(\hat{x}_{\text{mod}}(k|k-1))$
if $Rank < States$ **then**
'Current system is not fully observable'
end if
$\mathcal{Q}_{\text{k-1}} \leftarrow w(k-1)^2$
$\mathcal{R}_{\text{k}} \leftarrow v(k)^2$
$\mathcal{P}_{\text{k|k-1}} \leftarrow \mathcal{B}_{\text{k-1}} \mathcal{Q}_{\text{k-1}} \mathcal{B}_{\text{k-1}}^T$
$\mathcal{K}_{\text{k}} \leftarrow \mathcal{P}_{\text{k|k-1}} \mathcal{C}^T (\mathcal{C} \mathcal{P}_{\text{k|k-1}} \mathcal{C}^T + \mathcal{R}_{\text{k}})^{-1}$
$\hat{x}_{\text{est}}(k|k) \leftarrow \hat{x}_{\text{mod}}(k|k-1) + \mathcal{K}_{\text{k}}(y_{\text{p}}(k) - \mathcal{C}\hat{x}_{\text{mod}}(k|k-1))$
return $\hat{x}_{\text{est}}(k|k)$

Before employing this algorithm, the optimized control signals are applied in the simplified nonlinear model to predict the next-step states $\hat{x}_{\text{mod}}(k|k-1)$ and obtain the time step-dependent nonlinear state-space matrices $\mathcal{A}_{\text{k-1}}$ and $\mathcal{B}_{\text{k-1}}$, without considering the white-noise process and sensor disturbances, $w(k-1)$ and $v(k)$. The same control signals are simulated in the nonlinear plant model considering both the white-noise process and sensor disturbances so that the real system's measured output $y_{\text{p}}(k)$ is more closely approximated. Note that the system should be observable, which can be realized by positioning sensors on various state components. The sensor locations are described by output matrix $\mathcal{C}$, which is used to test the system's observability. Many combinations of 8 measured states appeared to be sufficient for the system to be observable. There may exist a more optimal sensor combination that allows full observability. However, such research is beyond the scope of this thesis.

Separating the state-update loops

The HMPC-2 extensions differ by assuming that the updated states for the NLMPC controller do not necessarily have to be shared with the LMPC agent. The agent controller functions as a reference trajectory optimizer and thermal controller in view of the long period. Therefore,

it benefits less from the estimated state-update by the Kalman filter than the slave controller, which aims for short period accuracy. The state-update for the LMPC agent can come from the linearized model in the upper layer. Then, the HMPC-2b's feedback is structured differently, as presented in Figures 3-17 and 3-18. According to Table 3-7, HMPC-2b slightly outperforms HMPC-2a. Therefore, the HMPC-2b structure is considered in the case study.

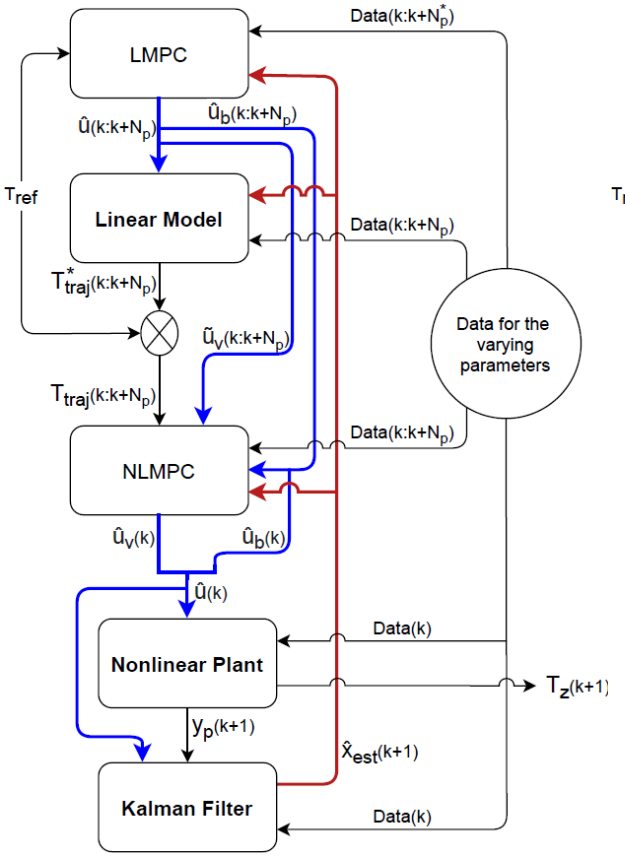

Figure 3-17: HMPC-2a structure flowchart.

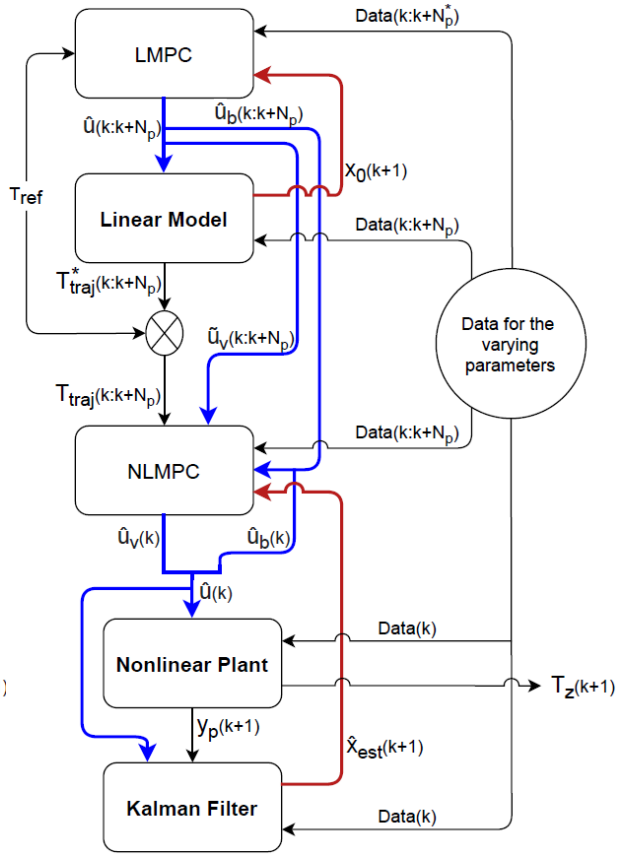

Figure 3-18: HMPC-2b structure flowchart.

	HMPC-2a						HMPC-2b					
Δt	$3600\,\mathrm{s} \rightarrow N_\mathrm{p}^* = 24$			$1800\,\mathrm{s} \rightarrow N_\mathrm{p}^* = 48$			$3600\,\mathrm{s} \rightarrow N_\mathrm{p}^* = 24$			$1800\,\mathrm{s} \rightarrow N_\mathrm{p}^* = 48$		
N_p	2	4	8	2	4	8	2	4	8	2	4	8
$\sum e^2[\mathrm{K}^2]$	210	204	200	208	204	200	202	197	195	199	196	192
$\sum e[\mathrm{K}]$	137	135	136	131	129	128	134	133	138	127	126	127

Table 3-7: Results of the HMPC-2 extensions for a 40-day simulation period.

3-3 Multi-objective control problem

The final step in the control system development is to add an auxiliary energy control signal so that thermal comfort is always achievable. In this way, a multi-objective optimization problem arises in which a conflict occurs between thermal comfort and energy consumption. For the LMPC agent controller, such a multi-objective problem is inevitable, because the control

performance of the hierarchical structure is highly dependent on the optimized reference temperature trajectory. The trajectory should therefore contain the information of additional auxiliary energy. For the NLMPC slave controller, a multi-objective problem only occurs when the auxiliary energy control signal is selected to be re-optimized.

A similar strategy as presented before can be applied, in which this control input is only optimized in the LMPC agent and provided as a non-optimizable parameter to the NLMPC slave and nonlinear plant. However, it was decided to re-optimize the auxiliary energy control signal in the slave controller, because this input, like the ventilation, quickly and directly influences the inner zone's state. This achieves a higher control performance, but the controller's computational cost will deteriorate from this. The following two subsections clarify the methods to deal with the multi-objective functions. The final MPC framework is applied in the case study and provided in Section 4-1-3.

3-3-1 ϵ-constraint method

For the LMPC agent, the ϵ-constraint method is applied to handle the multiple objectives. The LMPC optimization problem is modified so that the thermal comfort objective is omitted from the objective function and included as a constraint. Thermal comfort is then forced to be achieved during occupied hours by setting inequality constraints on the inner zone's state. The inequality constraints denote that the system output may only differ 0.2 K from T_{ref} during t_{occ}. The remaining function is of the single-objective type, in which only the control inputs are penalized. This method works well for LMPC since the calculation time of *quadprog* does not increase significantly when using such linear inequality state constraints. However, for *fmincon*, the computation time significantly deteriorates when the model's output is limited by nonlinear constraints. Therefore, this method is not applied in the NLMPC controller.

3-3-2 Pareto front construction

A common strategy for nonlinear MPC is to determine weighting values that indicate the trade-off point between the conflicting objectives. The challenge is to determine the weights for the desired trade-off point among all other possible points. This can be obtained by constructing the Pareto front of the optimization problem and selecting the optimal trade-off point. However, these fronts vary greatly for each problem, as the optimization problems differ per time step. MATLAB functions *gamultiobj* and *paretosearch* of the Global Optimization Toolbox were used to construct these 'local' Pareto fronts and to select desired trade-offs for each NLMPC problem. However, this was too computationally expensive, as this method was performed at every simulation step. Therefore, another strategy is applied for the NLMPC controller. A 'global' Pareto front construction, presented in Figure 3-19, is performed in which the trade-off points contain the information of a simulation period of 20 days instead of one time step. For this front, the standard deviation (SD) of the temperature error set and the required auxiliary energy of each simulation period are analyzed. A maximum standard deviation of 0.25 K is selected, such that 95% of all errors are within 0.5 K, assuming the error set e to be a normal distribution. The selected Pareto point is determined by considering both the Pareto front and corresponding computation times, shown in Figure 3-20. Hence, the corresponding $\mathcal{Q}$ and $\mathcal{R}$ weighting values, presented in Section 4-1-3, are the optimized values that contribute globally to the desired control performance.

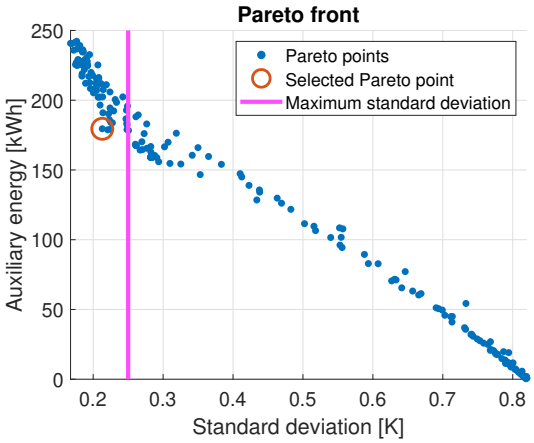

Figure 3-19: 200 Pareto trade-off points.

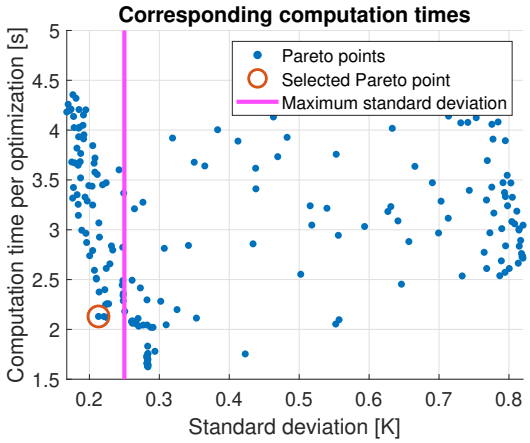

Figure 3-20: Mean computational costs.

3-4 Conclusions

In this chapter, the development methodology of the best-performing MPC architecture is provided. This is done by assessing multiple control architectures under varying control horizons and circumstances. To equally compare all control structures, three models are developed: the nonlinear plant model that serves as a simulation testbed, the simplified nonlinear model for the nonlinear optimization problem, and the linear model for the quadratic optimization problem. To better understand the optimization complexity of the two types of problems, a convexity analysis has been carried out. The linear optimization problems appear to be convex, as the Hessian matrix is under all tested conditions positive definite. For the nonlinear optimization problems, the non-convexity of those problems has been analyzed by mapping some solution spaces and evaluating multi-start. Applying multi-start turned out to be redundant, given the extra computational costs of executing multi-start.

Subsequently, a systematic comparison strategy is applied that will lead to the best-performing architecture. Firstly, the control performances of the centralized linear and nonlinear MPC controllers, which only consider passive energy sources for achieving thermal comfort, are analyzed. The NLMPC structure appears to be more accurate than the LMPC structure. However, centralized NLMPC seems impractical for on-line application. Hereafter, two hierarchical structures, which combine the main advantages of the linear and nonlinear MPC controllers, are developed and compared. Both structures are suitable for on-line control, but the HMPC-2 structure outperforms the HMPC-1 structure in terms of control performance and computation time. Namely, because the HMPC-2 structure divides the optimization of the control signal between two controllers and makes better use of future knowledge in its optimizations. As third, a linear Kalman filter is adopted and a new comparison is made between two structures that differ in their state-update locations.

Finally, the HMPC-2b structure appears to be the best-performing architecture to control the passive energy sources. Therefore, this structure is extended with an auxiliary energy source and its objective functions are rewritten, so that thermal comfort is always achievable while the active energy consumption is minimized. To cope with the multi-objective functions that have arisen, techniques, such as the Pareto front construction and the ϵ-constraint method, are applied. The final form of the HMPC-2b structure is employed in the case study.

Chapter 4

Case Study

To complete the thesis, a case study is included. This case study is conducted to find out whether the developed nonlinear plant model is indeed able to capture real-case thermodynamics in a building and if the HMPC-2b structure can maintain similar control performances in a more real-case scenario. First, the design of the case study is presented in Section 4-1. Hereafter, the case study results are provided in Section 4-2. Finally, the conclusions of this chapter are given in Section 4-3.

4-1 Case study details

The sensor measurements and rule-based controller of the CCC-building are used to evaluate the performances of the developed white-box model and MPC architecture. To compare the two controllers, it is essential to have a plant model that is accurate to the actual building. Therefore, the accuracy of the plant model should be analyzed and improved if necessary. Interesting is to analyze the improvements of the model and what the impact is by these model changes on the control performance. In this way, insight can be gained into the effects on the use of other materials or component geometry in such a building, as different material properties and component sizes lead to different control performances. Such a control structure can then contribute to optimizing the building design for passive energy harvesting.

However, this would only be a side-result as the main research question has not been answered until the HMPC-2b structure has proven to be on-line applicable and to reduce the building's energy consumption while maintaining thermal comfort. Therefore, a case study setup that ensures a fair comparison between the currently implemented rule-based controller and the developed HMPC-2b structure is proposed in this section.

4-1-1 Model validation setup

To get a good indication of how well the proposed control structure works on a real-case building, the applied white-box modeling methodology is validated using the field measurements of the CCC-building. The validation setup is realized by applying the following process.

What is measured

The aim is to validate the part of the white-box model that denotes the building's thermal response to the outdoor climate. This includes the heat transfer expressions between the different components and the solar irradiance expressions for modeling the Sun's impact. The ventilation system is not considered in the validation strategy, as the present ventilation system is not based on the working principle of a thermal chimney. Initially, it was the intention to use a buoyancy-driven thermal chimney for the CCC-building. However, due to the choice of a different chimney design, with the placement of fans, PCM, and heat exchangers, the system's friction dominates the natural airflow. Nevertheless, this thesis deals with the original design of the thermal chimney, as its dynamics have already been validated using CFD. Therefore, temperature changes in the CCC-building due to ventilation should be avoided during the measurement period. Moreover, all additional heat sources, i.e., occupancy and active energy sources, are disregarded as well. By omitting these sources, the validation method is focused on the building's response to the outdoor climate. Three practical actions are taken during the measurement period that comply with the proposed validation strategy:

- The solar blinds are open during the entire measurement period;
- The ventilation system is turned off and all windows and doors are kept closed;
- The heat pump and lights are switching off and no occupants are allowed;

When is it measured

Two measurement periods are completed in the spring, a 10-day period at the beginning of April and a 3-day period at the end of May. The spring period has the advantage that the weather can vary from day to day, but the solar irradiance is already quite strong. This results in some arbitrariness in ambient temperatures and cloud formation, while the sun has a large and steady impact on the building during clear skies.

How is it measured

Input and state data with a 5 minute sampling time is obtained by means of 41 sensors of the CCC-building. 35 sensors are applied to observe 8 components. This includes 3 sensors for the inner zone, 4 for the ceiling, 2 for each of the north, east, and west-facing interior glazed walls, 4 for the south-facing interior glazed wall, 9 for the raised floor, and 9 for the basement floor. The sensors per state are strategically distributed over the component. Therefore, averages of all sensor data per component are taken to estimate the mean temperature of each observed state. With this data, 8 states of the nonlinear plant model can be validated and the accuracy of the proposed white-box modeling methodology can then be verified.

To validate the model, climate data during the testing period is required as well. 6 sensors are applied to measure the local environmental climate. Of this, 5 sensors are incorporated in the weather station, which measures the ambient temperature, wind speed, air pressure, relative humidity, and average global irradiance. Besides the weather station, 1 sensor independently determines the ambient temperature. This provides a good indication of a part of the local climate during the testing period. However, no DNI and DHI sensors are used to measure the direct beam and diffused horizontal solar irradiances. Only the global irradiance is measured.

The global irradiance is easily determinable by means of the direct beam and diffused horizontal irradiances. However, these two irradiance types are required for the model and splitting the global irradiance accurately into DNI and DHI data is challenging. This problem is solved by using the empirical irradiance-splitting model of Reindl in the software program TRNSYS [11]. This model requires the data of the global irradiance, ambient temperature, and relative humidity to estimate the DNI and DHI values. However, the accuracy of the two estimated data types is questionable as these empirical splitting models are known to be not consistently accurate. In addition, the splitting models do not consider any surrounding obstacles, e.g., trees and adjacent buildings. Hence, a certain level of inaccuracy of the model inputs could lower the validation performance.

4-1-2 Control case formulation

The case study is primarily focused on the control performance of the final MPC architecture. Contrary to all previous analyses, this MPC architecture framework considers multi-objective control problems in which auxiliary energy is used to ensure thermal comfort. Thermal comfort is defined in this thesis as 293.15 K and the error set e determines how well thermal comfort is achieved. However, it is unrealistic and impractical to strive for perfect thermal comfort, since there will always be model mismatches between the predictive model and the plant. Therefore, the control performance in terms of the amount of required auxiliary energy and the standard deviation of the error set are both selected to be assessed. The latter would indicate that 95% of all temperature errors are less than the doubled standard deviation, assuming the error set is naturally distributed.

In the previous chapter, the maximum allowed standard deviation was set at 0.25 K, which is considered again in the case study analysis. In this case study, the amount of required auxiliary energy by the HMPC-2b structure will be compared with an experimental benchmark. The benchmark value is the amount of kWh that the CCC-building needed to consume to achieve thermal comfort during a 13-day field experiment. From May 3 to May 15, a rule-based controller was applied to realize thermal comfort by means of similar controllable devices as considered in this thesis. To validly compare the experimental benchmark with the HMPC-2b's performance, ten parameters of the nonlinear plant model are optimized such that the resulting grey-box model better represents the CCC-building. After this optimization, elaborated further in the next section, the same parameters are adjusted in the linear and nonlinear prediction models. Therefore, a new control performance comparison is performed in which the MPC frameworks stay the same but the prediction and plant models differ. This leads to interesting results as the optimized parameters are basically better property values for the real-case components. By changing the material or dimension values, the control performance will be altered. In this way, the developed MPC framework can serve as a tool to optimize the selection of component materials and geometry that would benefit such control strategies.

Firstly, the next section compares the initial white-box models with the grey-box models, both applied in the same MPC framework. For this comparison, hourly TMY data of a year and the occupancy set of Table 3-2 are considered. Hereafter, the MPC framework with the optimized prediction and plant models is simulated and assessed, using the climate data measured by the CCC-building sensors during the 13-day field experiment. During this experimental period, occupancy in the CCC-building is imitated by 6 electric heaters of 500 W each. With this,

30 occupants are simulated between 9 a.m. and 5 p.m. for weekdays only. Another difference with previous analyzes is that thermal comfort is set between 294.15 and 298.15 K. This new occupancy schedule and temperature reference bounds are therefore considered during the comparison of the rule-based controller and the final HMPC-2b structure.

4-1-3 MPC framework

To finalize the HMPC-2b structure, an essential addition is done to the MPC framework that is provided in Figure 3-18. The auxiliary energy input is added to allow the MPC controllers to add or remove an optimal amount of energy to or from the system. This energy input is limited between ±10 kW since an industrial heat pump should easily have such heating and cooling capacity. Furthermore, the two objective functions are changed to cope with the emerged multi-objective problem. These modifications are realized according to the ϵ-constraint method and the Pareto front construction. Note that for the quadratic optimization problem only the inputs are penalized and the output constraints are defined to ensure thermal comfort. In addition, in the nonlinear objective function, specific penalizing values are given to the $\mathcal{Q}$ and $\mathcal{R}$ matrices so that the maximum standard deviation is not exceeded. The full exposition of the final MPC framework is provided below.

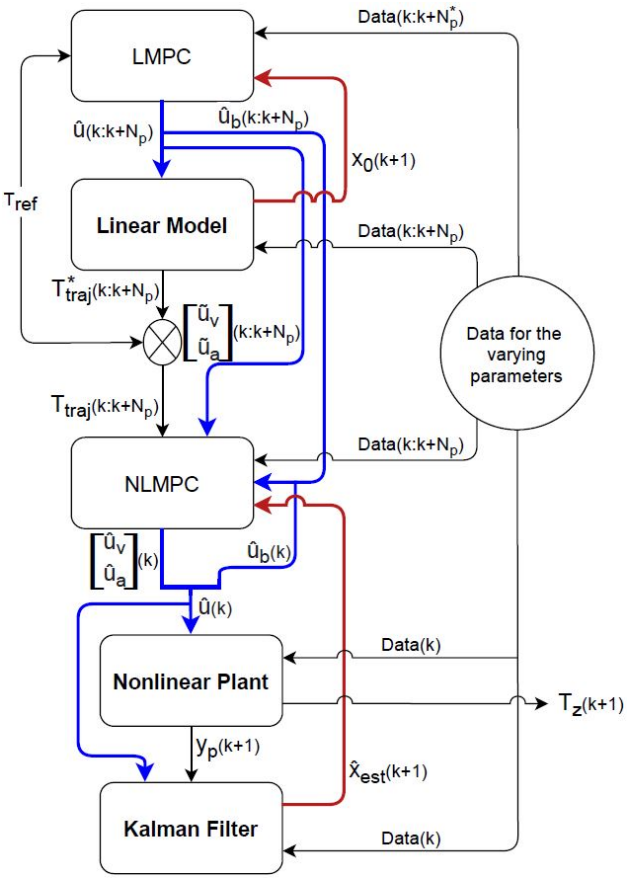

Figure 4-1: Final HMPC-2b structure flowchart.

The final quadratic optimization problem for the linear MPC agent is described as:

$$\min_{U \triangleq u(k),\ldots,u(k+N_{\mathrm{p}}^{*}-1)} \sum_{i=0}^{N_{\mathrm{p}}^{*}-1} (u(k+i)-u_{\mathrm{ref}})^{T}\mathcal{R}(u(k+i)-u_{\mathrm{ref}}) \tag{4-1}$$

$$\begin{aligned}
\text{s.t.} \quad & 0 \leq u_{\mathrm{v}}(k+i) \leq 1, && i \ni \{0,...,N_{\mathrm{p}}^{*}-1\}\\
& 0 \leq u_{\mathrm{b}}(k+i) \leq 1, && i \ni \{0,...,N_{\mathrm{p}}^{*}-1\}\\
& -10^{4} \leq u_{\mathrm{a}}(k+i) \leq 10^{4}, && i \ni \{0,...,N_{\mathrm{p}}^{*}-1\}\\
& 292.95 \leq T_{\mathrm{z}}(k+i) \leq 293.35 \ \Rightarrow\ k+i \in t_{\mathrm{occ}}, && i \ni \{0,...,N_{\mathrm{p}}^{*}\}\\
& 273.15 \leq T_{\mathrm{z}}(k+i) \leq 313.35 \ \Rightarrow\ k+i \notin t_{\mathrm{occ}}, && i \ni \{0,...,N_{\mathrm{p}}^{*}\}\\
& u_{\mathrm{ref}} = [0,1,1,1,1,0]^{T} &&\\
& x(k+i+1) = \mathcal{A}(p(k+i))x(k+i) + \mathcal{B}(p(k+i))u(k+i) + \mathcal{E}d(k+i), && i \ni \{0,...,N_{\mathrm{p}}^{*}-1\}\\
& T_{\mathrm{z}}(k+i) = \mathcal{C}x(k+i), && i \ni \{0,...,N_{\mathrm{p}}^{*}\}\\
& x(k+i) = x_{0}, && i = 0\\
& \mathcal{R} = \mathbf{diag}(3, 0.1, 0.1, 0.1, 0.1, 100) &&\\
& x(k+i) \in \mathbb{X}^{17}, && i \ni \{0,...,N_{\mathrm{p}}^{*}\}\\
& u(k+i) \in \mathbb{U}^{6}, && i \ni \{0,...,N_{\mathrm{p}}^{*}-1\}\\
& d(k+i) \in \mathbb{D}^{1}, && i \ni \{0,...,N_{\mathrm{p}}^{*}-1\}\\
& T_{\mathrm{z}}(k+i) \in \mathbb{Y}^{1}, && i \ni \{0,...,N_{\mathrm{p}}^{*}\}
\end{aligned}$$

The final nonlinear optimization problem for the nonlinear MPC slave is described as:

$$\min_{U \triangleq u(k),\ldots,u(k+N_{\mathrm{p}}-1)} \sum_{i=1}^{N_{\mathrm{p}}} \mathcal{Q}\,(T_{\mathrm{z}}(k+i) - T_{\mathrm{traj}}(k+i))^{2} + \mathcal{R}\,u_{\mathrm{a}}(k+i-1)^{2} \tag{4-2}$$

$$\begin{aligned}
\text{s.t.} \quad & 0 \leq u_{\mathrm{v}}(k+i) \leq 1, && i \ni \{0,...,N_{\mathrm{p}}-1\}\\
& -10^{4} \leq u_{\mathrm{a}}(k+i) \leq 10^{4}, && i \ni \{0,...,N_{\mathrm{p}}-1\}\\
& T_{\mathrm{traj}}(k+i) = \begin{cases} 293.15, & k+i \in t_{\mathrm{occ}} \\ T^{*}_{\mathrm{traj}}(k+i), & k+i \notin t_{\mathrm{occ}} \end{cases} && i \ni \{1,...,N_{\mathrm{p}}\}\\
& x(k+i+1) = f(x(k+i), u(k+i), p(k+i)) + \mathcal{E}d(k+i), && i \ni \{0,...,N_{\mathrm{p}}-1\}\\
& T_{\mathrm{z}}(k+i) = \mathcal{C}x(k+i), && i \ni \{1,...,N_{\mathrm{p}}\}\\
& x(k+i) = \hat{x}_{\mathrm{est}}, && i = 0\\
& \mathcal{Q} = 0.8 &&\\
& \mathcal{R} = 7.5\times10^{-9} &&\\
& x(k+i) \in \mathbb{X}^{17}, && i \ni \{0,...,N_{\mathrm{p}}\}\\
& u(k+i) \in \mathbb{U}^{2}, && i \ni \{0,...,N_{\mathrm{p}}-1\}\\
& d(k+i) \in \mathbb{D}^{1}, && i \ni \{0,...,N_{\mathrm{p}}-1\}\\
& T_{\mathrm{z}}(k+i) \in \mathbb{Y}^{1}, && i \ni \{1,...,N_{\mathrm{p}}\}
\end{aligned}$$

4-1-4 CPU specifications

All simulations are performed on an HP ZBook Studio x360 G5. This device has an Intel Core i7-8750H processor and 16 GB of RAM. MATLAB R2019b is applied as simulation environment and all optimization problems are solved by functions of the Optimization Toolbox.

4-2 Case study results

4-2-1 Validation results

The previously discussed validation setup is applied to evaluate the proposed white-box modeling methodology. However, one change was made to the original model prior to validation. Due to the fact that the irradiance-splitting model of Reindl does not consider surrounding obstacles, a major output error occurred during each late afternoon. This error was caused by the fact that trees and large buildings on the west-side of the CCC-building affect the incoming solar irradiance. The error was significantly reduced when a rule was added to the model that omits the direct beam irradiation after 5 p.m. The validation results of 8 states of the two periods are provided in Tables 4-1 and 4-2. Figures 4-2 and 4-3 present the inner zone temperature comparison between the CCC-building and the nonlinear plant model.

State	T_z	T_c	T_{rf}	T_{bf}	$T_{n,3}$	$T_{e,3}$	$T_{s,3}$	$T_{w,3}$
VAF	91.2	92.3	40.1	75.1	92.2	90.6	78.1	87.1
NRMSE	0.14	0.12	0.37	0.26	0.07	0.10	0.14	0.09

Table 4-1: White-box model validation results: April 2 to 11.

State	T_z	T_c	T_{rf}	T_{bf}	$T_{n,3}$	$T_{e,3}$	$T_{s,3}$	$T_{w,3}$
VAF	88.5	85.4	42.1	0.00	93.2	90.6	80.6	70.0
NRMSE	0.09	0.10	0.39	0.61	0.11	0.09	0.11	0.14

Table 4-2: White-box model validation results: May 22 to 24.

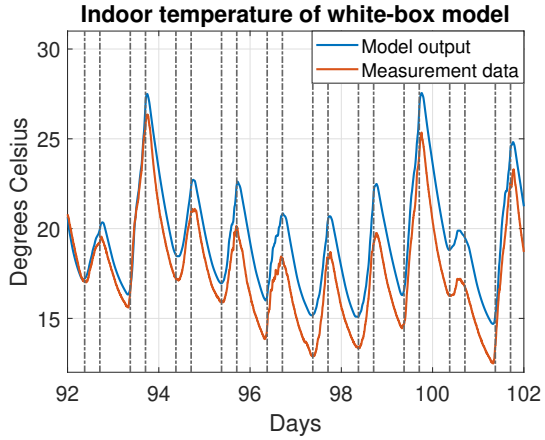

Figure 4-2: Validation on 10-day period.

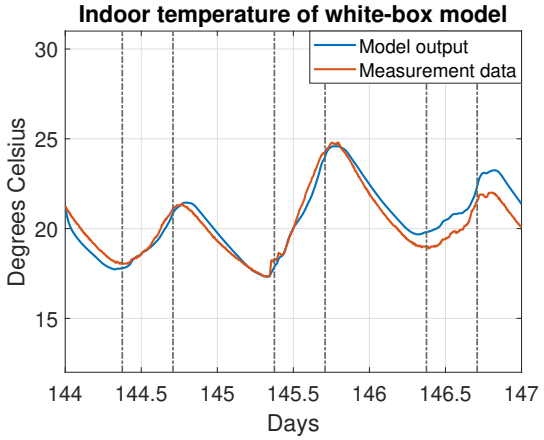

Figure 4-3: Validation on 3-day period.

Many model parameters are determined by means of architectural drawings and the database GRANTA EduPack. However, practice often tends to differ from theory. Some modeled components appeared to be better at capturing real thermodynamics than others. For instance, the raised floor and basement floor states show poor validation results. However, these states are less relevant, as the prime factor for good real-case control is the accuracy of the inner zone state. Although the validation results of the inner zone and several other components seem promising, a grey-box identification process has been performed. For this, ten model parameters are selected to be re-optimized on training data. As training data, the data from the 10-day measurement period in April is selected. The resulting model is tested on validation data of the 3-day measurement period in May. Both training and validation results are provided in Tables 4-3 and 4-4. Figures 4-4 and 4-5 present the inner zone temperature comparison between the CCC-building and the optimized nonlinear plant model. In addition, the optimized values of the selected parameters are provided in Table C-3 in Appendix C.

State	T_z	T_c	T_{rf}	T_{bf}	$T_{n,3}$	$T_{e,3}$	$T_{s,3}$	$T_{w,3}$
VAF	95.8	94.7	81.1	95.9	95.7	96.3	89.5	91.6
NRMSE	0.05	0.05	0.15	0.07	0.07	0.05	0.07	0.06

Table 4-3: Grey-box model validation results on training data: April 2 to 11.

State	T_z	T_c	T_{rf}	T_{bf}	$T_{n,3}$	$T_{e,3}$	$T_{s,3}$	$T_{w,3}$
VAF	93.8	87.2	76.9	89.4	95.8	95.6	89.3	83.47
NRMSE	0.10	0.10	0.16	0.09	0.16	0.12	0.10	0.11

Table 4-4: Grey-box model validation results on validation data: May 22 to 24.

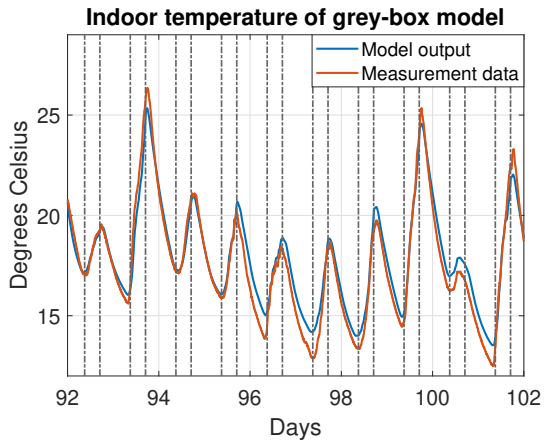

Figure 4-4: Training on 10-day period.

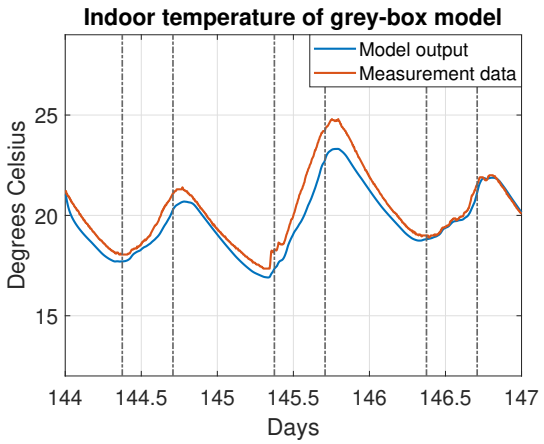

Figure 4-5: Validation on 3-day period.

4-2-2 Control performance of grey-box model

In the grey-box model, several parameters have been adjusted, as shown in Table C-3. The main difference between the original and optimized model is that the latter is less capable of harvesting solar energy, as the solar irradiance absorptance and effective optical transparency are significantly reduced. This presumably leads to lower control performance, as the energy

demand will increase to maintain thermal comfort. By analyzing this hypothesis, insight can be gained into optimal passive designs for offices with features like the CCC-building.

To evaluate the hypothesis, the grey-box model is compared to the initial white-box model. As previously mentioned, the same MPC framework with an N_p^* of 24, N_p of 4, and hourly control sampling time is used for both models. In addition, the TMY data of 200 consecutive days and the occupancy schedule of Table 3-2 are applied in the simulations and no objects surrounding the building are taken into account. Thus for this comparison, the rule that omits the direct beam irradiation after 5 p.m. is disregarded. Table 4-5 provides the results of this comparison. Note that this comparison is focused on other control characteristics besides the converging performance towards thermal comfort. The ventilated air mass and the total consumed auxiliary energy are both also examined. Furthermore, the total time that the solar blinds have been employed for thermal regulation is also analyzed. This total period is expressed as the sum of usage hours per blind. Note that the maximum use of blinds is 19200 hours since the simulation period is 4800 hours and 4 blinds are considered.

Control performance comparison	White-box model	Grey-box model
$\sum e^2$ [K^2]	67	64
$\sum e$ [K]	232	223
SD [K]	0.222	0.224
t_{op} [s]	1.87	1.83
Ventilated air mass [kg]	5003300	4802900
Total solar blind usage [h]	5842	5350
Energy [kWh]	1626	1830

Table 4-5: Model comparison on 200-day period, using the HMPC-2b scheme.

The results in Table 4-5 show that the white-box model is better in harvesting passive energy. Although the sums of the two error sets are higher, this model outperforms the grey-box model in maintaining thermal comfort as the standard deviation of the error set is slightly lower. The HMPC-2b structure with the white-box model achieves this standard deviation by making more use of passive energy source control and using less auxiliary energy. Applying the gray-box model results in 8.4% less use of the blinds and 4% less air ventilation, while consuming 12.5% more auxiliary energy. However, the output of the grey-box model better reflects what would actually happen, as the model is optimized on the current CCC-building. Therefore, this model is employed in the last case study comparison to solve the main research question. Still, these side-results indicate the effect of optimal passive design during construction. Good passive design decisions, such as integrating more thermal mass or using a floor with a higher solar absorptance value, can then benefit this building's control performance.

4-2-3 Control comparison with rule-based controller

This final comparison will indicate if the advanced HMPC-2b structure is able to outperform the rule-based controller that currently is applied as BEMS. To validly compare the two controllers, the grey-box models are applied in the HMPC-2b structure and the direct beam irradiation is omitted after 5 p.m. In this analysis, the reference temperature is set at 294.15 K, as this value was also considered by the rule-based controller. Furthermore, the simulation

is run with the same occupancy schedule and climate input from the 13-day testing period. Note that the measured climate data has a 5 minute sampling time. Therefore, the control time step is reduced from hourly steps to steps of 30, 20, and 15 minutes. Even smaller control steps are possible, but changing some actuators, such as the blinds, each 5 to 10 minutes is assumed to be unpleasant and thus undesired. To analyze the performance, multiple control time steps and prediction horizons are evaluated and presented below in Table 4-6.

Δt	$1800\,\text{s} \rightarrow N_\text{p}^* = 48$			$1200\,\text{s} \rightarrow N_\text{p}^* = 72$			$900\,\text{s} \rightarrow N_\text{p}^* = 96$		
N_p	4	6	8	6	9	12	8	12	16
$\sum e^2$ [K^2]	5.5	4.5	4.2	5.3	4.7	4.5	5.3	4.8	4.6
$\sum e$ [K]	14.4	13.3	12.9	13.2	12.7	12.5	13.4	12.6	12.3
SD [K]	0.254	0.237	0.237	0.255	0.249	0.250	0.259	0.253	0.257
t_op [s]	2.09	4.94	11.8	5.40	14.1	30.2	9.25	27.4	60.6
Energy [kWh]	113	117	119	109	112	114	109	114	115

Table 4-6: Results of the HMPC-2b structure for a 13-day field experiment period.

The evaluation shows that the results do not differ much. It seems that the standard deviation does not improve significantly when larger horizons are considered, as is in line with the result observation in Section 3-2-5. Nevertheless, the control time step of 20 minutes and the nonlinear prediction horizon of 9 lead to the desired results. Therefore, the following figures represent the control performance and input signals of the HMPC-2b structure with these control parameters during the 13-day field experiment period. Hereafter, the control performance and the ventilation inputs signals of the rule-based controller are provided.

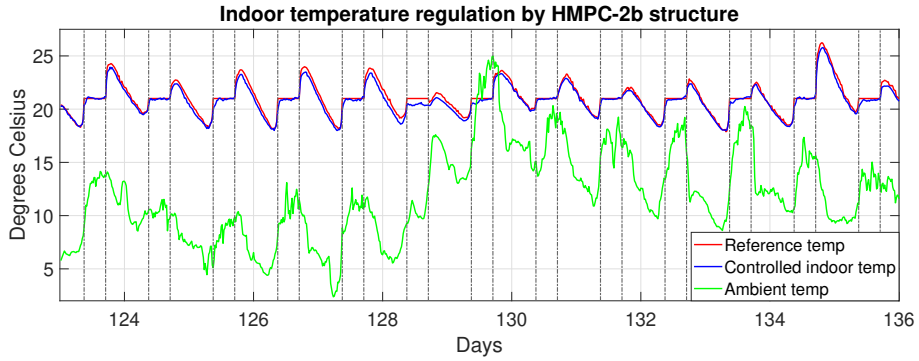

Figure 4-6: 13-day progression of T_z: $N_\text{p}^* = 72 \wedge N_\text{p} = 9$.

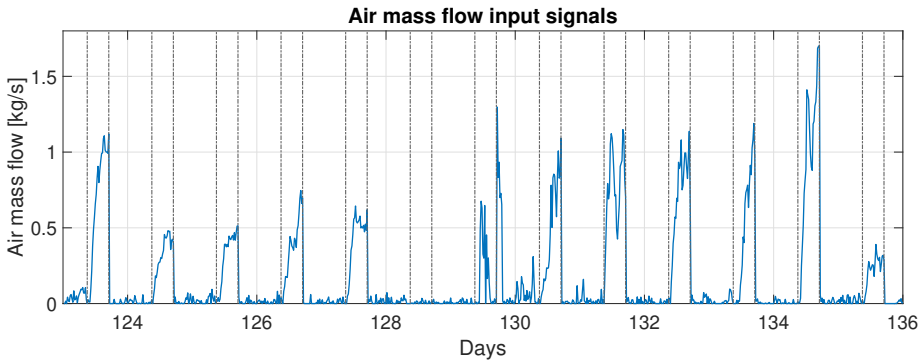

Figure 4-7: Supplied air through natural ventilation.

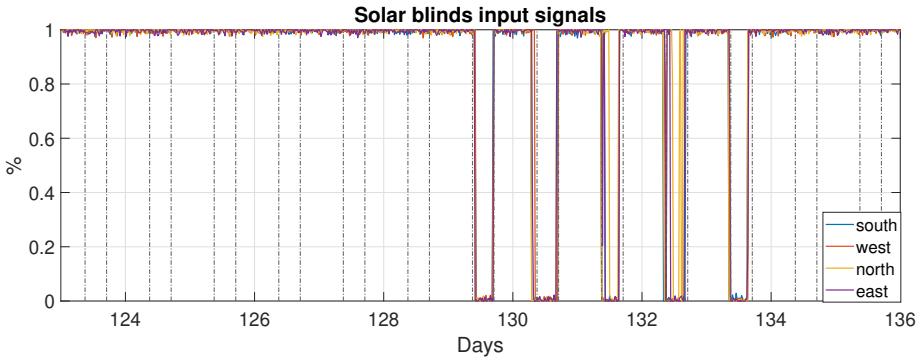

Figure 4-8: States of the 4 blinds to control solar irradiance.

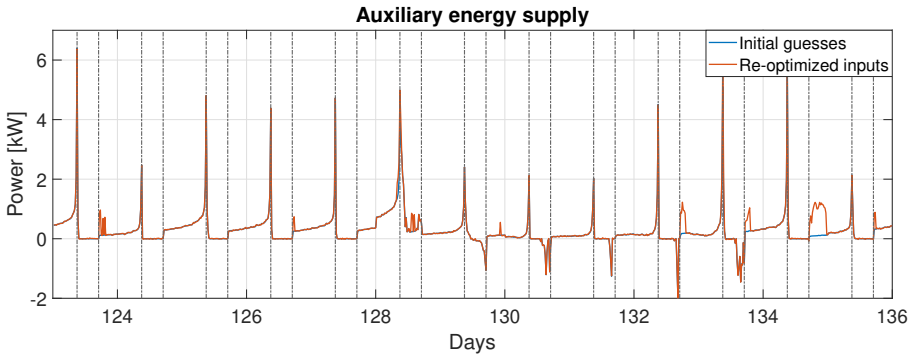

Figure 4-9: Auxiliary energy supply to ensure thermal comfort.

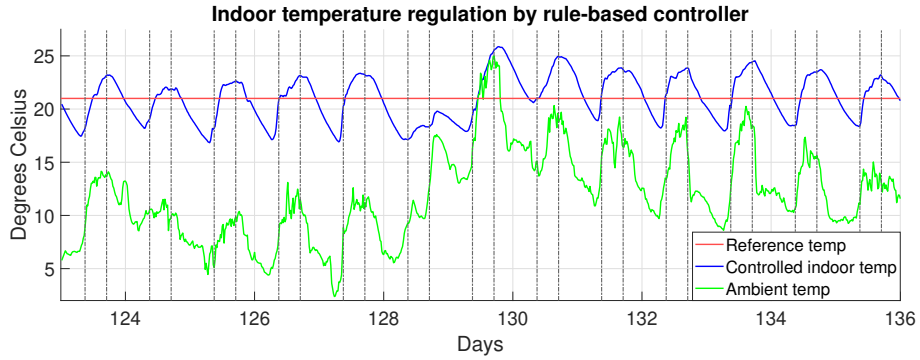

Figure 4-10: 13-day progression of the measured T_z of the CCC-building.

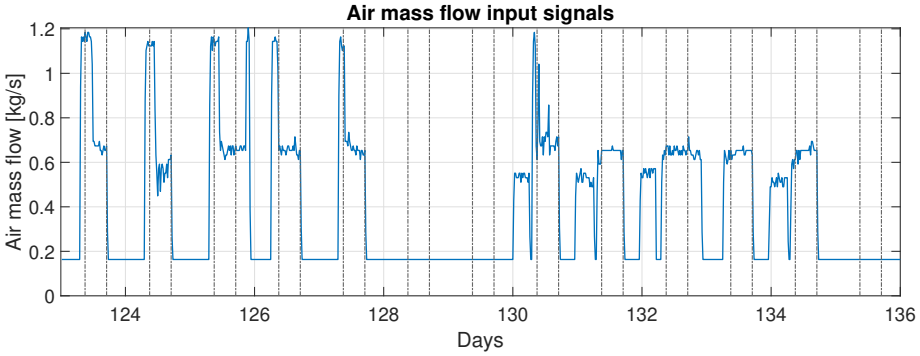

Figure 4-11: Supplied air through fans.

The first four figures indicate that thermal comfort is well achieved by the HMPC-2b structure. The blinds are applied during warmer days and auxiliary energy is mainly supplied during the night. The latter occurs since this control structure considers hard constraints for all occupied hours. In the morning, only auxiliary energy can be applied to achieve this constraint. In the later hours, the energy gain due to occupancy and the Sun is often sufficient in this climate period. Furthermore, natural ventilation is often applied to cool the building down during the day, but the air supply only benefits thermal comfort and not IAQ. According to ASHRAE Standard 62.1-2019 [28], 2.5 to 5 l/s per person is required in offices. Assuming the latter, at least 0.19 kg/s should be applied during occupied hours for this occupancy scheme.

However, the rule-based controller tries to realize both IAQ and thermal comfort by means of a ventilation and heat pump system. For simplicity, a full elaboration on the rule-based controller is not provided, but the differences in control objectives should be considered in the comparison. For example, the rule-based controller assumes that the thermal comfort is between 294.15 and 298.15 K. To reach these temperatures and achieve IAQ, the heat pump consumed 90 kWh over the 13-day period. Unfortunately, the energy consumption of the fans was not measured during that period due to a sensor installation error. Therefore, a direct energy consumption comparison between the two controllers is not possible. However, two simplified calculations to approximate the relative energy consumption difference between both control performances are conducted, as provided below.

$$U_{\text{add}} = \Delta t \sum \dot{m}(t_{\text{occ}}) C_{\text{p}} |21 - T_{\text{z}}(t_{\text{occ}})| \tag{4-3}$$

$$U_{\text{IAQ}} = \Delta t \sum (0.19 - \dot{m}(t_{\text{occ}})) C_{\text{p}} |21 - T_{\text{a}}(t_{\text{occ}})|, \qquad \dot{m}(t_{\text{occ}}) < 0.19 \tag{4-4}$$

Equation 4-3 determines the required energy U_{add} to reach thermal comfort of 21°C under the ventilation profiles of Figures 4-7 and 4-11. Equation 4-4 calculates the auxiliary energy U_{IAQ} for reaching the required ventilation of 0.19 kg/s. To maintain thermal comfort, U_{IAQ} should be compensated and therefore considered in the results. Table 4-7 provides these results.

Controller	U_{add} [kWh]	U_{IAQ} [kWh]	$U_{\text{add}} + U_{\text{IAQ}}$
HMPC-2b	4.4	45.6	50.0
Rule-based	102.6	4.6	107.2

Table 4-7: Additional energy comparison to realize thermal comfort and IAQ.

Although these results are obtained by simplified calculations and more energy is presumably required to achieve real thermal comfort and IAQ, the difference between the results loosely indicates the control performances. The HMPC-2b structure appears to achieve better thermal comfort and IAQ than the rule-based controller, but with less additional energy. Initially, 112 kWh is used to achieve the current T_{z} progression of figure 4-6, as opposed to the minimum 90 kWh consumption of the rule-based controller. However, as Table 4-7 indicates, much more energy is required to correct the latter's T_{z} progression, regardless of the HMPC-2b structure's energy demand for correcting IAQ. Therefore, it is concluded that the HMPC-2b structure outperforms the rule-based controller in terms of energy consumption.

Another method to determine the energy demand reduction is to compare the one-year energy demand per squared meter to the benchmark values of the BENG-requirements. Note, however, that this demand is caused by the building design and control strategy combined.

The HMPC-2b structure with the grey-box models and the occupancy scheme of Table 3-2 is simulated on a one-year period of TMY data. The building's energy consumption resulted in 9000 kWh with a standard deviation of 0.267 K from the 293.15 K reference temperature. Hence, the whole system has a theoretical energy demand of about 30 kWh/m^2 per year for thermal control. This energy demand is well below the 100-150 kWh/m^2 benchmark and well within the 90 kWh/m^2 maximum energy demand of the BENG-requirements [43, 50].

4-3 Conclusions

In this chapter, the final HMPC-2b structure is analyzed on measured climate data and compared to the CCC-building's rule-based controller. The goal of the MPC structure is to outperform the currently employed BEMS in terms of reducing the auxiliary energy consumption and maintaining thermal comfort. To validly compare the control types, the nonlinear plant model, that serves as a simulation testbed, should accurately represent the CCC-building. Therefore, ten parameters of the nonlinear plant model are trained on data of a 10-day measurement period and eight model states are validated on data of a 3-day measurement period. The validation results indicate that the grey-box model outperforms the white-box model in terms of accuracy. However, more training data is needed for the grey-box model to be accurate for all climate periods, as all field measurement periods were performed in the spring.

The ten optimized parameters denote the material and dimensional properties of the system components. Therefore, the CCC-building's components are better represented by the grey-box model. However, the control performance of the HMPC-2b structure can benefit from selecting other materials or component sizes during the construction phase. To analyze the influence of the model parameters, a comparison is made between the initial model, controlled by the HMPC-2b structure with white-box prediction models, and the optimized model, controlled by the HMPC-2b structure with grey-box prediction models. The results indicate that the white-box variant makes more efficient use of the passive energy sources, as the white-box model can harvest more solar energy than the grey-box model. Hence, the HMPC-2b structure can be used as a tool to make passive design decisions that benefit the control performance of such BEMS in buildings with similar characteristics to the CCC-building.

To solve the main research question, the HMPC-2b structure with grey-box models is simulated under similar conditions as the rule-based controller faced during a 13-day field experiment. The HMPC-2b structure proved to be able to achieve thermal comfort and to be on-line applicable for multiple prediction horizon conditions. However, the energy consumption is difficult to put into perspective, as the energy consumption of the rule-based controller is only partly known. In addition, the auxiliary energy analysis is even harder as the CCC-building's BEMS considers other control objectives, e.g., IAQ. Still, a rough comparison is made by applying simplified calculations to normalize the difference in control objectives. The theoretical results show that the HMPC-2b structure performs relatively better than the rule-based controller in terms of reducing auxiliary energy consumption while achieving thermal comfort and IAQ. Furthermore, the HMPC-2b structure with grey-box models is simulated on a one-year period of TMY data to obtain the theoretical energy demand per squared meter per year. The one-year energy demand of the system appeared to be 30 kWh/m^2 for thermal control only. This is well below the 100-150 kWh/m^2 benchmark. However, this energy demand reduction is achieved by the whole system and not just by the applied control strategy.

Chapter 5

Conclusions and Future Work

In this chapter, the conclusions of the work done in this thesis and suggestions for future research on this topic are provided. Section 5-1 gives the closing conclusions for the research sub-questions and main research question that are specified in the first chapter. In Section 5-2, several suggestions for future research on this topic are proposed.

5-1 Conclusions

This thesis is based on the literature gap found in the literature research conducted prior to this project. In the field of passive energy sources and the field of BEMS, a literature gap arises. It appeared that no extensive research has been done into optimally combining passive and active energy sources to regulate indoor temperatures by means of advanced MPC controllers. In addition, prior research was mainly focused on finding innovative and on-line applicable MPC architectures that benefit the building structure, rather than the available energy sources. In these studies, the authors developed their building models in simulated environments (EnergyPlus, TRNSYS), mainly considering one type of actuator that often consumes active energy. Therefore, this thesis is based on developing an MPC architecture with low computational costs and yet good control performance, which is realized for an existing office building built for optimal passive energy harvesting. In order to achieve this target, the main research question and several sub-questions were proposed. The conclusions for each sub-question are given below, followed by the conclusion on the main research question.

1. *In what way can a building be modeled such that the model has a high degree of accuracy but is not too computationally complex, so that it is suitable for model-based control?*

In this thesis, the choice was made to use the CCC-building as support for the building model. Research has shown that grey- and black-box modeling techniques are able to produce accurate and efficient models. However, construction delays due to the COVID-19 epidemic and the limited research period of this thesis meant that these modeling techniques were not

applicable due to the lack of much measurement data. In addition, applying construction simulation software tools to realize white-box models was considered undesirable, since coupling advanced controllers to these simulation environments proved impractical.

Hence, a white-box model is created in MATLAB by means of fundamental laws of thermodynamics. The model is based on the foundation of the CCC-building as all model parameters are derived from the geometry and material properties of CCC-building's components. In addition, the system disturbances, i.e., environmental climate, solar positions, occupancy, and ground temperature, are considered by means of historical data, pre-determined schedules, and disturbance models, e.g., the oriented solar irradiance models (Perez model) and the validated ground temperature grey-box model. For indoor temperature control through passive energy sources, models for natural ventilation in a thermal chimney and solar irradiance control by automated solar shading are being considered. To control the building model using MPC, simplified and linearized versions are developed that can serve as prediction models.

2. *How does the developed building model perform compared to the thermal progressions in a real-case building?*

The two prediction models proved to be accurate derivations of the developed nonlinear plant model, as the control performances of all MPC architectures appeared promising. However, the relevance of the control performances depends on the ability of the nonlinear plant model to approximate a realistic scenario. Therefore, a validation case study is performed by comparing eight measured components of the CCC-building with their represented model states. Most states showed promising correlations with their real-case measurements. In particular, the state of the inner zone proved its ability to capture the real-case temperature progression.

However, some significant validation errors occurred, caused by the model mismatch or disturbance input errors. The latter is highly plausible, as the Reindl model is used to obtain the direct beam and diffuse irradiation values. This model's performance is known to be questionable. Still, ten model parameters are chosen to be re-optimized on training data to improve the validation results. The resulting grey-box model showed improved validation results on the validation data set compared to the white-box model. However, the measurement data sets remain relatively small due to the lack of time to do more field studies. More training and validation data is needed to optimize a building model on all climate conditions of a year.

3. *In what way can an on-line applicable model predictive control strategy be developed such that it optimally combines the control of the two passive energy sources?*

To develop an MPC structure that optimally manages passive energy sources, multiple relevant control structures are compared in this work. Five architectures are analyzed, including a linear and nonlinear approach and three hierarchical variants. It is found that the highest performance is achieved when the main advantages of linear and nonlinear MPC are combined in a hierarchical structure. Of all hierarchical structures, the HMPC-2b structure turned out to be the most promising. The advantage of this architecture can be explained by the applied separation of control input optimizations and state-update locations in different control layers. In this way, the HMPC-2b structure makes more efficient use of the two MPC controllers. This is the main contribution of this thesis to the literature, since, to the best of the author's knowledge, no hierarchical structure-based BEMS that combines linear and nonlinear MPC to control multiple passive energy sources in such a way, has been considered yet.

4. *How does the developed model predictive control strategy optimally combines passive and active energy sources, while maintaining thermal comfort? Is it then possible to reduce the energy consumption of such a building compared to a real-case rule-based controller?*

The HMPC-2b structure is selected to be extended with an active energy source and compared to the rule-based controller of the CCC-building. The ϵ-constraint and Pareto front construction methods are applied to handle the conflicting objectives, i.e., minimizing auxiliary energy consumption and maximizing thermal comfort. For the linear MPC agent, hard constraints are set such that thermal comfort is to be achieved without considering trade-off solutions between the two objectives. The linear MPC objective function only defines that the passive systems take precedence in controlling the indoor temperature over the active system. Furthermore, the nonlinear MPC slave is tasked with tracking the reference temperature trajectory by means of a multi-objective function. By constructing the Pareto front, the desired penalizing values for the multi-objective function are found such that the standard deviation of all temperature errors is 0.25 K. Hence, 95% of all errors are within 0.5 K deviation from the reference temperature. This is concluded as satisfactory in terms of thermal comfort.

A direct comparison of the energy consumption is not possible as the measurements of the energy consumed are incomplete and the rule-based controller considers other objectives than the HMPC-2b structure. However, simplified calculations normalizing the difference in objectives imply that the HMPC-2b structure outperforms the real-case BEMS in terms of reducing energy consumption while maintaining thermal comfort and IAQ. Moreover, the combination of such a building with the developed control strategy leads to a theoretical energy demand of 30 kWh/m^2 per year, which is far below the 100-150 kWh/m^2 benchmark.

Main research question

"What is the best model predictive control strategy for on-line building energy management systems that combines solar shading with passive ventilation in order to maximize performance in terms of passive fraction of energy while maintaining indoor thermal comfort?"

In this thesis, an innovative hierarchical structure is developed that combines linear MPC for shading control and reference trajectory optimization with nonlinear MPC for passive ventilation control and thermal comfort maintenance. The developed MPC architecture is proven to be on-line applicable, as the applied models have the proven ability to capture real-case temperature progression, while the computation time of the operating control system is low enough for real-time control. Therefore, it is concluded that the main research question of this thesis has been solved. This resolves the literature gap in the fields of passive energy sources and BEMS and contributes to the state-of-the-art research.

5-2 Recommendations for future work

The aim of this thesis was the development of an optimal MPC structure, which has been successfully achieved. However, multiple interesting research opportunities emerged during the process, which are recommended to pursue in future research. In this section, several research topics are provided with a duration estimate of 1-2 years, half a year, or 1-2 months.

Extensive grey-box model identification (1-2 years)

In the case study, a grey-box identification method was performed to optimize several model parameters and to validate the grey-box model on relatively short periods of data. In addition, the questionable Reindl model was employed for obtaining essential disturbance input data. In future research, DNI and DHI sensors could be installed near the CCC-building, disregarding the Reindl model. Then, a more extensive grey-box model identification can be performed, as the errors of the disturbance inputs are presumably significantly reduced. In addition, more field measurements should be carried out over the year, so that the grey-box model is not only optimized for one or a few periods of similar climatic conditions.

Up-scaling the system to a multi-zone building (half a year)

Contrary to the CCC-building, most office buildings are multi-zoned. Therefore, an important research topic is to develop a control structure that combines innovative passive systems, like solar blinds and PCM, in a multi-zoned building environment. Prior research has shown that considering additional zones and model inputs increases the computational costs, which will therefore be the main challenge of this research topic. However, this can be solved by an extension of the developed hierarchical structure in which a linear MPC agent optimizes all solar blinds and reference trajectories, taking into account the coupled thermodynamics between the zones, and decentralized nonlinear MPC slaves independently control the ventilation, heating, and cooling systems to accurately track those trajectories.

Considering full indoor comfort for occupants (half a year)

In this thesis, solely thermal comfort is considered to be achieved. However, ISO and ASHRAE standards require achieving IAQ through minimum ventilation usage per occupant and the fully glazed walls may cause visual comfort problems which are solvable by applying solar blinds. Therefore, full indoor comfort for occupants leads to complex multi-objective optimization problems. Such complex optimization problems may drastically deteriorate both the computation time and auxiliary energy consumption. Hence, it is essential to study these multi-objective optimization problems and find relevant solutions.

Decreasing the computation time of the control system (1-2 months)

In this thesis, all considered MPC structures are assessed on their computational costs, which contributed to the development of the HMPC-2b structure. However, it is essential to find methods that reduce the computation time even further, as lowering computational costs opens doors to new possibilities. For instance, the building model complexity can be decreased by considering fewer states or applying grey- and black-box model identification approaches. However, it is not immediately known whether this will positively or negatively affect the accuracy of the model. Other measures could be taken that benefit the computation time without affecting the model accuracy. For example, the nonlinear programming problem solver *IPOPT* [14] is known to outperform *fmincon* in terms of optimization time and several other programming languages, like C++, can process code faster than MATLAB.

Appendix A

Models for Solar-Based Parameters

Algorithm 4 Oriented solar irradiance parameters **MATLAB**

Input: $Day, t, \beta_{\mathrm{c}}, \gamma_{\mathrm{c}}, I_{\mathrm{bn}}, I_{\mathrm{d}}, \rho_{\mathrm{r}}$
Output: $I_{\mathrm{o}}, I_{\mathrm{o,b}}, I_{\mathrm{o,r}}, I_{\mathrm{o,d}}, \theta_{\mathrm{z}}, \gamma_{\mathrm{azi}}$
Procedure:
$lat = 4.378$ % Latitude
$long = 51.996$ % Longitude

% Calculations for sun's elevation, zenith, oriented normal, and azimuth angles
$B \leftarrow \frac{360}{365}(Day - 81)$
$EoT \leftarrow 9.87\sin(2B) - 7.53\cos(B) - 1.5\sin(B)$
$TC \leftarrow EoT - 4(15t - long)$
$\omega \leftarrow 15(t + \frac{TC}{60} - 12)$
$\delta \leftarrow \sin^{-1}(\sin(-23.45)\cos(\frac{360}{365}(Day + 10)))$
$\theta_{\mathrm{e}} \leftarrow \sin^{-1}(\cos(lat)\cos(\delta)\cos(\omega) + \sin(lat)\sin(\delta))$
$\theta_{\mathrm{z}} \leftarrow 90 - \theta_e$
$\theta_{\mathrm{n}} \leftarrow \cos^{-1}(\sin(\delta)\sin(lat)\cos(\beta_{\mathrm{c}}) - \cos(lat)\sin(\delta)\sin(\beta_{\mathrm{c}})\cos(\gamma_{\mathrm{c}}) + \cos(\delta)\cos(lat)...$
$\cos(\beta_{\mathrm{c}})\cos(\omega) + \cos(\delta)\sin(lat)\sin(\beta_{\mathrm{c}})\cos(\gamma_{\mathrm{c}})\cos(\omega) + \cos(\delta)\sin(\omega)\sin(\beta_{\mathrm{c}})\sin(\gamma_{\mathrm{c}}))$
$\gamma_{\mathrm{azi}} \leftarrow \cos^{-1}(\frac{\sin(\delta)\cos(l) - \cos(\delta)\sin(l)\cos(\omega)}{\theta_{\mathrm{e}}})$

% Calculations for solar irradiance parameters
$a \leftarrow \mathbf{max}(0, \cos(\theta_{\mathrm{n}}))$
$b \leftarrow \mathbf{max}(\cos(85), \cos(\theta_{\mathrm{z}}))$
$[F_1, F_2] \leftarrow \mathbf{Perez\_model}(\theta_{\mathrm{z}}, I_{\mathrm{d}}, I_{\mathrm{bn}}, Day)$
$I_{\mathrm{o,b}} \leftarrow I_{\mathrm{bn}}\cos(\theta_{\mathrm{n}})$
$I_{\mathrm{o,r}} \leftarrow \frac{\rho_{\mathrm{r}}}{2}(I_{\mathrm{d}} + I_{\mathrm{bn}}\cos(\theta_{\mathrm{z}}))(1 - \cos(\beta_{\mathrm{c}}))$
$I_{\mathrm{o,d}} \leftarrow I_{\mathrm{d}}(\frac{1}{2}(1 - F_1)(1 + \cos(\beta_{\mathrm{c}})) + F_1\frac{a}{b} + F_2\sin(\beta_{\mathrm{c}}))$
$I_{\mathrm{o}} \leftarrow I_{\mathrm{o,b}} + I_{\mathrm{o,r}} + I_{\mathrm{o,d}}$
return $I_{\mathrm{o}}, I_{\mathrm{o,b}}, I_{\mathrm{o,r}}, I_{\mathrm{o,d}}, \theta_{\mathrm{z}}, \gamma_{\mathrm{azi}}$

Algorithm 5 Oriented optical parameters **MATLAB**

Input: $\theta_{\mathrm{n}}, \alpha, \xi$
Output: $\alpha_{\mathrm{o}}, \xi_{\mathrm{o}}$
Procedure:
$\theta_{\mathrm{ref}} = [0, 20, 40, 50, 60, 70, 80, 90]$
$\alpha_{\mathrm{ref}} = [\alpha{+}0.01, \alpha{+}0.01, \alpha{+}0.02, \alpha{+}0.02, \alpha{+}0.02, \alpha{+}0.02, \alpha{+}0.02, 0]$
$\xi_{\mathrm{ref}} = [\xi{+}0.02, \xi{+}0.02, \xi, \xi{-}0.01, \xi{-}0.06, \xi{-}0.17, \xi{-}0.38, 0]$
$\alpha_{\mathrm{o}} \leftarrow$ **interp1**$(\theta_{\mathrm{ref}}, \alpha_{\mathrm{ref}}, \theta_{\mathrm{n}})$
$\xi_{\mathrm{o}} \leftarrow$ **interp1**$(\theta_{\mathrm{ref}}, \xi_{\mathrm{ref}}, \theta_{\mathrm{n}})$
return $\alpha_{\mathrm{o}}, \xi_{\mathrm{o}}$

Algorithm 6 Unshaded floor area parameter **MATLAB**

Input: $\theta_{\mathrm{z}}, \gamma_{\mathrm{azi}}, X_{\mathrm{z}}, Y_{\mathrm{z}}, Z_{\mathrm{z}}$
Output: A_{u}
Procedure:
$OH = 1.86$ % The overhang of the roof is 1.86 m on all sides
$H = Z_{\mathrm{z}} - OH \tan(90 - \theta_{\mathrm{z}})$
$\gamma_{\mathrm{east}} = 90$
$\gamma_{\mathrm{south}} = 180$
$\gamma_{\mathrm{west}} = 270$
$\gamma_{\mathrm{south}} = 360$
if $0 > \gamma_{\mathrm{azi}} < 180$ **then**
$x_{\mathrm{e}} \leftarrow H \frac{\cos(|\gamma_{\mathrm{azi}} - \gamma_{\mathrm{east}}|)}{\tan(90 - \theta_{\mathrm{z}})}$
$x_{\mathrm{e}}(x_{\mathrm{e}} > X_{\mathrm{z}}) = X_{\mathrm{z}}$
end if
if $90 > \gamma_{\mathrm{azi}} < 270$ **then**
$x_{\mathrm{s}} \leftarrow H \frac{\cos(|\gamma_{\mathrm{azi}} - \gamma_{\mathrm{south}}|)}{\tan(90 - \theta_{\mathrm{z}})}$
$x_{\mathrm{s}}(x_{\mathrm{s}} > Y_{\mathrm{z}}) = Y_{\mathrm{z}}$
end if
if $180 > \gamma_{\mathrm{azi}} < 360$ **then**
$x_{\mathrm{w}} \leftarrow H \frac{\cos(|\gamma_{\mathrm{azi}} - \gamma_{\mathrm{west}}|)}{\tan(90 - \theta_{\mathrm{z}})}$
$x_{\mathrm{w}}(x_{\mathrm{w}} > X_{\mathrm{z}}) = X_{\mathrm{z}}$
end if
if $\gamma_{\mathrm{azi}} < 90 \;||\; \gamma_{\mathrm{azi}} > 270$ **then**
$x_{\mathrm{n}} \leftarrow H \frac{\cos(|\gamma_{\mathrm{azi}} - \gamma_{\mathrm{north}}|)}{\tan(90 - \theta_{\mathrm{z}})}$
$x_{\mathrm{n}}(x_{\mathrm{n}} > Y_{\mathrm{z}}) = Y_{\mathrm{z}}$
end if
if $\gamma_{\mathrm{azi}} < 180$ **then**
$A_{\mathrm{u}} \leftarrow x_{\mathrm{e}} Y_{\mathrm{z}} + x_{\mathrm{s}} X_{\mathrm{z}} + x_{\mathrm{n}} X_{\mathrm{z}} - x_{\mathrm{e}} x_{\mathrm{s}} - x_{\mathrm{e}} x_{\mathrm{n}}$
else if
$A_{\mathrm{u}} \leftarrow x_{\mathrm{w}} Y_{\mathrm{z}} + x_{\mathrm{s}} X_{\mathrm{z}} + x_{\mathrm{n}} X_{\mathrm{z}} - x_{\mathrm{w}} x_{\mathrm{s}} - x_{\mathrm{w}} x_{\mathrm{n}}$
end if
return A_{u}

Appendix B

Model Predictive Control

Model Predictive Control (MPC) is a widely applied control method in the field of BEMS. Actuators, sensor data, optimization algorithms, and white or data-driven models can be integrated into such controllers. Appendix B elaborates on the principles of MPC. Hence, an overview of the general concept and the mathematical background of MPC are given.

B-1 Overview

The term MPC does not refer to a specific controller, but rather to a range of control approaches. MPC control schemes as Dynamic Matrix Control, Model Algorithmic Control, Predictive Functional Control, and Generalized Predictive Control are successfully used in many engineering fields. Although there are differences between these schemes, all of them practically contain three main elements [18], all illustrated by Figure B-1:

1. Explicit use of a model to predict the system's output at specific instants in the future time horizon.
2. Calculation of a control sequence minimizing an objective function at each time step.
3. Receding horizon control strategy, which involves the application of the first control signal of the predicted sequence at each time step.

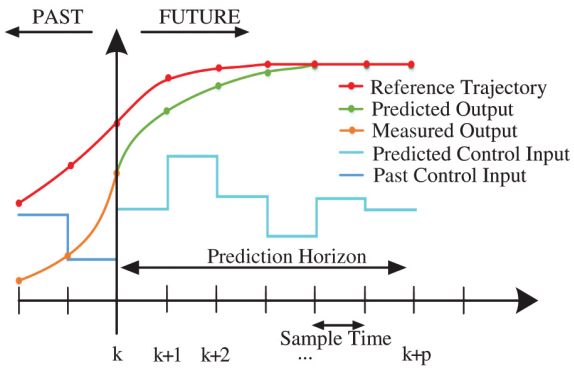

Figure B-1: Schematic representation of the discrete MPC scheme [54].

A control cycle of MPC starts with a measurement of the current state of the system and, subsequently, an optimization problem is solved at each following discrete-time step. This optimization problem utilizes an internal prediction model with operational constraints, to find the input signal that results in the optimal predicted output behavior over a predefined prediction horizon. In addition, MPC operates in a receding horizon fashion, meaning that at each time step only the first input of the optimized input control sequence is applied into the system and the remaining input signals are discarded. The cycle is then repeated. Various MPC methods differ in the model and constraint representation, noise handling, and cost function minimization. While Dynamic Matrix Control performs well with multi-variable processes, Predictive Functional Control allows nonlinear system dynamics, and Generalized Predictive Control shows good performance and a significant degree of robustness. Despite this distinctness, Ref. [18] states that all MPC approaches share a series of advantages over non-MPC approaches, making them very popular commercially:

- MPC can control a great variety of processes, from relatively simple to more complex dynamics, including systems with long time delays, non-minimum phase, or unstable characteristics;
- Multi-variable cases can easily be solved.
- The built-in feed-forward control makes the system more robust for measurable disturbances;
- The controller is relatively easy to implement;
- MPC is attractive to employees with limited knowledge of control because the concepts are intuitive but the tuning is relatively easy;
- The constraint extensions are conceptually simple and these can be systematically included during the design process;
- MPC is very useful when desired future references are known;
- The MPC methodology is open and is based on certain basic principles which allow for future research and extensions;

Nonetheless, MPC also holds several limitations:

- The performance of the MPC highly correlates with the accuracy of the model. For some engineering problems, obtaining an accurate model is very challenging;
- Although the control law is easy to implement and requires little computational burden, its derivation can be more complex than that of classical controllers;
- On-line implementation might become problematic as the computational complexity of MPC significantly increases with the model complexity and size;

B-2 General Model Predictive Control Framework

Whether the process is linear or nonlinear, state-space or in a transfer function, stable or unstable, etc., a universal MPC framework can be sketched according to Ref. [18]. Generally, the following expressions describe the behaviour of the dynamical system:

$$x(k+1) = f(x(k), u(k), d(k)) \tag{B-1}$$

$$y(k) = h(x(k), u(k), w(k)) \tag{B-2}$$

in which $x(k)$ denotes the state of the system at time step k, $u(k)$ refers to the control input at time step k, $d(k)$ stands for the input disturbances, $y(k)$ is the system's output, and $w(k)$ represents the system's noise.

In the general framework, the controller determines the optimal input sequence $\hat{u}(k)$ from time k to the end of the prediction horizon N_p by minimizing a specific objective function $J(y(k), x(k), u(k))$ while respecting the constraint set. These constraint sets represent the physical and operational limitations of the system. In addition, i denotes the time step ordinals of the prediction horizon. For reducing the computational load, the control horizon N_c is introduced. Since only the first input vector is applied to the real system, less emphasis is placed on the input vectors later in the predicted control horizon. Therefore, the computational load can be reduced and good control performances can be maintained, by choosing a smaller N_c than the N_p and keeping the remaining input vectors between the N_c and N_p constant. The general MPC problem can be formulated in the following way:

$$\min_{u(k)} J(y(k), x(k), u(k)) \tag{B-3}$$

s.t.

$$\begin{aligned}
x(k{+}i{+}1) &= f(x(k{+}i), u(k{+}i), d(k{+}i)), && i \ni \{0, ..., N_\mathrm{p}{-}1\} && \text{(B-4)}\\
x(k{+}i) &= x_0, && i = 0 && \text{(B-5)}\\
u(k{+}i) &= u(k{+}N_\mathrm{c}{-}1), && i \ni \{N_\mathrm{c}, ..., N_\mathrm{p}{-}1\} && \text{(B-6)}\\
y(k{+}i) &= h(x(k{+}i), u(k{+}i), w(k{+}i)), && i \ni \{1, ..., N_\mathrm{p}\} && \text{(B-7)}\\
x(k{+}i) &\in \mathbb{X}^n, && i \ni \{1, ..., N_\mathrm{p}\} && \text{(B-8)}\\
u(k{+}i) &\in \mathbb{U}^m, && i \ni \{0, ..., N_\mathrm{c}{-}1\} && \text{(B-9)}\\
d(k{+}i) &\in \mathbb{D}^m, && i \ni \{0, ..., N_\mathrm{c}{-}1\} && \text{(B-10)}\\
w(k{+}i) &\in \mathbb{W}^s, && i \ni \{1, ..., N_\mathrm{p}\} && \text{(B-11)}\\
y(k{+}i) &\in \mathbb{Y}^s, && i \ni \{1, ..., N_\mathrm{p}\} && \text{(B-12)}
\end{aligned}$$

The optimal input $\overline{u}(k)$ consists of $[\hat{u}^T(k), ..., \hat{u}^T(k + N_\mathrm{p} - 1)]^T$ in which $\hat{u}(k)$ denotes the optimal control vector for each step in the predicted horizon. Furthermore, x_0 is the measured initial state of the system for the optimization problem at time k. The state, input and output constraints must be satisfied in the spaces $\mathbb{X}$, $\mathbb{U}$, and $\mathbb{Y}$ with dimensions n, s, and m, respectively. n refers to the number of states, s the number of outputs, and m the number of inputs.

B-3 Objective Function Formulation

The objective function describes the desired performance of the system. A general elaboration about the mathematical background of the objective function for an MPC problem is given below. Oldewurtel et al. argue in [45] that the objective function generally serves two purposes:

1. Stability. The structure of the objective function is commonly chosen to be a Lyapunov function for a closed-loop system. In theory, Lyapunov functions guarantee stability of the system. In practice, it is simpler for an MPC controller to keep stability with

slow-moving stable dynamics, such as in buildings. The Lyapunov criteria can be taken more relaxed which leaves the designer free to select the function on a performance basis.

2. Performance target. The objective function can be described as a combination of performance targets. The parameter weights specify the preference of one target over another.

An important mathematical characteristic of an objective function is convexity. Convex cost functions are solvable by simple optimization algorithms, such as (Modified) Simplex, Interior Point, and Cutting Plane. Non-convex cost functions, which are often nonlinear or mixed-integer, benefit more from the stochastic optimization algorithms, such as Global Gradient methods and Genetic Algorithms. Knowing the degree of non-convexity helps with selecting the algorithm. The common objective functions $l_{\mathrm{k}}(x(k), u(k))$ from Table B-1 are:

- Quadratic costs. The weight matrices $\mathcal{Q}$ and $\mathcal{R}$ linked to the state and the input offer a trade-off between control quality and input energy. If the model doesn't hold constraints or the constraints are inactive, the cost function is equal to the function of the Linear Quadratic Regulator or Linear Quadratic Gauss controller (classical optimal control).
- Linear costs. It outperforms quadratic functions in minimizing 'amounts', outliers, or economical signals. This function is often used to minimize the building's energy load.
- Probabilistic costs. When a system is influenced by random disturbances, then one can minimize the expected value of the function $g_{\mathrm{k}}(x(k), u(k))$. For example, $g_{\mathrm{k}}(x(k), u(k))$ can be a quadratic or linear objective functions, as discussed above.

Objective function type	Mathematical formulation
Quadratic costs	$l_{\mathrm{k}}(x(k), u(k)) = x^T(k)\mathcal{Q}x(k) + u^T(k)\mathcal{R}u(k)$
Linear costs	$l_{\mathrm{k}}(x(k), u(k)) = c^T u(k)$
Probabilistic cost	$l_{\mathrm{k}}(x(k), u(k)) = \mathbb{E}[g_{\mathrm{k}}(x(k), u(k))]$

Table B-1: Common types of objective functions [45].

B-4 Constraints Formulation

The main advantage of MPC over other control methods is the ability to add constraints. Since different constraints can be applied in optimization problems, it is important to understand the mathematical background and purpose of those different types of constraints. Ref. [45] provides an overview of commonly used constraints in building climate control; summarized in Table B-2:

- Linear constraint. This popular type of constraint is utilized to set upper and/or lower bounds on variables. Linear constraints are easy to solve and they are used to approximate any convex constraint to an arbitrary degree of accuracy.
- Convex quadratic constraint. This type is used to bound a variable to be within an ellipsoidal form (higher dimensional). In building climate control problems, this constraint can be utilized when bounding the sum of input energy amongst multiple actuators.
- Chance-constraint. When uncertainties influence the optimization problem, this constraint can formulate the condition that has to be satisfied with the predetermined prob-

ability value α. Since solely deterministic variables can be solved in an optimization problem, chance-constraints require to be transformed into deterministic constraints.

- Second-order cone constraint. The feasible region of this constraint has the form of a cone. Second-order cone constraints arise from reformulations of chance-constraints.
- Switched constraint. This constraint includes a set of constraints, where one is chosen to be relevant when the predefined condition for that particular one is met. This is commonly used in hybrid systems, i.e., systems that hold both continuous and discrete-time behavior.
- Non-linear constraint. This constraint includes any type of constraint that is not classified in the above categories and where $h(x(k), u(k))$ is any nonlinear function. Generally speaking, it is challenging to cope with these constraints when solving optimization problems.

Constraints type	Mathematical formulation
Linear	$Ax(k) \leq b$
Convex quadratic	$(x(k) - \overline{x})^T \mathcal{Q}(x(k) - \overline{x}) \leq 1, \quad \mathcal{Q} \succcurlyeq 0$
Chance-constraint	$\mathbb{P}[Ax(k) \leq b] \geq 1 - \alpha, \quad \alpha \in (0, 0.5]$
Second order cone	$\|\|Ax(k) + b\|\|_2 \leq Cx(k) + d$
Switched	if condition, then $A_1 x(k) \leq b_1$ else $A_2 x(k) \leq b_2$
Nonlinear	$h(x(k), u(k)) \leq 0$

Table B-2: Common types of constraints [45].

Appendix C

Supportive Tables with Optimization and Validation Results

$\overline{h}_{\mathrm{i,j}}$	View	Inputs	Flow	Mean	VAF	NRMSE
$\overline{h}_{1,2}$	south	$T_{\mathrm{s},1}, T_{\mathrm{s},2}$	Natural	0.554	99.3	0.011
$\overline{h}_{1,2}$	west	$T_{\mathrm{w},1}, T_{\mathrm{w},2}$	Natural	0.541	99.2	0.012
$\overline{h}_{1,2}$	north	$T_{\mathrm{n},1}, T_{\mathrm{n},2}$	Natural	0.537	99.0	0.013
$\overline{h}_{1,2}$	east	$T_{\mathrm{e},1}, T_{\mathrm{e},2}$	Natural	0.556	99.4	0.009
$\overline{h}_{2,3}$	south	$T_{\mathrm{s},2}, T_{\mathrm{s},3}$	Natural	0.481	98.2	0.017
$\overline{h}_{2,3}$	west	$T_{\mathrm{w},2}, T_{\mathrm{w},3}$	Natural	0.491	99.1	0.011
$\overline{h}_{2,3}$	north	$T_{\mathrm{n},2}, T_{\mathrm{n},3}$	Natural	0.494	99.0	0.013
$\overline{h}_{2,3}$	east	$T_{\mathrm{e},2}, T_{\mathrm{e},3}$	Natural	0.482	98.6	0.016
$\overline{h}_{1,\mathrm{a}}$	south	$T_{\mathrm{a}}, v_{\mathrm{a}}$	Forced	16.74	99.9	0.003
$\overline{h}_{1,\mathrm{a}}$	west	$T_{\mathrm{a}}, v_{\mathrm{a}}$	Forced	16.74	99.9	0.003
$\overline{h}_{1,\mathrm{a}}$	north	$T_{\mathrm{a}}, v_{\mathrm{a}}$	Forced	16.74	99.9	0.003
$\overline{h}_{1,\mathrm{a}}$	east	$T_{\mathrm{a}}, v_{\mathrm{a}}$	Forced	16.74	99.9	0.003
$\overline{h}_{\mathrm{r,a}}$	-	$T_{\mathrm{a}}, v_{\mathrm{a}}$	Forced	17.46	99.9	0.003
$\overline{h}_{3,\mathrm{z}}$	south	$T_{\mathrm{s},3}, T_{\mathrm{z}}$	Natural	1.599	99.0	0.013
$\overline{h}_{3,\mathrm{z}}$	west	$T_{\mathrm{w},3}, T_{\mathrm{z}}$	Natural	1.623	98.9	0.015
$\overline{h}_{3,\mathrm{z}}$	north	$T_{\mathrm{n},3}, T_{\mathrm{z}}$	Natural	1.629	99.3	0.012
$\overline{h}_{3,\mathrm{z}}$	east	$T_{\mathrm{e},3}, T_{\mathrm{z}}$	Natural	1.588	98.9	0.015
$\overline{h}_{\mathrm{c,z}}$	-	$T_{\mathrm{c}}, T_{\mathrm{z}}$	Natural	1.350	99.3	0.019
$\overline{h}_{\mathrm{rf}\uparrow,\mathrm{z}}$	-	$T_{\mathrm{rf}}, T_{\mathrm{z}}$	Natural	1.777	99.4	0.016
$\overline{h}_{\mathrm{rf}\downarrow,\mathrm{z}}$	-	$T_{\mathrm{rf}}, T_{\mathrm{z}}$	Natural	0.6588	99.3	0.017
$\overline{h}_{\mathrm{bf,z}}$	-	$T_{\mathrm{bf}}, T_{\mathrm{z}}$	Natural	0.879	99.5	0.013

Table C-1: Results of the nonlinear convection coefficient fitted models.

$\overline{h}_{\mathrm{i,j}}$	View	x_{op}	VAF	NRMSE
$\overline{h}_{1,2}$	south	2e−3	90.1	0.048
$\overline{h}_{1,2}$	west	2e−3	89.6	0.048
$\overline{h}_{1,2}$	north	2e−3	89.7	0.050
$\overline{h}_{1,2}$	east	2e−3	86.3	0.051
$\overline{h}_{2,3}$	south	3e−3	80.7	0.071
$\overline{h}_{2,3}$	west	3e−3	90.7	0.040
$\overline{h}_{2,3}$	north	3e−3	93.3	0.039
$\overline{h}_{2,3}$	east	3e−3	88.3	0.055
$\overline{h}_{3,\mathrm{z}}$	south	-2e−4	70.4	0.076
$\overline{h}_{3,\mathrm{z}}$	west	5e−4	72.2	0.083
$\overline{h}_{3,\mathrm{z}}$	north	5e−4	81.2	0.067
$\overline{h}_{3,\mathrm{z}}$	east	2e−4	67.0	0.072
$\overline{h}_{\mathrm{c,z}}$	-	2e−4	83.7	0.088
$\overline{h}_{\mathrm{rf}\uparrow,\mathrm{z}}$	-	2e−3	88.0	0.072
$\overline{h}_{\mathrm{rf}\downarrow,\mathrm{z}}$	-	6e−4	83.1	0.073
$\overline{h}_{\mathrm{bf,z}}$	-	-8e−3	79.0	0.088

Table C-2: Results of the linear convection coefficient fitted models.

State	Parameter	Initial value	Optimized value
T_{c}	Z	0.003	0.0026
T_{rf}	Z	0.038	0.0361
T_{rf}	α	0.200	0.1558
T_{bf}	Z	0.225	0.2281
T_{bf}	κ	0.3125	0.344
$T_{\mathrm{i,j}}$	c_{p}	900	792.33
$T_{\mathrm{i,j}}$	α	0.085	0.078
$T_{\mathrm{i,j}}$	ξ	0.83	0.78
$T_{\mathrm{i,j}}$	ϵ	0.82	0.77
$T_{\mathrm{i,j}}$	ϵ_{low}	0.16	0.13

Table C-3: Results of the optimized parameters for the grey-box model.

Appendix D

Conference Paper

Model Predictive Control for Optimal Integration of a Thermal Chimney and Solar Shaded Building*

Thomas Joseph Ceha, Luigi Antonio de Araujo Passos, Simone Baldi, and Bart De Schutter,
MED2021, 29th Mediterranean Conference on Control and Automation, June 22-25, 2021, Bari, Puglia, Italy

***Abstract* — Energy-saving devices are extensively sought in several fields, including heating, ventilation, and air-conditioning (HVAC) tasks in buildings. This paper investigates six model predictive control (MPC) strategies as a way to optimize the operation of a solar shaded, natural ventilated building located at TU Delft campus. Such building is based on an innovative combination of a thermal chimney and glazing walls for harvesting passive energy. The main challenge is dealing with the system dynamics. The predictive controllers we consider include both linear and nonlinear MPC, and four hierarchical MPC strategies. All controllers aim to minimize auxiliary power consumption and, consequently, increasing the energy savings. The six control strategies performance are evaluated using reference values for thermal comfort, while relying on simulations performed in MATLAB for calculations. The hierarchical MPC architecture which considers a hybrid structure with nonlinear tracker for ventilation and linear agents for heating purposes appears the most promising one.**

I. INTRODUCTION

As the quest for energy efficiency is trending now, several innovative technologies have been proposed for HVAC (Heating, Ventilation, and Air-Conditioning) in buildings. This is because of the high energy consumption in indoor spaces, which, for instance, reaches half of the total energy consumption in European Union [1]. The HVAC solutions considered mostly rely on passive systems, renewable energy sources, and efficient processes/devices, e.g., steerable solar shadings, smart windows, thermal chimneys, phase-change materials (PCM), and photovoltaic panels [2].

While these systems are mainly driven by unsteady weather conditions, the development of operational control strategies plays an essential role for achieving the best system performance and energy dispatchability. Such operational strategies rely on control algorithms and optimization methods for establishing optimal decisions and to assess relevant figures of merit (energy savings, thermal comfort levels, ventilation rates, etc.). MPC (Model Predictive Control) has demonstrated to be a promising method for energy management in buildings [3]. Many MPC variants have been considered in the literature, e.g., robust, adaptative schemes [4], scenario-based stochastic control [5], off-line distributed MPC [6], and stochastic MPC [7]. In addition, multiple control structures have been compared, such as centralized, decentralized, distributed, and hierarchical MPC controllers [8-10], often concluding that the last two are superior in performance and computational efforts, depending on the complexity of the building. Some examples of analysis may include controlling the thermal stratification in shopping malls [11], air flows in libraries [12], and nighttime ventilation in office buildings [13].

In this work, we aim to develop and compare a set of MPC strategies to optimize the operation of a novel HVAC system installed in a living lab office-building based at TU Delft campus, in the Netherlands. Such system relies on the combination of a thermal chimney and glazed shaded walls, while considering PCM for latent thermal storage. While different MPC approaches have been suggested for buildings equipped with active HVAC systems, such control method has not been investigated for this combination of passive actuators for heating and ventilation. Therefore, the analysis explores six different MPC architectures to systematically operate the system actuators, which consist of the thermal chimney flow area and the solar shadings aperture. The control algorithms rely on a fully transient thermal model numerically implemented in MATLAB to explore different control strategies in order to guarantee the maximum passive fraction, and, consequently, the minimum use of auxiliary heating.

II. SYSTEM DESCRIPTION AND DYNAMIC MODELLING

A. Building and HVAC system configuration

The thermal system of this study is currently installed at TU Delft in a space particularly designed for testing passive technologies in co-working conditions. Figure 1 shows the schematic representation. As one can see, the configuration shown in Figure 1 includes a thermal chimney, in which the stack effect due to buoyancy provides natural ventilation, and a fully glazed walls building, where the solar heat gain coming into the place is controlled by external shades. Additionally, the chimney is supported by an auxiliary heater and PCM battery for thermal buffering. Therefore, the system mainly relies on the combination of passive technologies (i.e., thermal chimney and solar shadings) to meet indoor thermal comfort requirements, in which an optimal controller should contribute to a satisfactory performance. The building space is designed to support up to 240 people and the activities performed include meetings, presentations, and office work. Regarding the operation modes, the building is open for occupancy every day, in a time schedule from 8 a.m. to 4 p.m. Therefore, thermal comfort is only relevant to be achieved during those hours.

*Research supported by the Netherlands Enterprise Agency (RVO) CONVERGE Project TEUE318008.

Thomas Joseph Ceha, Luigi Antonio de Araujo Passos, and Bart De Schutter are with the Delft Center for Systems and Control, Faculty of Mechanical, Maritime and Materials Engineering, Delft University of Technology, Delft, 2628CD, Netherlands (e-mail: thom_ceha@hotmail.com, l.a.dearaujopassos@tudelft.nl, b.deschutter@tudelft.nl).

Simone Baldi (corresponding author) is with the School of Mathematics, Southeast University, Nanjing, 210096, China (email: s.baldi@tudelft.nl).

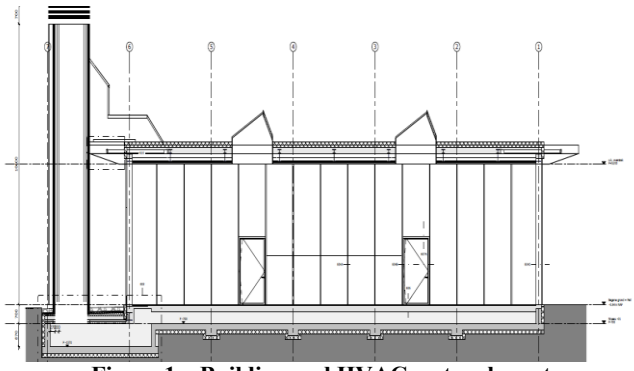

Figure 1 – Building and HVAC system layout

The building dimensions, materials and thermal-physical properties considered, are shown in Table 1. The theoretical values are obtained by means of the technical database CES EduPack [14].

Table 1 – Dimensions and materials where *V* means volume, *ρ* specific mass, *C* specific heat and ε thermal emissivity.

Section	Material	V [m³]	ρ [kg/m³]	C [J/kg/K]	ε [−]
N-S walls	Low-e glass	2.11	2470	900	0.86[a]
E-W walls	Low-e glass	3.51	2470	900	0.86[a]
Roof	Bitumen	1.22	1050	1800	0.93
Ceiling	Galvanized steel	0.46	7850	500	0.23
Floor	Concrete	75.94	2000	840	0.60
Room	Air	1579.5	1	1000	-

[a] The value of 0.2 is considered on the internal side of the glasses.

B. Thermal modelling

The physical system introduced in Figure 1 is mathematically modeled according to the principles of conservation of energy and heat transfer [15]. The data is provided at discrete time instant $t^k = k\Delta t$, in which Δt is the sample time. Therefore, the air flow rates coming across the building at the time step k is expressed as follows:

$$\dot{m}^k = \rho^k C_\mathrm{D} \phi \hat{u}_\mathrm{v}^k \sqrt{2gH \frac{|T_\mathrm{i}^k - T_\mathrm{o}^k|}{T_\mathrm{o}^k}} \tag{1}$$

where C_D refers to a nondimensional discharge coefficient, ϕ is the chimney's flow area, $\hat{u}_\mathrm{v}^k$ is the control input for optimal flow area fraction, g the gravitational constant, H the chimney height, ρ^k the air specific mass, and T_i^k and T_o^k refer to the temporal indoor and outdoor air temperatures, respectively. One should note that (1) assumes incompressible flow (and disregards friction losses). Therefore, the time variance of ambient temperature guarantees the variation of flowrate. In addition, the coefficient C_D is fixed to 0.62, based on calibrations with CFD simulations, while regarding the tower dimensions, $\phi = 4\ \mathrm{m}^2$ and $H = 4\ \mathrm{m}$.

For determining the evolution of the indoor temperature along time, an energy balance is applied to the fluid volume considered and to the 6 solid surfaces of the building (i.e., s_1 for the ceiling, s_2-s_5 for the walls, and s_6 for the floor). The fluid modelling mainly assumes a full-mixed temperature node inside the building (i.e., the air temperature inside the building is uniform along the space and it is only a function of time), so the temporal heat interaction regarding the air indoor and its surroundings is expressed as:

$$T_\mathrm{i}^k = T_\mathrm{i}^{k-1} + (\dot{q}_\mathrm{p}^k - \dot{q}_\mathrm{v}^k - \dot{q}_\mathrm{ci}^k) \frac{\Delta t}{M_\mathrm{i} C_\mathrm{i}} \tag{2}$$

where $\dot{q}_\mathrm{p}^k$ refers to internal heat gain from occupants, $\dot{q}_\mathrm{v}^k$ is the indoor ventilation rate, and $\dot{q}_\mathrm{ci}^k$ the total convective heat transfer between the air and bordering solids. Moreover, M_i refers to the mass of air, and C_i to the specific heat at constant pressure. The heat transfer rates considered in (2) are:

$$\dot{q}_\mathrm{p}^k = 100(P^k) \tag{2.1}$$

$$\dot{q}_\mathrm{v}^k = \dot{m}^k C_\mathrm{i} (T_\mathrm{i}^k - T_\mathrm{o}^k) \tag{2.2}$$

$$\dot{q}_\mathrm{ci}^k = \sum_{s=s_1}^{s_6} \dot{q}_\mathrm{cs}^k \tag{2.3}$$

where s_1-s_6 refers to the corresponding solid surfaces, P^k refers to the number of people inside the building, and $\dot{q}_\mathrm{cs}^k$ is the individual convective heat transfer for each solid surface. Note that the number 100, included in (2.1), refers to the metabolic heat generation per person. For determining the solid temperatures, a general energy balance for all surfaces results in the following expression:

$$T_\mathrm{s}^k = T_\mathrm{s}^{k-1} + (\hat{U}_\mathrm{s}^k \dot{q}_\mathrm{s}^k - \dot{q}_\mathrm{r}^k - \dot{q}_\mathrm{cs}^k - \dot{q}_\mathrm{d}^k) \frac{\Delta t}{M_\mathrm{s} C_\mathrm{s}} \tag{3}$$

where $\hat{U}_\mathrm{s}^k$ is the control input set for optimal shadings aperture, $\dot{q}_\mathrm{s}^k$ is the solar heat rate, $\dot{q}_\mathrm{r}^k$ the radiative heat rate and $\dot{q}_\mathrm{d}^k$ the conductive heat rate, while M_s refers to the solid mass, and C_s the specific heat of the respective solid considered. It is important to mention that when considering the ceiling (i.e., s=s_1), $\hat{u}_{s_1}^k = 1$, since there is no shading over the roof. Moreover, the heat rates between the brackets, in (3), depend on the kind of solid considered. Therefore,

$$\dot{q}_\mathrm{s}^k = I^k A_\mathrm{s} \tau_\mathrm{s} \alpha_\mathrm{s} \tag{3.1}$$

$$\dot{q}_r^k = \frac{\sigma A_\mathrm{s} \varepsilon_\mathrm{s} [(T_\mathrm{s}^k)^4 - (T_\mathrm{o}^k - 8)^4]}{F_{1-2}} \tag{3.2}$$

$$\dot{q}_\mathrm{cs}^k = h_\mathrm{s}^k A_\mathrm{s} (T_\mathrm{s}^k - T_\mathrm{o}^k) \tag{3.3}$$

$$\dot{q}_d^k = \lambda_\mathrm{s} A_\mathrm{s} (T_\mathrm{s}^k - T_\mathrm{g}^k) \tag{3.4}$$

where I^k refers to the solar radiation incidence, τ_s refers to transmittance, α_s to absorptance, ε_s the thermal emissivity, σ the radiative constant, F_{1-2} the radiative view factor, h_s^k the convective coefficient, λ_s the thermal conductivity, and T_g^k the ground temperature. At this moment, it is important to mention other assumptions regarding (3). For instance, when dealing with the ceiling (s_1) and the floor (s_6), $\dot{q}_r^k = 0$. On the other hand, $\dot{q}_\mathrm{d}^k = 0$ in the walls (s_2-s_5). Additionally, T_g^k in (3.4)

denotes the roof temperature when using (3) for the ceiling (s_1). In this paper, the convective coefficients are calculated according to the solid geometry, fluid velocity, and thermal-physical properties, such as thermal conductivity, specific mass and viscosity, generally written in terms of non-dimensional numbers [15]. On the other hand, the view factor $F_{1-2} = 1$ for external surfaces and $F_{1-2} = 2 - \varepsilon_s$ for enclosure surfaces [15]. For predicting ground temperatures, a plain cosines model is developed, based on ground data from the Royal Dutch Meteorological Institute [16].

For modelling the weather conditions acting as system disturbance, i.e., ambient temperature, solar irradiance, and wind velocity, TMY (Typical Meteorological Year) data for Amsterdam is considered. One should note that the radiation values typically provided by weather databases account only measurements at the horizontal and at a solar-tracked surface. In this case, I^k is particularly accounted for each surface considering the vertical tilting, orientation, solar angles, and Perez model for diffuse components, as fully described in [17]. However, for simplicity, such details will not be covered in this paper (see [17] for more details).

III. CONTROL ARCHITECTURE

While the system under consideration contains variable energy sources (i.e., solar and buoyancy), the HVAC design includes active components that may be controlled in order to provide effective energy management. For instance, the shadings aperture area determines solar heat gains, the chimney flow aperture form the ventilation rates across the building, etc. Hence, the challenge is to find optimal control signals for these actuators, while sufficiently suppressing the computation time for on-line application. Six distinct MPC architectures are analyzed to tackle this challenge.

The two single-level MPC architectures implemented in this work consider linear and nonlinear modelling approaches. In addition, four hierarchical MPC structures are introduced, employing a linear MPC reference determining agent and a nonlinear MPC reference tracker slave. Since the thermal model described above is nonlinear, a number of simplifications are made when considering the linear model:

- The heat transfer coefficients (h_s^k) do not depend on the actual solid and air temperatures.
- The radiative heat transfer rates are linearized around their current working points into terms of linear radiation coefficients, similar to the convection rates.
- The ventilation flow rates calculated in (1) are determined in terms of the outdoor and reference temperature T_{ref} instead of the transient indoor temperature state T_i^k.

The flowchart shown in Figure 2 displays the centralized nonlinear MPC (NLMPC) scheme. The full prediction model is constructed out of prediction functions, with each function representing the thermal model for one of the prediction steps of the receding prediction horizon, N_p. Each function is adjusted for each prediction step by considering a new set of time, occupation, ground temperature, weather data and input dependent model states from the previous prediction function. The optimization algorithm, employed by MATLAB function *fmincon*, is active-set, as it shows similar results but faster convergence than interior-point and Sequential Quadratic Programming. The MPC strategy is split in two periods, i.e., daytime, when solar shade control is relevant, and night-time. Such approach optimizes 5 input values (1 for the ventilation and 4 for the shaded walls), where the bounds are all set between 1 and 0, representing 100% and 0%, respectively. During night-time, it is only relevant to control the ventilation input. Note that at each time step k, the initial guess set $\tilde{u}$ is set equal to the optimized inputs $\hat{u}$ of the previous time step.

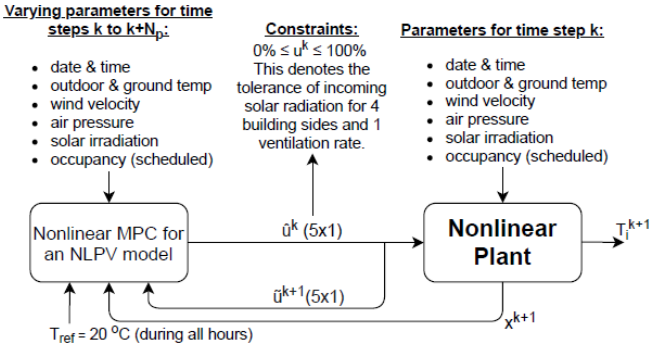

Figure 2 – Centralized nonlinear MPC (NLMPC)

For linear MPC (LMPC), a faster, quadratic programming optimization algorithm is adopted. In this case, the full prediction model encapsulates all prediction step dependent prediction matrices throughout the receding horizon, N_p^*. Each matrix also represents the thermal model which is modified by a new set of time, occupancy, ground temperature and weather data, but not by input dependent states, making the prediction model linear. This model is then inserted into a quadratic cost function with penalizing matrices on the stage and terminal costs, resulting in an augmented matrix. The stage and terminal costs are chosen so that the resulting augmented matrix is symmetric positive definite, and the global optimum is guaranteed when the optimal solution is found. The LMPC structure optimizes 5 inputs which are also bounded between 1 and 0. Figure 3 shows the flowchart for LMPC.

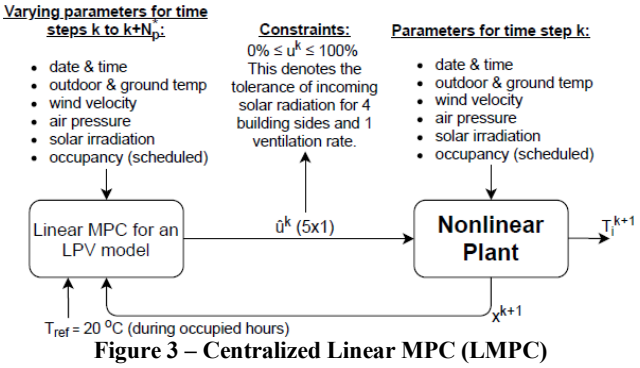

Figure 3 – Centralized Linear MPC (LMPC)

The first hierarchical control structure regarded combines the main advantages of the last two structures, i.e., it uses linear MPC and the linearized model of the plant to optimize a reference trajectory for the unoccupied hours, T_{traj}, that the nonlinear MPC controller has to track. The control flowchart is illustrated in Figure 4. In this case, the nonlinear plant will be controlled according to the re-optimized input values by the more accurate nonlinear MPC controller. The computation time of the linear controller is low enough to employ easily prediction horizons of 48 prediction steps,

while the nonlinear controller does not use a horizon larger than 4, due to heavy computational burdens which increase exponential in relation to the chosen horizon. The choice of horizon is further explained in Section IV.

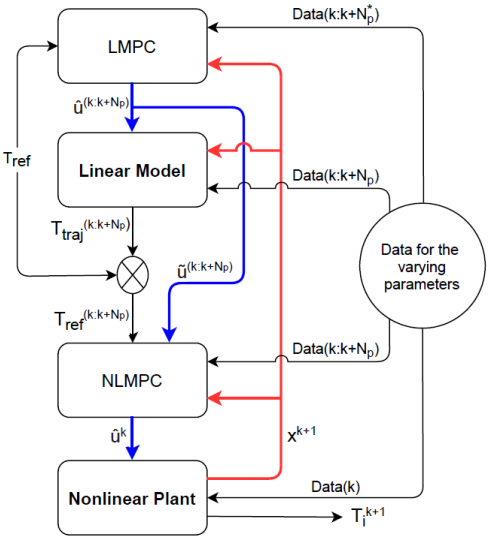

Figure 4 – Hierarchical MPC #1 (HMPC-1)

A second hierarchical structure is introduced to analyse the relevance of the state update strategy, assuming full state knowledge. This is done because the output of the linear model, controlled by linear MPC, could provide better reference trajectories when the two hierarchical layers are separated into their own closed loops. Such MPC flowchart is illustrated in Figure 5.

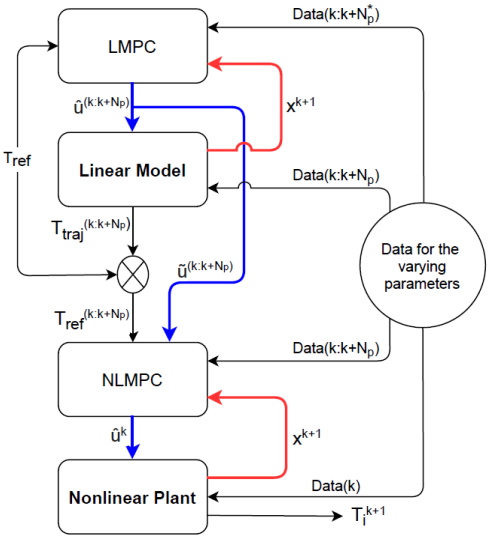

Figure 5 – Hierarchical MPC #2 (HMPC-2)

The third MPC architecture is set forth assuming that the building's heating response due to solar irradiance is relatively slow when compared to the heating response by ventilation. The former response is therefore less sensitive to nonlinearities and the ventilation can compensate quickly with its fast dynamics for thermal errors in the short period. Such approach is illustrated in Figure 6. In this case, the optimal solutions for the input values for the solar shades are applied directly to the nonlinear plant and are not re-optimized by the nonlinear MPC controller. However, they are taken into account by the nonlinear MPC controller for the optimization of the ventilation input. Therefore, the nonlinear MPC controller solely has to optimize the ventilation input, which saves a lot of computation time.

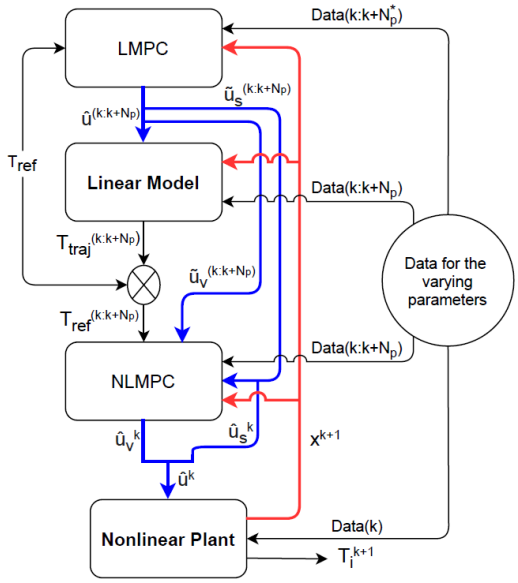

Figure 6 – Hierarchical MPC #3 (HMPC-3)

Lastly, a fourth hierarchical MPC structure is developed, according to Figure 7, for the same reason why hierarchical MPC structure 2 was considered: to analyse the optimal strategy for the state update process.

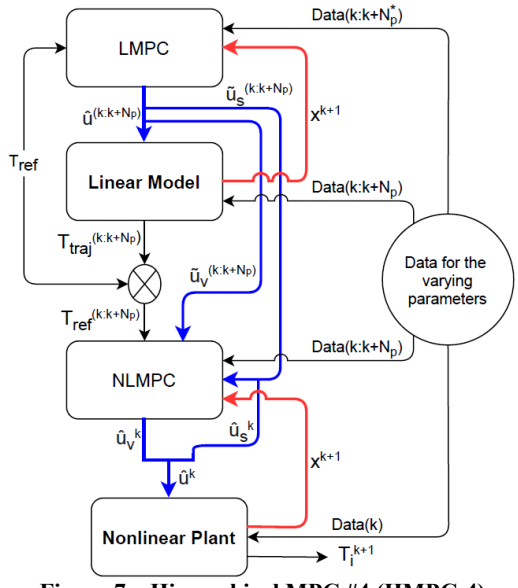

Figure 7 – Hierarchical MPC #4 (HMPC-4)

All five nonlinear MPC controllers presented aim at the minimization of the same objective function, such that

$$\min \sum_{k=1}^{N_\mathrm{p}} (T_\mathrm{i}^k - T_\mathrm{ref}^k)^2 \tag{5}$$

where T_ref^k is time depended and N_p the prediction horizon considered. In addition, the non-convexity of the nonlinear optimization problems has been analyzed by integrating a

multi-start approach with 40 random initial input guesses in the optimization algorithms.

IV. RESULTS AND DISCUSSION

The six MPC architectures were assessed in terms of attending the variance minimization with the reference values, as expressed by the objective function and computation time spent. The results are obtained during occupied hours for 40 days over the early spring. The prediction horizons N_p used, and the results dependent on the chosen control time step Δt, are summarized in Tables 2 and 3. The percentages indicate the degree of improvement per structure with respect to the NLMPC structure, e.g., the absolute error of HMPC-1 is 135 ^{o}C which is an improvement of -9.3% compared to the 149 ^{o}C of the NLMPC architecture.

Table 2 - Results of the MPC structures: Δt = 3600 s

Architecture	N_p	Squared error	Absolute error	Processing time per Δt
NLMPC	8	313 ^{o}C^2	149 ^{o}C	21.1 s
LMPC	24	-14.1%	+1.3%	-99.0%
HMPC-1	4[b]	-15.0%	-9.3%	-76.9%
HMPC-2	4[b]	-11.8%	-8.1%	-75.0%
HMPC-3	4[b]	-20.8%	-12.8%	-92.6%
HMPC-4	4[b]	-20.1%	-12.1%	-92.5%

[b] N_p^* is 24 for the linear block inside the HMPC architecture.

Table 3 – Results of the MPC structures: Δt = 1800 s

Architecture	N_p	Squared error	Absolute error	Processing time per Δt
NLMPC	8	342 ^{o}C^2	146 ^{o}C	31.2 s
LMPC	48	-24.3%	-0.7%	-97.7%
HMPC-1	4[c]	-3.5%	-6.2%	-76.5%
HMPC-2	4[c]	-1.5%	-5.5%	-74.5%
HMPC-3	4[c]	-26.0%	-14.4%	-92.1%
HMPC-4	4[c]	-26.3%	-14.4%	-92.5%

[c] N_p^* is 48 for the linear block inside the HMPC architecture.

Even though NLMPC holds the most representative dynamics of the actual plant, the current analysis shows that its control performance is impaired by computational requirements. For instance, the nonlinear controller requires a prediction horizon that should overbridge at least the unoccupied period in order to find optimal solutions which take into account the disturbance knowledge of the unoccupied and next occupied periods. Otherwise, the controller will not make preparatory decisions, benefitting that next occupied period. The unoccupied period is assumed to be 16 hours long. This implies, depending on the control time step of 60 or 30 minutes, that a minimum horizon of 17 to 33 prediction steps is required. When the horizon is doubled, the computation time is multiplied by 5.5 to 6. With a standard Intel computer and MATLAB, one time step with a horizon of 17 takes 2 to 3 minutes to solve the NLMPC optimization problem. However, such an MPC controller has minimal information about the next day and operates hourly. It is more preferable to have a longer horizon, such that more information about the next day is included in the optimization problem, and to have a control time step of 30 minutes or even shorter. In this case, the computation time will approach 20 minutes per time step. Full-fledged MPC controllers should have plug-and-play capabilities to accommodate more actuators, e.g., PCM, heat pumps, and operational windows. In that case, the computation time will surpass the control time step, making on-line control impossible. Therefore, it was noted that when the horizon cannot be increased to overbridge the unoccupied period, it is better to set N_p at 8 and track the 20 ^{o}C reference temperature during all hours, even if the building is unoccupied. In this case, the system makes no preparatory decisions for future occupied periods, but tries to hold 20 ^{o}C. Therefore, the NLMPC structure experiences the largest errors and it is used as benchmark for the other architectures.

For LMPC, the computation time is much lower, while employing a larger horizon. It was noted that when the horizon is doubled, the computation time to solve the LMPC optimization problem increases by 2 to 2.5 times. The horizon thus can easily be set to 24 or even 48 prediction steps. The controller can therefore choose optimal control inputs for the dynamics of the building, which benefits the performance of both the current and next day. The performance in terms of the squared error is significantly improved, but the absolute error results show no improvement. This indicates that the variance of the errors has decreased, but the mean of the errors is increased with respect to the results of the NLMPC structure. This can be explained by the mismatch between the linear prediction model and the nonlinear plant, resulting in small errors and oscillations around the 20 ^{o}C reference temperature.

Regarding the hierarchical structures, in general the algorithms demonstrate lower processing times, due to a lower employed prediction horizon, but also improved performance with respect to the NLMPC structure. Moreover, they are more accurate structures than the LMPC structure, resulting in smaller errors and less oscillations and thus better performance. The higher accuracy is due to the nonlinear MPC lower slave layer that overrules the solutions of the linear MPC higher agent layer, while respecting the optimal reference trajectory. Note that when the nonlinear slave re-optimizes the solutions of the linear agent, which employs a horizon of 24 or 48, it does so with disturbance knowledge of the shorter receding future, as the prediction horizon of the slave controller is set at 4. The results showed that, in case of HMPC-1 and HMPC-2, over the shorter period, the nonlinear slave prefers the ventilation to control the indoor temperature over that of the shading control, since the transient response is faster. However, the shades have a significant effect over a longer period, because they have a large influence on the thermal mass of the floor, which can be beneficial on later notice. For instance, the HMPC-1 structure may prioritize to open the shades and fully use the ventilation in order to cool down the indoor air during a semi-hot day. However, when even warmer weather follows, a better solution might have been to close the shades and make less use of ventilation. This is a scenario that can occur when the shading operations are re-optimized on a shorter future of disturbance knowledge. Additionally, the performances of HMPC-1 and HMPC-2 are comparable, with slightly better results for HMPC-1.

Meanwhile, HMPC-3 seems to solve the problem of HMPC-1 and HMPC-2 regarding the optimal control solutions of the thermal mass by the solar shading. HMPC-3 increases the system's performance by 4% to 9%, depending on the control time step, with respect to HMPC-1. The processing time of HMPC-3 is 68% faster than HMPC-1 and HMPC-2. Therefore, despite its complex structure, this control structure seems to be the best option so far analysed, while the HMPC-4 architecture does not seem to increase the system's performance significantly.

Figure 8 presents the performance of HMPC-3 over 15 days during April and May. The occupied periods are indicated by vertical dotted lines. The figure shows clearly that the building prepares itself for the next day, e.g., during the cold period, it heats the indoor air (blue line) up after the occupied period has ended and during the hot period, it tries to cool down the thermal mass of the floor (green line) as much as possible during the night.

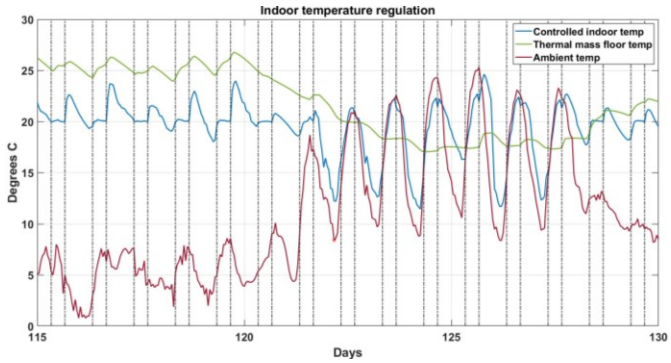

Figure 8 – Performance of HMPC-3 with a 20 ºC reference temperature during occupied hours

V. Conclusions

This work has investigated effective MPC methods to optimize the integration of a thermal chimney and a solar shading system for passive HVAC of an office building at the TU Delft campus. Six architectures were tested, including a linear and nonlinear approach, and four hierarchical variants. The results indicate that the hierarchical architecture HMPC-3 presents promising performance. The advantages of this architecture can be explained by the separation of controllable actuators, based on their effect on the dynamical system, into distinct control strategies, suppressing the computation time.

On-going and future work include the analyze of other computational demand reducing methods for MPC, e.g., shorten the control horizon relative to the prediction horizon and applying more efficient nonlinear solvers, like IPOPT.

References

[1] European Commission, "Mapping and analyses of the current and future (2020-2030) heating/cooling fuel deployment (fossil/renewables)", 2016.

[2] X. Cao, X. Dai and J. Liu, "Building energy-consumption status worldwide and the state-of-the-art technologies for zero-energy buildings during the past decade", *Energy and Buildings,* pp. 198-213, 2016.

[3] J. Drogna et al., "All you need to know about model predictive control for buildings", *Annual Reviews in Control*, pp. 190-232, 2020.

[4] M. Tanaskovic et al., "Robust adaptive model predictive building climate control", *IFAC-PapersOnLine*, pp. 1871-1876, 2017.

[5] A. Parisio et al., "A scenario-based predictive control approach to building HVAC management systems", *IEEE International Conference on Automation Science and Engineering*, pp. 428–435, 2013.

[6] J. Drgoňa et al., "Explicit stochastic MPC approach to building temperature control", *IEEE Conference on Decision and Control*, pp. 6440-6445, 2013.

[7] S. Koehler and F. Borrelli, "Building temperature distributed control via explicit MPC and trim and respond methods", *European Control Conference*, pp. 4334-4339, 2013.

[8] H. Scherer et al., "Efficient building energy management using distributed model predictive control", *Journal of Process Control*, pp.740-749, 2014.

[9] V. Putta et al., "Distributed model predictive control for building HVAC systems: A case study", *International High Performance Buildings Conference*, pp. 3611-3619, 2014.

[10] Y. Long et al., "A hierarchical distributed MPC for HVAC systems", *2016 American Control Conference*, pp. 2385-2390, 2016.

[11] G. Mantovani, L. Ferrarini, and S. Member, "Temperature control of a commercial building with model predictive control techniques", *Transactions on Industrial Electronic*, pp. 2651-2660, 2015.

[12] M. Maasoumy and A. Sangiovanni-Vincentelli, "Total and peak energy consumption minimization of building HVAC systems using model predictive control", *Design and Test of Computers*, pp. 26–35, 2012.

[13] Y. Ma, J. Matusko, and F. Borrelli, "Stochastic model predictive control for building HVAC systems: Complexity and conservatism," *Transactions on Control Systems Technology*, pp. 101–116, 2015.

[14] ANSYS, "GRANTA EduPack, Formerly CES EduPack: Materials Education Support", www.ansys.com/products/materials/granta-edupack, Accessed on January 15, 2020.

[15] T. L. Bergman et al., "Fundamentals of Heat and Mass Transfer", New York: *John Wiley & Sons*, 2011.

[16] KNMI, "Soil Temperatures", www.knmi.nl/nederland-nu/klimatologie/bodemtemperaturen, Accessed on January 15, 2021.

[17] J. Duffie and W. Beckman, "Solar Engineering of Thermal Processes", New York: *John Wiley & Sons*, 2013.

Appendix E

Draft of Journal Paper

Bibliography

[1] RICHTLIJN 2010/31/EU VAN HET EUROPEES PARLEMENT EN DE RAAD. *Publicatieblad van de Europese Unie*, 06 2010.

[2] CONVERGE, Project plan Urban Energy tender. *Delft University of Technology*, 2018.

[3] A. Afram and F. Janabi-Sharifi. Review of modeling methods for hvac systems. *Applied Thermal Engineering*, 67:507–519, 06 2014.

[4] A. Afram and F. Janabi-Sharifi. Theory and applications of hvac control systems – a review of model predictive control (mpc). *Building and Environment*, 72:343–355, 2014.

[5] Z. Afroz, G. Shafiullah, T. Urmee, and G. Higgins. Modeling techniques used in building hvac control systems: A review. *Renewable and Sustainable Energy Reviews*, 12 2017.

[6] K. Ahmed, A. Akhondzada, J. Kurnitski, and B. Olesen. Occupancy schedules for energy simulation in new pren16798-1 and iso/fdis 17772-1 standards. *Sustainable Cities and Society*, 35:134–144, 2017.

[7] A. Albatayneh, D. Alterman, A. Page, and B. Moghtaderi. The significance of sky temperature in the assessment of the thermal performance of buildings. *Applied Sciences*, 10(22), 2020.

[8] K.T. Andersen. Theoretical considerations on natural ventilation by thermal buoyancy. *ASHRAE Transactions*, (101):1–15, 1995.

[9] ANSYS. Granta edupack, formerly ces edupack: Materials education support. www.ansys.com/products/materials/granta-edupack. Accessed: 16-06-2021.

[10] G.S. Bakken, D.M. Gates, T.H. Strunk, and M. Kleiber. Linearized heat transfer relations in biology. *Science*, 183(4128):976–978, 1974.

[11] W.A. Beckman, L. Broman, A. Fiksel, S.A. Klein, E. Lindberg, M. Schuler, and J. Thornton. Trnsys the most complete solar energy system modeling and simulation software. *Renewable energy*, 5(1-4):486–488, 1994.

[12] I.H. Bell, J. Wronski, S. Quoilin, and V. Lemort. Pure and pseudo-pure fluid thermophysical property evaluation and the open-source thermophysical property library coolprop. *Industrial & Engineering Chemistry Research*, 53(6):2498–2508, 2014.

[13] W. Bernal, M. Behl, T.X. Nghiem, and R. Mangharam. Mle+ a tool for integrated design and deployment of energy efficient building controls. In *Proceedings of the Fourth ACM Workshop on Embedded Sensing Systems for Energy-Efficiency in Buildings*, pages 123–130, 2012.

[14] L.T. Biegler and V.M. Zavala. Large-scale nonlinear programming using ipopt: An integrating framework for enterprise-wide dynamic optimization. *Computers & Chemical Engineering*, 33(3):575–582, 2009.

[15] A. Boodi, K. Beddiar, M. Benamour, Y. Amirat, and M. Benbouzid. Intelligent systems for building energy and occupant comfort optimization: A state of the art review and recommendations. *Energies*, 11(10), 2018.

[16] S. Brisset and F. Gillon. 4 - approaches for multi-objective optimization in the ecodesign of electric systems. In Jean-Luc Bessède, editor, *Eco-Friendly Innovation in Electricity Transmission and Distribution Networks*, pages 83–97. Woodhead Publishing, Oxford, 2015.

[17] B. Bronsema, R. Bokel, and W. van der Spoel. *Earth, Wind & Fire–Natural Air Conditioning*. PhD thesis, PhD Thesis. Delft University of Technology, 2013.

[18] E. Camacho and C. Bordons. *Model Predictive Control*, volume 13. 01 2004.

[19] CHAM. Phoenics (parabolic, hyperbolic or elliptic numerical integrated code series). http://www.cham.co.uk/phoenics.php. Accessed: 17-12-2020.

[20] Z. Chen, M. K. Masood, and Y.C. Soh. A fusion framework for occupancy estimation in office buildings based on environmental sensor data. *Energy and Buildings*, 133:790–798, 2016.

[21] D.B. Crawley, L.K. Lawrie, F.C. Winkelmann, W.F. Buhl, Y.J. Huang, C.O. Pedersen, R.K. Strand, R.J. Liesen, D.E. Fisher, M.J. Witte, et al. Energyplus: creating a new-generation building energy simulation program. *Energy and buildings*, 33(4):319–331, 2001.

[22] L.A. de Araujo Passos, P. van den Engel, S. Baldi, and B. De Schutter. Dynamic optimization of a thermal chimney, solar shades, and latent heat buffer system for passive hvac. pages 1–35, 2021.

[23] M. de Simón-Martín, C. Alonso-Tristán, and M. Díez-Mediavilla. Diffuse solar irradiance estimation on building's façades: Review, classification and benchmarking of 30 models under all sky conditions. *Renewable and Sustainable Energy Reviews*, 77:783–802, 2017.

[24] A.I. Dounis and C. Caraiscos. Fuzzy comfort and its use in the design of an intelligent coordinator of fuzzy controller-agents for environmental conditions control in buildings. *Journal of Uncertain Systems*, 2(2):101–112, 2008.

[25] J. Drgoňa, J. Arroyo, I. Cupeiro Figueroa, D. Blum, K. Arendt, D. Kim, E. Perarnau Ollé, J. Oravec, M. Wetter, D.L. Vrabie, and L. Helsen. All you need to know about model predictive control for buildings. *Annual Reviews in Control*, 50:190–232, 2020.

[26] D. D'Agostino, P. Zangheri, and L. Castellazzi. Towards nearly zero energy buildings in europe: A focus on retrofit in non-residential buildings. *Energies*, 10(1), 2017.

[27] EnergyPlus. Weather data sources. https://energyplus.net/weather/sources. Accessed: 16-10-2020.

[28] M. Falih. *Ventilation for Acceptable Indoor Air Quality*. 10 2020.

[29] P.O. Fanger et al. Thermal comfort. analysis and applications in environmental engineering. *Thermal comfort. Analysis and applications in environmental engineering.*, 1970.

[30] R. Forristall. Heat transfer analysis and modeling of a parabolic trough solar receiver implemented in engineering equation solver. 01 2003.

[31] J.E. Hay. A revised method for determining the direct and diffuse components of the total short-wave radiation. *Atmosphere*, 14(4):278–287, 1976.

[32] I. Hazyuk, C. Ghiaus, and D. Penhouet. Optimal temperature control of intermittently heated buildings using model predictive control: Part i – building modeling. *Building and Environment*, 51:379 – 387, 2012.

[33] F.P. Incropera, D.P. DeWitt, T.L. Bergman, and A.S. Lavine. *Fundamentals of Heat and Mass Transfer*. Wiley, 2007.

[34] F. Jorissen, D. Picard, I. Cupeiro Figueroa, W. Boydens, and L. Helsen. Towards real mpc implementation in an office building using taco. 2018.

[35] D. Kim and J.E. Braun. Hierarchical model predictive control approach for optimal demand response for small/medium-sized commercial buildings. In *2018 Annual American Control Conference (ACC)*, pages 5393–5398. IEEE, 2018.

[36] KNMI. Soil temperatures of four locations in the netherlands. www.knmi.nl/nederland-nu/klimatologie/bodemtemperaturen. Accessed: 15-01-2021.

[37] P.S. Koronakis. On the choice of the angle of tilt for south facing solar collectors in the athens basin area. *Solar Energy*, 36(3):217–225, 1986.

[38] B. Liu and R. Jordan. Daily insolation on surfaces tilted towards equator. *ASHRAE J.;(United States)*, 10, 1961.

[39] Y. Long, S. Liu, L. Xie, and K.H. Johansson. A hierarchical distributed mpc for hvac systems. In *2016 American Control Conference (ACC)*, pages 2385–2390. IEEE, 2016.

[40] P.G. Loutzenhiser, H. Manz, C. Felsmann, P.A. Strachan, T. Frank, and G.M. Maxwell. Empirical validation of models to compute solar irradiance on inclined surfaces for building energy simulation. *Solar Energy*, 81(2):254–267, 2007.

[41] A.F. Mills. *Basic Heat and Mass Transfer*. Pearson, 2 edition, 1999.

[42] T. Muneer. Solar irradiance and illuminance models for japan i: Sloped surfaces. *International Journal of Lighting Research and Technology*, 27(4):209–222, 1995.

[43] NIEMAN. BENG eis vanaf 01-01-2021. https://www.nieman.nl/specialismen/energie-en-duurzaamheid/beng-eis-vanaf-01-01-2021/. Accessed: 03-06-2020.

[44] S. Obyn and G. van Moeseke. Variability and impact of internal surfaces convective heat transfer coefficients in the thermal evaluation of office buildings. *Applied Thermal Engineering*, 87:258–272, 2015.

[45] F. Oldewurtel, A. Parisio, C. Jones, D. Gyalistras, M. Gwerder, V. Stauch, B. Lehmann, and M. Morari. Use of model predictive control and weather forecasts for energy efficient building climate control. *Energy and Buildings*, 45:15–27, 02 2012.

[46] R. Perez, P. Ineichen, R. Seals, J. Michalsky, and R. Stewart. Modeling daylight availability and irradiance components from direct and global irradiance. *Solar Energy*, 44(5):271–289, 1990.

[47] D. Picard, J. Drgoňa, M. Kvasnica, and L. Helsen. Impact of the controller model complexity on model predictive control performance for buildings. *Energy and Buildings*, 152:739–751, 2017.

[48] K. Shukla and S. Rangnekar. Comparative study of isotropic and anisotropic sky models to estimate solar radiation incident on tilted surface: A case study for bhopal, india. *Energy reports*, 1:96–103, 03 2015.

[49] C. Toledo, A.M. Gracia Amillo, G. Bardizza, J. Abad, and A. Urbina. Evaluation of solar radiation transposition models for passive energy management and building integrated photovoltaics. *Energies*, 13(3), 2020.

[50] R. van der Loos and I. Kuijpers. BENG is veranderd, maar wat betekent dat nu echt? *Praktijk*, 06 2019.

[51] M. Verhaegen and V. Verdult. *Filtering and System Identification: A Least Squares Approach*. Cambridge University Press, 2007.

[52] Rijksdienst voor Ondernemend Nederland. Energieprestatie - BENG. https://www.rvo.nl/onderwerpen/duurzaam-ondernemen/gebouwen/wetten-en-regels/nieuwbouw/energieprestatie-beng. Accessed: 03-06-2020.

[53] Rijksdienst voor Ondernemend Nederland. Phase change materials PCM. https://www.rvo.nl/onderwerpen/duurzaam-ondernemen/gebouwen/technieken-beheer-en-innovatie/phase-change-materials-pcm. Accessed: 03-06-2020.

[54] Y. Wang, Q. Zheng, H. Zhang, and Y. Gao. A study on nonlinear model predictive control for helicopter/engine with variable rotor speed based on linear kalman filter. *International Journal of Turbo Jet-Engines*, 2019.

[55] M. Wetter and P. Haves. A modular building controls virtual test bed for the integration of heterogeneous systems. *Proceedings of SimBuild*, 3(1):69–76, 2008.

[56] M. Wetter, W. Zuo, T.S. Nouidui, and X. Pang. Modelica buildings library. *Journal of Building Performance Simulation*, 7(4):253–270, 2014.

[57] A. Yahiaoui, J.L.M. Hensen, and L.L. Soethout. Integration of control and building performance simulation software by run-time coupling. In *IBPSA Conf. & Exhib*, volume 3, pages 1435–1441, 2003.

Glossary

List of Acronyms

TU Delft	Delft University of Technology
MPC	Model predictive control
BENG	Almost Energy Neutral Buildings
PCM	Phase Change Materials
HVAC	Heating Ventilating and Cooling
ANN	Artificial Neural Networks
RMSE	Root mean squared error
NRMSE	Normalized root mean squared error
VAF	Variance accounted for
CFD	Computational Fluid Dynamics
BES	Building energy simulation
SVM	Support Vector Machines
SQP	Sequential Quadratic Programming
IAQ	Indoor air quality
CCC	Co-Creation Centre
BEMS	Building energy management system
TMY	Typical Meteorological Year
LMPC	Linear model predictive control
NLMPC	Nonlinear model predictive control
HMPC	Hierarchical model predictive control
SD	Standard deviation

List of Symbols

A	Area [m^2]
A^*	Effective opening area [m^2]
A_b	Chimney outlet area [m^2]
A_t	Chimney inlet area [m^2]
A_u	unshaded floor area [m^2]
$A_{\vec{x}}$	Area perpendicular to the transfer direction [m^2]
C_d	Natural ventilation coefficient for discharge and friction [-]
D	Cavity thickness [m]
Day	The specific day number of the year [-]
H	Thermal chimney height [m]
I_{bh}	Direct beam radiation to Earth's horizon [W/m^2]
I_{bn}	Direct beam radiation to tracking surface [W/m^2]
I_d	Diffused radiation [W/m^2]
$I_{o,b}$	Oriented direct beam radiation [W/m^2]
$I_{o,d}$	Oriented diffused radiation [W/m^2]
$I_{o,r}$	Oriented reflected radiation [W/m^2]
I_o	Total oriented solar irradiance [W/m^2]
M	Adjacent medium for convection [-]
N_p^*	Prediction horizon for linear MPC [-]
N_c	Control horizon [-]
N_{occ}	Number of occupants [-]
N_p	Prediction horizon for nonlinear MPC [-]
Q	Heat energy [J]
T	Temperature [K]
T_M	Adjacent medium temperature [K]
T_a	Ambient temperature [K]
T_{bf}	Temperature state of basement floor [K]
T_c	Temperature state of ceiling [K]
T_{diff}	Difference between two temperatures [K]
$T_{e,j}$	Temperature states of the three east glazed walls [K]
$T_{g,B}$	Ground temperature data set of De Bilt [K]
$T_{g,w}$	Ground temperature data set of Wilhelminadorp [K]
T_g	Ground temperature [K]
$T_{n,j}$	Temperature states of the three north glazed walls [K]
T_{nom}	Nominal temperature [K]
T_{ref}	Reference temperature [K]
T_{rf}	Temperature state of raised floor [K]
T_r	Temperature state of roof [K]
$T_{s,j}$	Temperature states of the three south glazed walls [K]

T_{sky}	Sky temperature [K]
T_{s}	Surface temperature [K]
T_{traj}	Optimized reference temperature trajectory [K]
$T_{\text{w,j}}$	Temperature states of the three west glazed walls [K]
$T_{\text{z,0}}$	Temperature constant of inner zone [K]
T_{z}	Temperature state of inner zone [K]
U	Thermal energy [J]
U_{IAQ}	Additional thermal energy to reach IAQ [kWh]
U_{add}	Additional thermal energy to reach thermal comfort [kWh]
V	Volume [m^3]
W	Work [J]
X	Component width [m]
Y	Component length [m]
Z	Component depth [m]
$\dot{Q}_{\text{cond}}$	Energy gain rate by conduction [W]
$\dot{Q}_{\text{conv}}$	Energy gain rate by convection [W]
$\dot{Q}_{\text{gen}}$	Internally generated energy gain rate [W]
$\dot{Q}_{\text{hp}}$	Energy gain rate by the heat pump [W]
$\dot{Q}_{\text{in}}$	Energy gain rate by absorption [W]
$\dot{Q}_{\text{out}}$	Energy gain rate by energy transfer [W]
$\dot{Q}_{\text{rad}}$	Energy gain rate by radiation [W]
$\dot{Q}_{\text{vent}}$	Energy gain rate by ventilation (advection) [W]
$\dot{m}$	Mass flow rate [kg/s]
$\hat{u}_{\text{k}}$	Set of optimized inputs [-]
$\tilde{u}_{\text{k}}$	Set of initial input guesses [-]
α	Solar irradiance absorptance [-]
α_{o}	Oriented solar irradiance absorptance [-]
β	Angle between a component's surface and the horizon [Deg]
ϵ	Surface emissivity [-]
ϵ_{low}	Surface emissivity for low-e glass [-]
γ_{azi}	Azimuth angle [Deg]
$\hat{x}_{\text{est}}$	Set of updated states by the Kalman filter [K]
$\hat{x}_{\text{mod}}$	Set of updated states by the model [K]
κ	Thermal conductivity of a solid [W/(mK)]
λ_{M}	Thermal conductivity of a fluid or gas [W/(mK)]
$\mathcal{A}$	System matrix [-]
$\mathcal{B}$	Input matrix [-]
$\mathcal{C}$	Output matrix [-]
$\mathcal{E}$	Disturbance input matrix [-]
$\mathcal{F}_{12}$	Radiation transfer factor between two surfaces [-]

$\mathcal{K}$	Kalman filter matrix [-]
$\mathcal{P}$	Penalizing terminal matrix (Ricatti) [-]
$\mathcal{Q}$	Penalizing state matrix [-]
$\mathcal{R}$	Penalizing input matrix [-]
Nu	Nusselt number [-]
$Nu_{\downarrow}$	Nusselt number for downwards-facing surfaces [-]
$Nu_{\uparrow}$	Nusselt number for upwards-facing surfaces [-]
Pr	Prandtl number [-]
Ra	Rayleigh number [-]
Re	Reynolds number [-]
$\overline{h}_{\mathrm{j,j^*}}$	Average heat transfer coefficient between two components [W/(m^{2}K)]
$\overline{u}_{\mathrm{k}}$	Set of optimized inputs over the whole horizon [-]
ρ	Density [kg/m^3]
ρ_{r}	Albedo value [-]
σ	Stefan-Boltzmann constant [W/(m^{2}K^4)]
θ_{n}	Angle between a surface's normal and the solar beam direction [Deg]
θ_{z}	Zenith angle [Deg]
$\vec{x}$	Distance over the direction's length of transferred energy [m]
ξ	Effective optical transparency [-]
ξ_{o}	Oriented effective optical transparency [-]
c_{p}	Constant-pressure specific heat [J/(kgK)]
d_{k}	Set of time-varying model disturbances [-]
e	Set of temperature errors [K]
g	Gravitational acceleration [m/s^2]
i	Index of control horizon step [-]
k	Index of simulation time step [-]
l	Characteristic length for convection [m]
n	Number of glazings in series before an component [-]
p_{M}	Pressure of a medium [N/m^2]
p_{k}	Set of time-varying model parameters [-]
t	Time in seconds [s]
t_{h}	Time in hours [h]
t_{occ}	Occupied hours [h]
t_{op}	Computation time of a optimization step [s]
u_{a}	Controllable input of additional auxiliary energy [W]
u_{b}	Controllable input of the solar blinds [%]
u_{k}	Set of time-varying model inputs [-]
u_{ref}	Reference states of the inputs [-]
u_{v}	Controllable input of the natural ventilation [%]
v	White-noise sensor disturbances [K]

v_{a}	Ambient wind speed [m/s]
w	White-noise process disturbances [-]
x_0	Set of initial states [K]
x_{k}	Set of time-varying model states [K]
y_{k}	Set of time-varying model outputs [K]
y_{p}	Plant's measured outputs [K]